



Università Campus Bio-Medico di Roma
School of Engineering
PhD Course in Biomedical Engineering
(XXIV - 2009/2011)

Biomechatronic design of novel compliant active and passive joints for wearable robots

Giorgio Carpino

Supervisors

Prof. Eugenio Guglielmelli

Dr. Dino Accoto


PhD Program Coordinator

Prof. Giulio Iannello

March 2012

A handwritten signature in black ink, which appears to read 'Giorgio Carpino', is located in the bottom right corner of the page.

Tesi di dottorato in Ingegneria Biomedica, di Giorgio Carpino,
discussa presso l'Università Campus Bio-Medico di Roma in data 20/03/2012.
La disseminazione e la riproduzione di questo documento sono consentite per scopi di didattica e ricerca,
a condizione che ne venga citata la fonte

A handwritten signature in black ink, appearing to read "Giorgio Carpino". The signature is written in a cursive, flowing style with some loops and flourishes.

Biomechatronic design of novel compliant active and passive joints for wearable robots

A thesis presented by

Giorgio Carpino

in partial fulfillment of the requirements for the degree of

Doctor of Philosophy

in Biomedical Engineering

Università Campus Bio-Medico di Roma

School of Engineering

Supervisors

Prof. Eugenio Guglielmelli

Dr. Dino Accoto

PhD Program Coordinator

Prof. Giulio Iannello

March 2012



Tesi di dottorato in Ingegneria Biomedica, di Giorgio Carpino,
discussa presso l'Università Campus Bio-Medico di Roma in data 20/03/2012.
La disseminazione e la riproduzione di questo documento sono consentite per scopi di didattica e ricerca,
a condizione che ne venga citata la fonte

COMMITTEE:


Prof. Giulio Iannello (Università Campus Bio-Medico di Roma)

Prof. Riccardo Pietrabissa (Politecnico di Milano)

Prof. Salvatore Andrea Sciuto (Università degli Studi Roma Tre)

REVIEWER:

Prof. Dirk Lefeber (Vrije Universiteit Brussel)

A handwritten signature in black ink, appearing to read 'Giorgio Carpino', is located in the lower right quadrant of the page.

Tesi di dottorato in Ingegneria Biomedica, di Giorgio Carpino,
discussa presso l'Università Campus Bio-Medico di Roma in data 20/03/2012.
La disseminazione e la riproduzione di questo documento sono consentite per scopi di didattica e ricerca,
a condizione che ne venga citata la fonte

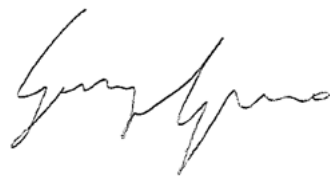
To my parents and my family

“Stay hungry, stay foolish”

(S. J., 2005)

A handwritten signature in black ink, appearing to read 'Giorgio Carpino', written in a cursive style.

Tesi di dottorato in Ingegneria Biomedica, di Giorgio Carpino,
discussa presso l'Università Campus Bio-Medico di Roma in data 20/03/2012.
La disseminazione e la riproduzione di questo documento sono consentite per scopi di didattica e ricerca,
a condizione che ne venga citata la fonte

A handwritten signature in black ink, appearing to read "Giorgio Carpino". The signature is fluid and cursive, with the first name "Giorgio" and the last name "Carpino" clearly distinguishable.

Abstract

Wearable robots are a class of mechatronic systems intended to exchange energy with the environment and the human body for assistive, prosthetic or rehabilitative purposes. The conventional design approach starts with the definition of suitable technical specifications, which provide a set of constraints to the designer. The objective of the design phase is to find a solution of such constrained problem. While the conventional design methodology is still effective in several fields of robotics, a number of issues arise in the case of wearable robots, mainly related to the need of high efficiency, robustness and safety levels. Moreover, wearable robots have to cope with the human body own dynamics, which is rather complex and influenced by a number of concurrent biomechanical and neurological factors. In particular, the application of the concept of structural intelligence, as form of embodied intelligence, in the design of wearable robots can greatly simplify the achievement of the emergence of dynamic behaviors derived from the coupling of the human body and the wearable robot. Such machine would expectedly be lighter, more energy efficient and possibly simpler than machines designed in a conventional way.

The development of efficient wearable robotic systems for rehabilitation and assistive purposes requires the synergistic deployment of advanced solutions involving multiple aspects, such as the design of the kinematic structure and of the actuation system. New compliant actu-



ation solutions have been developed in recent years to establish a safe and effective physical human-robot interaction in rehabilitation and assistive wearable robots. The introduction of intrinsic compliance, as a form of structural intelligence, in the actuation system and in the passive joints of wearable robots is motivated by the necessity of improving safety and dynamical adaptability. Furthermore, in wearable robots for gait assistance, the exploitation of conservative compliant elements as energy buffers mimics the intrinsic dynamical properties of legs.

In order to address this design challenge, this thesis described the design of novel active and passive joints for lower limbs wearable robots embedding innovative solutions to render different viscoelastic behaviors. Commercially available compliant components do not generally allow to obtain the desired requirements in terms of admissible peak loading demanded by gait assistance, while guaranteeing a compact and lightweight design. The high torque and power necessary for gait assistive robotic systems requires the use of custom-made springs, able to guarantee high performances with a compact and lightweight design. Two rotary Series Elastic Actuators and a passive viscoelastic joint have been developed. The working principles, the basic design choices regarding the overall architectures and the single components and the systems characterization are presented and discussed.

The developed joints have been integrated in two wearable robots concepts: an active orthosis for knee assistance and a non-anthropomorphic lower limbs wearable robot for gait assistance. The wearable robot include two modules for the actuation of the hip/knee flexion/extension in the sagittal plane and for the actuation of the hip degrees of freedom outside the sagittal plane. The integration of the modules and the concept of the wearable robot are finally reported.



Acknowledgments

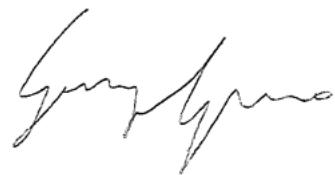
Here I am...last but not least the acknowledgments for this work, probably the harder piece to write!

This three-year experience has stretched me academically and personally. I am very grateful to the people that have been with me to share this whole experience. First of all, I would like to thank my supervisors Eugenio Guglielmelli and Dino Accoto for their advice, guidance, help, time, and enthusiasm. I appreciate all that I have learned from them as advisors, teachers, mentors and men. I am also very grateful to Andras Toth that has received me to work in his lab for three months.


The Biomedical Robotics and Biomicrosystems Lab is a great place to work with young researchers having the same objective: to apply their findings to improve the quality of human life. I had passed great moments with all of my colleagues and friends in the lab (Nino, Peppe, Simone, Michelangelo, Maria Teresa, Antonella, Mimmo, Baffo, Massimo, Loredana, Flavia, Alessandro, Marco, Eugenia, Anna Lisa, Valentina, Angelo, Francesco, Alessio) and I would like to thank them for all the time spent together.

I especially appreciate my good friends Fabrizio and Nevio with whom I have shared the Ph.D. road working closely and spending many nights in the lab. Nothing more to say than "thanks". I hope to still work with you having the opportunity to create something great one day.

I thank my parents, my sister, my nephew and niece, and the whole family for their constant support, encouragement, and words of confidence. Mom and Dad are the ones who made it possible to start this journey and who have always trusted in me.




Last but not least, I say “thank you” to all the special people present in my life; with your constant presence you have supported me to reach this hard achievement. They know how much I have loved, I love and I will love them!


A handwritten signature in black ink, appearing to read 'Giorgio Carpino', located in the bottom right corner of the page.

Contents

Contents	xi
List of Tables	xiv
List of Figures	xv
List of Acronyms	xix
1 Introduction	1
1.1 Thesis overview	2
2 State of the art and design methodologies for lower limbs wearable robots	5
2.1 Wearable robots and pHRI	5
2.2 Wearable robots for the lower limbs: conventional design approach .	7
2.2.1 "Stand-alone" WRs	8
2.2.1.1 Human performance augmentation WRs	9
2.2.1.2 Mobile medical WRs	17
2.2.2 "Treadmill-based" wearable robots	24
2.2.3 Hybrid solutions for wearable robots	29
2.3 Structural intelligence-based design methodology for wearable robots	31
2.4 Conclusions	36
3 Active and passive joints for wearable robots for the lower limbs	39
3.1 Active joint for wearable robots: Series Elastic Actuator 90W	40
3.1.1 SEA 90W design requirements	42



3.1.2	SEA 90W design	45
3.1.2.1	SEA 90W custom torsional spring	48
3.1.2.2	Spring design requirements	50
3.1.2.3	Spring design methodology	52
3.1.2.4	SEA 90W spring design	55
3.1.2.5	FEM simulations	57
3.1.2.6	Characterization of the torsional spring	63
3.1.3	SEA 90W experimental characterization	66
3.1.4	Conclusions and future works	70
3.2	Active joint for wearable robots: Series Elastic Actuator 300W	72
3.2.1	SEA 300W requirements	74
3.2.2	SEA 300W design	75
3.2.2.1	SEA 300W springs pack	78
3.2.2.2	SEA 300W custom torsional spring	79
3.2.2.3	Characterization of SEA 300W torsional spring	84
3.2.3	Conclusions and future works	89
3.3	Passive joint for wearable robots: passive viscoelastic joint	91
3.3.1	pVEJ requirements	94
3.3.2	pVEJ concept and dimensioning	95
3.3.2.1	Torsional stiffness	95
3.3.2.2	Torsional damping	98
3.3.3	pVEJ design	101
3.3.3.1	Torsional stiffness module	101
3.3.3.2	Torsional damping module	105
3.3.4	pVEJ characterization	105
3.3.4.1	Stiffness module	105
3.3.4.2	Damping module	106
3.3.5	Conclusions and future works	107
4	Non-anthropomorphic lower limbs wearable robot for gait assistance	111
4.1	Introduction	111
4.1.1	Objectives	114



4.2	Hip/knee flexion/extension module	115
4.2.1	Wearable robot topology and morphology	115
4.2.1.1	Particularization to a hip/knee orthosis	120
4.2.1.2	Simulation environment	121
4.2.2	Design of hip/knee flexion/extension module	125
4.2.2.1	Thigh and calf cuffs	128
4.3	Hip module	131
4.3.1	Hip abduction/adduction and intra/extrarotation module . .	132
4.3.1.1	ACHM requirements	132
4.3.1.2	ACHM design	133
4.4	Modules integration and future works	136
5	Conclusions	139
A	Selection of spring stiffness for SEA	143
	List of Publications	147
	Bibliography	151



List of Tables

3.1	SEA 90W requirements.	44
3.2	SEA 90W torsional spring requirements.	53
3.3	Definition of the search space for the optimization problem of topology 3.	59
3.4	Parameters defining the best morphologies produced by the optimization, for each of the three considered topologies.	60
3.5	SEA 90W torsional spring properties.	65
3.6	SEA 300W requirements.	75
3.7	SEA 300W springs pack requirements.	81
3.8	SEA 300W torsional spring requirements.	82
3.9	SEA 300W torsional springs and springs pack properties.	89
3.10	pVEJ requirements.	95
3.11	pVEJ springs main characteristics.	103
3.12	Results for Constant, Linear and Quadratic torsional Stiffness Characteristics.	103
4.1	Number of topologies generated and filtered for HR-isomorphism and for HR-degeneracy for the case of hip and knee orthosis.	120
4.2	Requirements for range of motion, peak torque and peak power of ACHM133	



List of Figures

2.1	Block scheme of conventional design for wearable robots	7
2.2	First examples of exoskeleton-like robots	8
2.3	DARPA program exoskeletons	9
2.4	Exoskeleton for human performances augmentation	14
2.5	Mobile medical exoskeletons	18
2.6	Treadmill-based exoskeletons	26
2.7	Hybrid solutions for wearable robots	30
2.8	Emerging behaviours and low-level adaptations to the environment	32
2.9	Block scheme of evolutionary design approach for wearable robots	35
2.10	Examples of wearable robots exploiting embodied intelligence	37
3.1	Torque control scheme for a rotary SEA	41
3.2	SEA 90W prototype	45
3.3	Block scheme of SEA 90W.	46
3.4	Cross section of rotary SEA 90W	47
3.5	Compliant components for rotary SEA prototypes	49
3.6	Schematic representation of springs possible arrangements	52
3.7	Flowchart of the spring design methodology	54
3.8	Three analyzed springs topologies	55
3.9	Sketch of an arbitrary morphology based on topology 3	57
3.10	Specific energy for the three investigated topologies	58
3.11	Frontal view of the custom made torsional spring	58
3.12	Boundary conditions and swept mesh for spring FEM simulations	61




3.13	von Mises stress and deformation from FEM simulations	62
3.14	Custom dynamometric test-bed	63
3.15	Experimental data from the characterization of the torsional spring under different loads	64
3.16	Series and parallel springs arrangements	67
3.17	SEA torque control scheme	68
3.18	SEA 90W position tracking for a typical knee profile during overground walking	69
3.19	Response of the system to torque step commands (amplitude 3 N·m and 10 N·m, with blocked actuator output.	69
3.20	Steady-state response of the system to a torque reference sinusoid	70
3.21	Knee orthosis concept	71
3.22	Cross section of the second version of SEA 90W	73
3.23	SEA 300W prototype	75
3.24	Block scheme of SEA 300W.	76
3.25	Sensorization block scheme of SEA 300W	77
3.26	3D CAD view of rotary SEA 300W	78
3.27	Springs pack: serial configuration of two equal torsional springs	80
3.28	Custom torsional springs for SEA300W	83
3.29	Boundary conditions and swept mesh for spring FEM simulations	84
3.30	von Mises stress and deformation from FEM simulations	85
3.31	Custom dynamometric test-bed for the characterization of SEA 300W spring	86
3.32	Experimental data from the characterization of the torsional springs of SEA 300W under different loads	87
3.33	Second version of the springs pack	91
3.34	3D CAD view of the second version of SEA 300W	92
3.35	Schematic representation of pVEJ torsional spring module	96
3.36	Cam profiles for constant, linear and quadratic torsional stiffness characteristics	98
3.37	Schematic representation of pVEJ torsional damping module	99



3.38	pVEJ exploded view	101
3.39	3D CAD and picture of pVEJ stiffness module	102
3.40	Constant, linear and quadratic cam profiles	104
3.41	Cam discs with constant, linear and quadratic stiffness-angle characteristics	104
3.42	3D CAD and picture of pVEJ damping module	106
3.43	Custom dynamometric test-bed for pVEJ characterization	107
3.44	pVEJ torque vs. angle profiles	108
3.45	Torques vs. angular velocities for the damping module	109
4.1	Overview of the design methodology	115
4.2	Schematic of a wearable robot attached to the planar model of a lower limb	118
4.3	Atlas of topologies with 4 robot links, 2 DOFs, for the design of a planar orthosis assisting the hip and the knee flexion/extension.	121
4.4	Structural representations of morphologies with 4 robot links, 2 DOFs, for the design of a planar orthosis assisting the hip and the knee flexion/extension	122
4.5	Selected morphology for the hip/knee flexion/extension module	126
4.6	3D CAD of hip/knee flexion/extension module	127
4.7	Thigh and calf cuffs	129
4.8	FEM analysis of the C-shaped inserts of thigh and calf cuffs	130
4.9	Three views of ACHM module 3D CAD	134
4.10	Serial mechanism of ACHM module	135
4.11	Four views of the rendering of the lower limbs WR concept	137
A.1	Minimal model and block diagram for a Series Elastic Actuator	144



Tesi di dottorato in Ingegneria Biomedica, di Giorgio Carpino,
discussa presso l'Università Campus Bio-Medico di Roma in data 20/03/2012.
La disseminazione e la riproduzione di questo documento sono consentite per scopi di didattica e ricerca,
a condizione che ne venga citata la fonte

A handwritten signature in black ink, appearing to read "Giorgio Carpino". The signature is fluid and cursive, with the first name "Giorgio" and the last name "Carpino" clearly distinguishable.

List of Acronyms

AAN	Assistance As Needed
ACAM	Actively Controlled Ankle Module
ACHM	Actively Controlled Hip Module
AFO	Ankle Foot Orthosis
ALEX	Active Leg EXoskeleton
BLEEX	Berkeley Lower Extremity Exoskeleton
BWS	Body Weight Support
CPG	Central Pattern Generator
DARPA	Defense Advanced Research Projects Agency
DOF	Degree Of Freedom
ECCG	ElectroCardioGram
EHPA	Exoskeletons for Human Performance Augmentation
EXPOS	EXoskeleton for Patients and the Old by Sogang
FDA	Food and Drug Administration
FEM	Finite Element Method
HB	Human Body



HULC	Human Universal Load Carrier
ICR	Istantaneous Centre of Rotation
IHMC	Institute for Human and Machine Cognition
LFB	Large Force Bandwidth
LOPES	LOWer-extremity Powered ExoSkeleton
PAM	Pelvic Assist Manipulator
PD	Proportional-Derivative
pHRI	physical Human-Robot Interaction
POGO	Pneumatically Operated Gait Orthosis
PSO	Particle Swarm Optimization
pVEJ	passive ViscoElastic Joint
ROM	Range Of Motion
SF	Safety Factor
SCI	Spinal Cord Injured
SEA	Series Elastic Actuator
SUBAR	Sogang Universitys Biomedical Assistive Robot
SVEA	Series ViscoElastic Actuator
VIA	Variable Impedance Actuators
VIJ	Variable Impedance Joints
WPAL	Wearable Power-Assist Locomotor
WR	Wearable Robot
WWH	Wearable Walking Helper
ZMP	Zero Moment Point




Chapter 1

Introduction

Wearable robotics represents a challenging research topic in current robotics. In the design of robots intended to strictly interact with humans the classic paradigm applied to traditional industrial robots “rigidity by design, safety by sensors and control”, more suited for conventional industrial robotics, to the “safety by design, performance by control” philosophy [1].

Physical human-robot interaction (pHRI) represents one of the most motivating, challenging, and ambitious research topic in this area. Many of the future and emerging applications of robotics, be they in service, assistance and care, rehabilitation, or in more traditional working contexts, will indeed require robots to work in direct contact with humans. Tasks unifying the workspace of humans and robots will require safe and dependable robot design and control. The novel additional optimality criteria for pHRI lead to redesign robots starting from the mechanics.

In robots interacting with humans for assistive or rehabilitation purposes, traditional stiff and high-precision actuators have been replaced by systems with intrinsic compliance, in order to improve the level of adaptability and safety. The development of robots that can establish dynamic interactions with the human body thus requires the use of joints and actuators whose mechanical impedance can be tuned. The tuning of the mechanical impedance allows improving the dynamical performances of a joint, similarly to the variation of human joints stiffness, which is usefully exploited to perform different tasks.



The possibility of tuning the dynamical properties of the robotic systems is even more crucial in the design of wearable robots in strict contact with the human body in order to give rise to useful emerging dynamical behaviours from the symbiotic interaction between the wearable robot and the human body. Compliant elements, if properly exploited, can lower actuation requirements thanks to effective energy bouncing between the wearable robot and human body. This kind of dynamic interaction may be exploited, for instance, in order to produce emerging dynamical behaviors (e.g. stable limit cycles resembling to physiological movements) without the need of forcing the assisted limbs to follow a specified pattern. As a corollary of this approach, the robot becomes intrinsically capable of offering assistance as needed, with an expectedly safer pHRI, as required in assistive or rehabilitation scenarios.

1.1 Thesis overview

This thesis is focused on the application of the above-mentioned general paradigms to the scenario of lower limbs wearable robots for human gait assistance. The thesis is organized as follows.

Chapter 1 gives a brief introduction to the background and motivation of the thesis. It also includes the main aspects covered in the different chapters.

Chapter 2 provides a critical analysis of the state of the art of mechatronic devices for gait assistance based on different design methodologies. On the basis of such analysis, the objectives of this thesis are defined.

Chapter 3 describes the main original contribution of this thesis: the design, development and characterization of innovative solutions for mechatronic active and passive joints for wearable robots integrating novel compact compliant components to enhance a safer physical Human-Robot Interaction. Two Series Elastic Actuator (i.e. SEA 90W and SEA 300W), each integrating compact custom torsional springs, and a passive viscoelastic joint (i.e. pVEJ), able to render a non linear torque vs. angle and tunable torque vs. angular velocity profiles, have been developed. The possible implementation of SEA 90W as actuation system for a knee orthosis for gait assistance is shown.



Chapter 4 describes the integration of SEA 300W in a wearable robot for lower limbs. The design of the robot is based on a methodology which allows to generalize and to solve in a complete and computationally efficient way the problem of kinematic synthesis of a non anthropomorphic wearable robot for gait assistance. The candidate contribution is focused on the hardware implementation of the optimal morphological solution related to the chosen wearable robot topology. The wearable robot includes two modules: one for the actuation of the hip/knee flexion/extension in the sagittal plane and one for the actuation of the hip degrees of freedom outside the sagittal plane. The integration of the modules and the concept of the complete wearable robot are finally reported.

Chapter 5 gives concluding remarks and outlines future avenues of investigation.



Tesi di dottorato in Ingegneria Biomedica, di Giorgio Carpino,
discussa presso l'Università Campus Bio-Medico di Roma in data 20/03/2012.
La disseminazione e la riproduzione di questo documento sono consentite per scopi di didattica e ricerca,
a condizione che ne venga citata la fonte

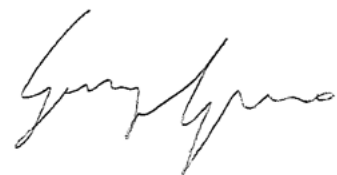
A handwritten signature in black ink, appearing to read "Giorgio Carpino". The signature is fluid and cursive, with the first name "Giorgio" and the last name "Carpino" clearly distinguishable.

Chapter 2

State of the art and design methodologies for lower limbs wearable robots

2.1 Wearable robots and pHRI

Wearable robots (WRs) are robots worn by human operators, whether to supplement the function of a limb or to replace it completely. Wearable robots may operate alongside human limbs, as in the case of orthotic robots or exoskeletons, or they may substitute for missing limbs, for instance following an amputation. Wearability does not necessarily imply that the robot is ambulatory, portable or autonomous [2]. A wearable robot can be seen as a technology that extends, complements, substitutes or enhances human function and capability or empowers or replaces (a part of) the human limb where it is worn. The exoskeleton is a species of wearable robot. The definition of exoskeleton has been given by [3] as an active mechanical device that is essentially anthropomorphic in nature, is worn by an operator and fits closely to his or her body, and works in concert with the operators movements. Robot kinematic chain is not a free design parameter for robotic exoskeletons, while wearable robots can be designed to have a possibly non-anthropomorphic kinematic structure also according to the classification introduced in [4].



The purpose of such devices is to enhance the strength or performance of the person that wears it, where performance can be speed or coordination or some other desired attributes. Potential uses of a wearable robot are in rehabilitation, training, strength augmentation or simply as an assistance device for normal daily living.

The strict cooperation between WR and human body (HB) poses the accent on the safety of this connection. The close physical interaction through this interface imposes strict requirements on wearable robots as regards safety and dependability. In this scenario, the physical human-robot interaction (pHRI) is explicit embedded by the flow of power between the human and the robot. pHRI represents the most critical form of interaction between humans and machines. The design of the robot structure, sensors, actuators and control architecture need to be considered all together, from the specific point of view of interaction with humans. In this framework the WR design goals should be:

- *safety*, the WR should avoid unnatural or arbitrary movements, for instance excessive excursions that could hyperextend or hyperflex human joints;
- *actuator performance*, in order to comply with the specific application requirements;
- *ergonomics and comfort*, as ability to adapt to the specific needs and ergonomic particularities of humans [5]. The WR and the human joints must be exactly aligned for proper operation. Misalignment of joints could generate interaction forces and may produce pressure sores on the skin of the wearer. Moreover, the robots operational workspace should be compatible with the human limbs workspace;
- *transfer of power* from WR to the soft tissues of the HB with the question of the intensity, the mode and the areas on the human body where it is possible to apply loads.
- *enhancing the adaptation of two dynamic control systems*, i.e. human motor control and robot control, to each other;



- *reducing the WR size and weight* as minimum as possible and stress the ease of use for the tester.

2.2 Wearable robots for the lower limbs: conventional design approach

The conventional design approach adopted for WRs follows the scheme depicted in Fig. 2.1 where the optimization phase closes the design loop composed by the cascade of mechanical design, dynamical modeling and control design.

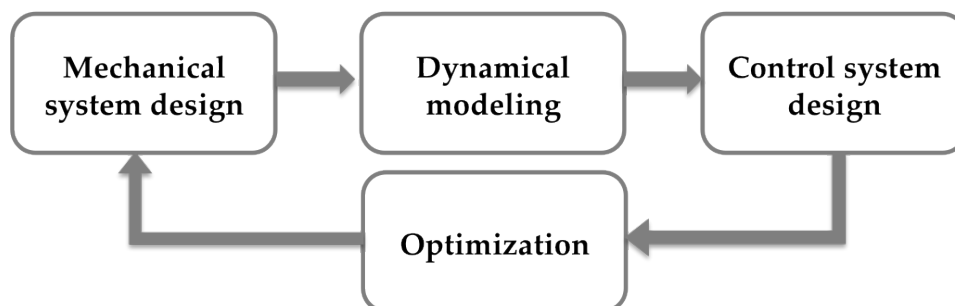


Figure 2.1: Block scheme of conventional design for wearable robots.

In the following the objective is to analyze and give a classification of the lower limbs WRs at the state of the art. During the last five years several review papers and books on wearable robotics have been published [2, 3, 6, 7, 8, 9, 10, 11, 12]. This proves the high interest of the scientific community in this research area. The following dissertation is inspired by the above mentioned papers. Only wearable robots acting on lower limbs and actuating more than one human joints have been considered. The lower limbs wearable robots have been divided in three main categories: *stand-alone* devices, *treadmill-based* devices and *hybrid solutions* for WRs.

The earliest mention of a device resembling an exoskeleton is described by Yagn [13] in the U.S. Patents granted in 1890. This concept, shown in Fig. 2.2-a consisted of long bow /leaf springs operating in parallel to the legs and was intended to augment human running and jumping capabilities. Each leg spring was engaged

during the stance phase of the gait so to compress the spring and was disengaged during the swing phase in order to release the elastic energy to the human leg. This was only a concept and no prototype was built.

Many years later, General Electric Co. developed the concept of human-amplifiers through the *Hardiman* project from 1966 to 1971. The Hardiman robot, in Fig. 2.2-b, was more of a robotic masterslave configuration than a real wearable robot configuration.

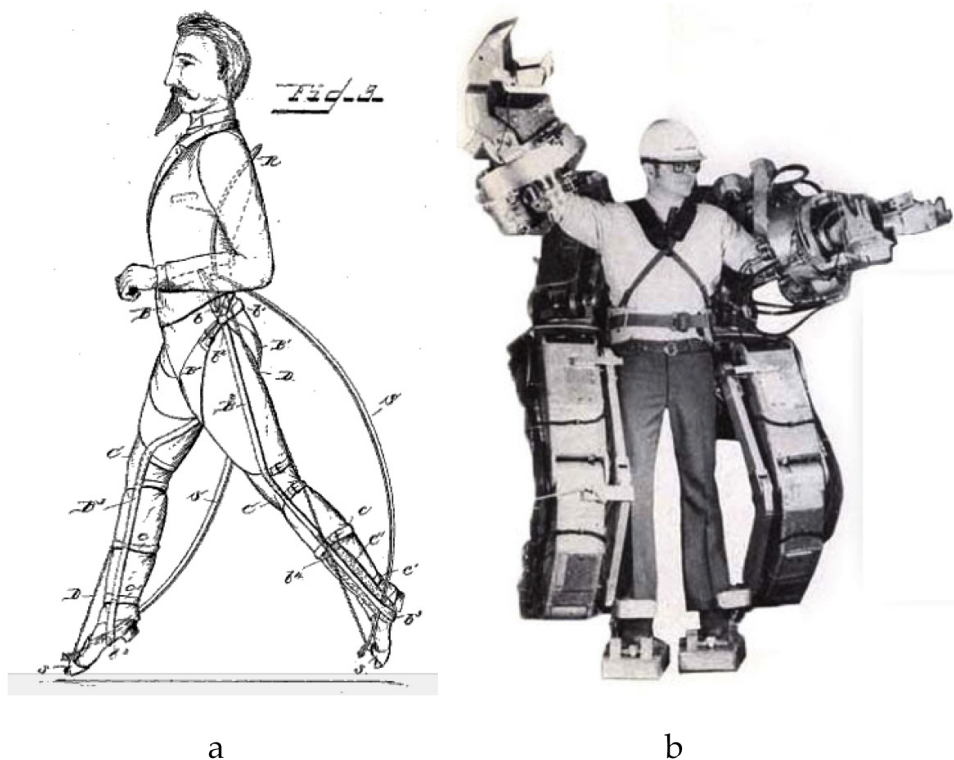


Figure 2.2: First examples of exoskeleton-like robots. (a) Yawn concept, (b) Hardiman extender by General Electric Co.

2.2.1 "Stand-alone" WRs

The "stand-alone" WRs can in turn be divided in two subcategories: the *human performance augmentation* and the *mobile medical devices*.

2.2.1.1 Human performance augmentation WRs

A big jump forward in the design of wearable robots has been registered after the program promoted by the US Defense Advanced Research Projects Agency (DARPA), called Exoskeletons for Human Performance Augmentation (EHPA) started in 2001, in order to encourage the development of exoskeletons helping soldiers to carry backpack during military missions and to reduce the soldiers fatigue during this task. This type of leg exoskeleton could benefit people who carry load by increasing their load capacity, lessening the possibility of leg or back injury, improving metabolic locomotory economy, and/or reducing the perceived level of difficulty. These exoskeletons are thus for human capabilities augmentation and three of them were reported in literature as working prototypes: the *Berkeley exoskeleton*, the *Sarcos exoskeleton* and the *MIT exoskeleton*, shown in Fig. 2.3.

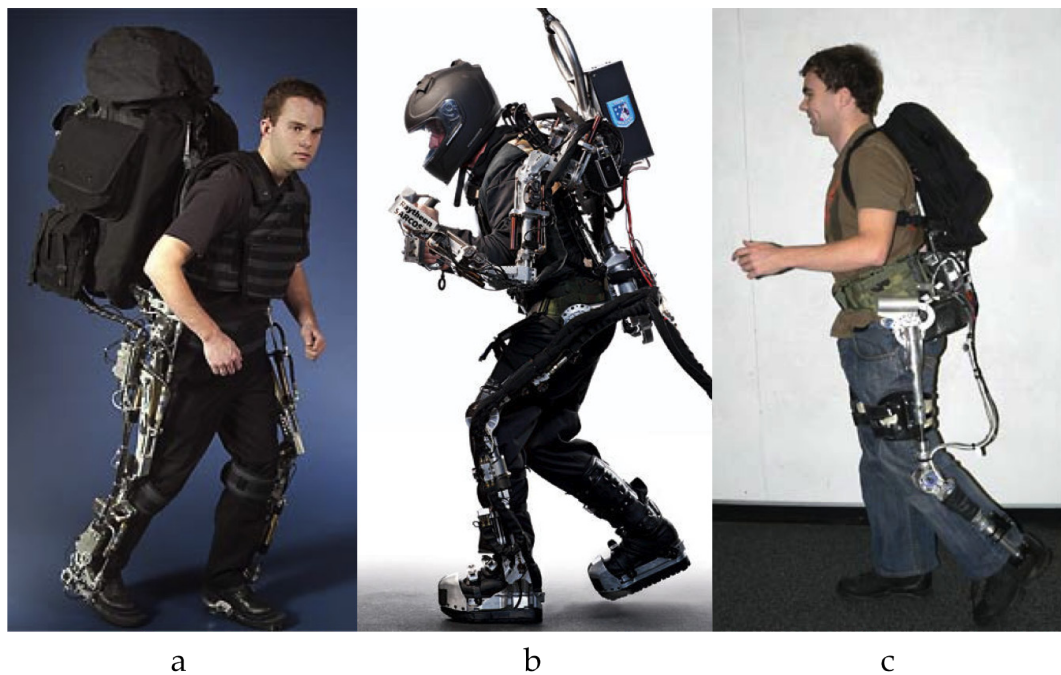


Figure 2.3: DARPA program exoskeletons. (a) BLEEX, (b) Sarcos, (c) MIT exos.

The **Berkeley Lower Extremity Exoskeleton (BLEEX)** has been developed by Professor Kazerooni and his group at the University of California [14] (Fig. 2.3-a).

A handwritten signature in black ink, which appears to read 'Giorgio Carpino'.

It is energetically autonomous and carries its own power source. BLEEX features three degrees of freedom (DOFs) at the hip, one at the knee, and three at the ankle. Of these, four are actuated: hip flexion/extension, hip abduction/adduction, knee flexion/extension, and ankle flexion/extension. Of the non-actuated joints, the ankle inversion/eversion and hip rotation joints are spring-loaded, and the ankle rotation joint is completely free [15]. The kinematics and actuation requirements of the exoskeleton were designed by assuming behavior similar to that of a 75 kg human and utilizing clinical gait analysis data for walking [16].

The first version of the exoskeleton was actuated via bidirectional linear hydraulic cylinders consuming an average of 1143 W of hydraulic power during level-ground walking, as well as 200 W of electrical power for the electronics and control. In contrast, a similarly sized, 75 kg human consumes approximately 165 W of metabolic power during level-ground walking [15, 16]. A more recent version of the BLEEX has been actuated by electric motors significantly decreasing power consumption during level walking in comparison to hydraulic actuation [17]. The weight of the implementation of the electrically-actuated joint, however, was approximately twice that of their hydraulically-actuated joint (4.1 kg vs. 2.1 kg).

The control system utilizes the information from eight encoders and sixteen linear accelerometers to determine angle, angular velocity, and angular acceleration of each of the eight actuated joints, a foot switch, and load distribution sensor per foot to determine ground contact and force distribution between the feet during double stance, eight single-axis force sensors for use in force control of each of the actuators, and an inclinometer to determine the orientation of the backpack with respect to gravity [15].

In terms of performance, users wearing BLEEX can reportedly support a load of up to 75 kg while walking at $0.9 \text{ m}\cdot\text{s}^{-1}$, and can walk at speeds of up to $1.3 \text{ m}\cdot\text{s}^{-1}$ without the load.

After the first prototypal version of the system, the Berkeley Robotics & Human Engineering Laboratory worked on new versions of the device for military applications developing the *ExoHiker* and the *ExoClimber* systems, tailored for load carrying during overground walking or during slopes ascent. The third generation



of their exoskeletal system, the *Human Universal Load Carrier (HULC)* has reduced bulkiness and weight, since structural parts are titanium made. The system is now ready for commercialization for military applications. Interestingly, the HULC is claimed in the group webpage [11] to be the first system able to provide a reduction in the order of 5 to 15% of the metabolic cost associated to overground walking. Despite of these claims, no data published in peer-reviewed journals or conference proceedings demonstrating such reduction in metabolic cost could be retrieved.

Similar to the BLEEX project and the Berkeley Robotics & Human Engineering Laboratory exoskeletons, Sarcos (recently purchased by Raytheon) has developed an exoskeleton also based on hydraulics. However, their exoskeleton, the **Sarcos XOS**, has been designed to encompass the entire body as seen in Fig. 2.3-b. Similarly to the Berkeley exoskeleton, Sarcos has advanced a hydraulically actuated exoskeleton concept. However, instead of linear hydraulic actuators, the Sarcos exoskeleton employs rotary hydraulic actuators located directly on the powered joints of the device. The device can lift heavy loads with minimal effort exerted by the wearer, while maintaining the dexterity to allow the motions of continuously punching a boxing speed bag. This exoskeleton also relies on monitoring and measuring the actions of the wearer to process and derive its own assistive actions. The XOS robot includes 30 actuated DOFs and is controlled using a number of multi-axis force-moment transducers that are located between the feet, the hands and the torso of the operator and the machine. A force interaction between XOS and the wearer let this latter control smoothly the movements of the exoskeleton. At this stage, development of the device is undergoing and the goals planned by the company are as follow: walk at $5.6 \text{ km}\cdot\text{hr}^{-1}$ with a 68 kg load, run at $8 \text{ km}\cdot\text{hr}^{-1}$, walk up a 25% grade carrying a 45 kg load, and use less than 6.5 kg of fuel to travel 100 km on level ground [18]. However, this system is not without its drawbacks; the exoskeleton does not hug the human form as closely as some other exoskeletons. The arm control handles remove any functionality of the hands, forcing the wearer to rely on attachments to the ends of the arms to manipulate objects. However, the largest drawback to this device is its lack of a mobile power source. At this stage of



development, it relies on a separate power source that it is tethered to with cables. This is a very large issue when trying to implement a freestanding exoskeleton, and will require much development achieve independence in its activities. However, the company has planned to design a capable exoskeleton first, and then design the mobile power source to accommodate its specific predetermined needs. The development of the device continued as a military project and for these reasons many detailed technical information on the device were not published.

A quasi-passive exoskeleton, the **MIT exoskeleton** (Fig. 2.3-c), has been designed in the Biomechanics Group at the Massachusetts Institute of Technology Media Laboratory by the group of professor Hugh Herr. This concept seeks to exploit the passive dynamics of human walking in order to create lighter and more efficient exoskeleton devices with the aim of replicate in wearable robots the achievements obtained in the field of passive bipedal walkers [19], which demonstrated that a walking machine, whose mechanical structure is designed in order to optimize the exchange of elastic, gravitational and kinetic energy during the gait cycle, has an increased energetic efficiency when compared to conventional walking machine designed through a kinematically anthropomorphic design and controlled via zero moment point (ZMP) technique [20, 21]. The MIT exoskeleton employs a quasi-passive design that does not use any actuators for adding power at the joints. Instead, the design relies completely on the controlled release of energy stored in springs during the negative power phases of the walking gait [22]. The quasi-passive elements in the exoskeleton (springs and variable damper) were chosen based on an analysis of the kinetics and kinematics of human walking. The 3 DOF hip employs a spring-loaded joint in the flexion/extension direction that stores energy during extension that is released during flexion. The hip abduction/adduction direction is also spring-loaded, but only to counter the moment induced by the backpack load. Additionally, a cam mechanism was incorporated at the hip to compensate for the relative change in length between the thigh of the exoskeleton and the user due to the joint offset during abduction/adduction. Additionally, spring-loaded hip rotation and ankle rotation joints were included to allow non-sagittal



plane limb movements. The knee of the MIT exoskeleton consists of a magneto-rheological variable damper (motion in the flexion/extension direction) that is controlled to dissipate energy at appropriate levels throughout the gait cycle. For the ankle, separate springs for dorsiflexion/plantarflexion are implemented in order to capture the different behaviors during these two stages of motion, and store/release the optimum amount of energy. The ankle also features a carbon fiber plate that attaches to the boot and doubles as a subtalar joint inversion/eversion spring. Additionally, there is a carbon fiber spring under the heel that reduces impact losses and aids in lifting the heel at the beginning of the powered plantarflexion. Finally, an artificial elastic spine attaches to the backpack that allows for coronal and sagittal plane human spine movements. The quasi-passive exoskeleton is controlled simply by using sensory information provided by a set of full-bridge strain gages on the exoskeleton shin and a potentiometer on the knee joint. Without a payload, the exoskeleton weighs 11.7 kg and requires only 2 W of electrical power during loaded walking. This power is used mainly to control the variable damper at the knee. Experimental work with this quasi-passive exoskeleton demonstrated a working device that successfully supported a 36 kg load during walking at $1 \text{ m}\cdot\text{s}^{-1}$. It was also shown that the exoskeleton structure transferred on average 80% of the 36 kg payload weight to the ground during the single-support phase of walking. However, metabolic studies with the quasi-passive exoskeleton showed a 10% increase in walking metabolic cost of transport for a subject carrying the 36 kg load via the quasi-passive exoskeleton versus a standard laden backpack [22]. While this is an undesirable result, it is thought to be the first reported study on the metabolic cost associated with walking under the aid of an exoskeleton and, furthermore, no one has yet demonstrated an exoskeleton that reduces the metabolic cost of transport when compared to the load-carriage with a standard backpack. Further experimental work with the MIT quasi-passive exoskeleton showed a significant reduction in metabolic cost of walking versus the same exoskeleton without the springs at the hip and ankle and the variable damper at the knee, demonstrating the utility of the quasi-passive elements. Additionally, tests were conducted to determine the effect of the added mass and the inertial load of the exoskeleton on the wearer. From these



studies, it was concluded that, in addition to the added mass and inertia, a dominant cause for the observed cost of transport increase are the additional kinematic constraints inadvertently imposed on the wearer, upsetting the efficient dynamics normally seen during human walking [22].

In the area of human performances augmentations, other exoskeleton has been developed such as *HAL-5*, *NTU exos* and the *Kanagawa Institute of Technology exos* as shown in Fig. 2.4.

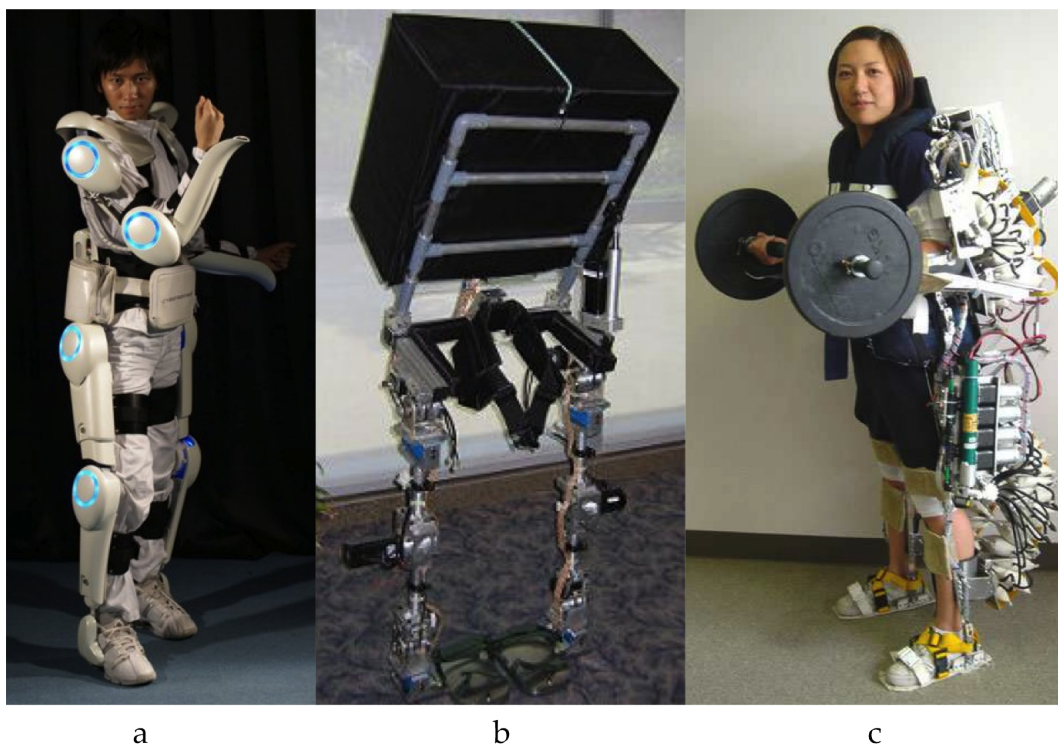


Figure 2.4: Exoskeleton for human performances augmentation. (a) HAL-5, (b) NTU exoskeleton, (c) Kanagawa Institute of Technology exoskeleton.

The group of professor Yoshiyuki Sankai at the University of Tsukuba in Japan has been developed an exoskeleton that is targeted for both performance-augmenting and rehabilitative purposes [23, 24]. The leg structure of the full-body **HAL-5** exoskeleton (Fig. 2.4 -a) powers the flexion/extension joints at the hip and knee via a

Giorgio Carpino

DC motor with harmonic drive placed directly on the joints. The ankle dorsi/plantar flexion DOF is passive. The lower limbs components interface with the wearer via a number of connections: a special shoe with ground reaction force sensors, cuffs on the calf and thigh, and a wide waist belt. The HAL-5 system utilizes a number of sensing modalities for control: skin-surface EMG electrodes placed below the hip and above the knee on both the anterior (front) and posterior (back) sides of the wearer's body, potentiometers for joints angles measurement, ground reaction force sensors, a gyroscope and accelerometer mounted on the backpack for torso posture estimation. Reportedly, it takes two months to optimally calibrate the exoskeleton for a specific user [25].

The first published control strategy for HAL is the "phase sequence algorithm" that was demonstrated for the stepping-up motion [26]. In this approach the stepping up movement is subdivided into five phases which are handled by a state-machine: leg raising, stepping up, leaning forward, hind leg raising, torso erection. Transition to the next state is performed when the joint angles and the center of gravity measured beneath both feet meet certain criteria. Each phase has an associated predefined trajectory for all actuated joints. An improved version of this control structure with an extended state machine incorporating standing up, sitting down and walking can be found in [27].

HAL-5 is currently commercialized by the spinoff company Cyberdine (Tsukuba, Japan). On the company website, it is declared that an operator wearing HAL can lift up to 40 kg more than they can manage unaided; additionally, the device increases the user's leg press capability from 100 to 180 kg. However, to date no peer-reviewed, quantitative results have been published highlighting the effectiveness of the exoskeleton's lower limbs components for the improvement of locomotory function.

The exoskeleton developed at the Nanyang Technological University, **NTU Exoskeleton** in Fig. 2.4-b, is designed for performance augmentation of healthy people, like soldiers or emergency personnel. It should allow the operator to carry heavy loads faster and over longer distances compared to normal conditions. In



contrast to more traditional exoskeletons, the NTU exoskeleton does not embrace the operator at the legs, except for some sensors to read current joint angles. Instead, it features two actuated legs which hold a payload frame, and the operator is standing only on the footplates of the exoskeleton. The exoskeleton is completely carrying itself and the payload, and is only guided by the operator. The idea of the control scheme is to follow the trajectory of the operators foot with its own footplate during the swing phase of each leg. This allows the operator to provide information about the desired velocity and stride length of gait. The required information is taken from the operators joint angles, and not from contact forces between the exoskeleton and the human. In theory, it should be hard to perform a target motion with the foot while being rigidly attached to the footplate of the exoskeleton that should follow the motion. Unfortunately, it is not mentioned in the publications how this problem is solved. The exoskeleton maintains balance during the motion by utilizing the ZMP technique [20, 21]: the controller moves the actuated joints in such a way that the ZMP remains within the support region. The support region is defined as the footprint, if only one foot touches the ground, otherwise it is defined as the convex area encompassing both footprints. Modification of the ZMP by the controller is performed by changing the angle of the exoskeleton "trunk", which is the payload frame. The target ZMP the controller tries to follow is the ZMP measured from the human body alone. The ground reaction forces for computation of the ZMP are measured with force sensors embedded in the feet of the exoskeleton [28, 29].

Researchers of the Kanagawa Institute of Technology have developed an exoskeleton, **Kanagawa Power Assisting Suit** shown in Fig. 2.4-c, for assisting nursing personnel when handling patients. The suit covers shoulders, arms, torso, waist and both legs, weighting a total of 30 kg. It supports the operator at the elbows, waist and knees with pneumatic actuators. The controller structure calculates the joint torques required to maintain a statically stable pose by computing the inverse of a rigid body model that takes into account the current joint angles and masses of the components of the exoskeleton and the weight of the patient. The weight of



the patient is measured beforehand. The operators own muscle force is recorded by muscle hardness sensors which consist of mini-load cells with contact plates taped to the skin sitting on top of the muscle bellies, and will probably be integrated into the control in later versions. Interaction with the exoskeleton is based on the fact that the torques imposed by the operator on the joints of the exoskeleton overlay with the torques produced by the actuators. Arbitrary movement patterns are possible, although not necessarily intuitively at first: depending on the accuracy of the inverse calculation and the effects of the omitted dynamics of the system, necessary muscle activations to move in concert with the exoskeleton and the load can be very different from the intuitive activation patterns. Handling the patient with the exoskeleton may require some training.

2.2.1.2 Mobile medical WRs

The second family of stand-alone WRs has been represented by rehabilitation and assistive robots called *mobile medical exoskeletons*. They act both for assistive and/or rehabilitative purposes. Different from the performance-augmenting exoskeletons which are used by healthy human, this kind of device is designed for person with gait disability. Also compared to rehabilitation robots where usually exists a body weight support system to keep balance and help to support body weight, the mobile medical exoskeletons requires the patient to balance themselves which means the patient must have a healthy upper body. The mobile medical exoskeleton should provide enough external joint moment to compensate the lack of force in the lower body joints and also body weight support to minimize the weight loaded on these joints. So a good human robot physical interfacing design is very important.

Improving the quality of life of wheelchair users is the aim of a three-year project entitled Exoskeleton Orthotic Systems for Individuals with Mobility Disorder, which is being conducted by Ekso Bionics with financial support from NISTs (National Institute of Standards and Technology) Advanced Technology Programme. In this framework, the more recent device is the **Ekso** designed and commercialized






Figure 2.5: Mobile medical exoskeletons for rehabilitative and assistive purposes. (a) Ekso, (b) ReWalk, (c) REX, (d) MINA, (e) Vanderbilt powered orthosis, (f) Wearable Walking Helper.

Giorgio Carpino

by the Ekso Bionics (Berkeley, CA, US), see Fig. 2.5-a. This device is a second version of the exoskeleton *eLegs* developed by the same company (the company has recently changed its name from Berkeley Bionics to Ekso Bionics). The robot is intended for people with lower extremity weakness or paralysis due to neurological disease or injury (spinal cord injuries, multiple sclerosis, Guillain Barr syndrome). The system requires from the user a sufficient upper extremity strength to balance with crutches or walker and the ability to self-transfer from wheelchair to a regular chair. Battery pack is attached to the back of the system and the battery life is declared to be four hours [30].

Data retrieved from literature are based on the first prototype (*eLegs*) of this exoskeleton that seems to be very similar to the Ekso device. Its architecture is almost anthropomorphic and it has four actuated DOFs, which minimize the complexity and weight of the machine while still providing the functionality needed. The hip and knee joints are actuated in the sagittal plane (the main direction of the walking motion). The range of motion (ROM) of these joints is comparable to that of a healthy individual. The other DOFs at those joints are locked out or are passive, supported with a spring. The ankle joints are not actuated but are highly sprung in the sagittal plane and locked out in the other DOFs. This minimizes weight and complexity while still allowing the necessary flexibility for sitting down and standing up with the feet flat on the ground. These DOFs allow for the exoskeleton to sit, walk, and stand while minimizing uncontrolled robot DOFs [31, 32].

Testing of the device was performed on four paraplegic patients with complete or incomplete paralysis [33] and on three chronic stroke patients [32]. The testing with paraplegic subjects was performed on three patients with incomplete paralysis and one with complete paralysis [33]. A state machine was implemented with a position control, which tracks a trajectory set whose profile is derived from Clinical Gait Analysis data, and adapted to guarantee a safer clearance from ground during the swing phase, and parametrized in terms of step length and step speed, which could be adjusted according to the subject's and the therapist feeling. During the stance phase, the hip is driven through a zero-impedance controller, which avoids problems of torso rotation which arise due to the lack of vertical support for the



torso link, which is not fixed to a rigid frame as in the case of treadmill-based machines. During stance phase, the momentum of the body, whose center of mass is moving forward, is sufficient to provide motion to the hip during the stance phase.

Founded in 2001 and originally operating under the auspices of the Technion-Seed (Technion, Institute of Technology, Israel), Argo Medical Technologies has developed a robotic ambulation system for wheelchair users named **ReWalk** (see Fig. 2.5-b).

ReWalk is a wearable robotic device which helps the paralyzed people to walk. It is actuated by DC motors at hip and knee joint only in the sagittal plane. The ankle joint is not actuated. Battery and controllers are attached at the back of the user. The system is designed with a remote controller which can be used to change the motion mode of the system such as ground walking or climbing stairs. There is a posture detection sensor at the torso to detect the upper body movement of the user and the information is used estimate the users' walking intention and drive ReWalk accordingly. Upper-body motions are analyzed through apposite algorithms and used to trigger and maintain gait patterns and other operations such as climbing stairs and shifting from sitting to standing, leaving the hands free for self-support or other tasks. While ReWalk has been demonstrated climbing stairs, neither device has been demonstrated on rough or irregular terrain. The wearer also has to use crutches for stability and safety reasons.

No technological detail of the system has ever been published in the scientific literature; however since 2008 the system has gone through the stages of final engineering and is currently in the process of undergoing the first clinical trials at MossRehab (Philadelphia, PA, USA). Pilot clinical trials are also presently starting in Italy, in particular at the Centro Protesi INAIL di Vigorso di Budrio (Bologna, Italy) on 18 paraplegic subjects.

The device is now available on the market in two version: *ReWalk-I* for institutional use that allows institutions to use it as a multi-user rehabilitation and training solution (it is supplied in two sizes to accommodate users height from about



1.60m to 1.90m) and *ReWalk-P* for personal use intended for a daily use by qualified paraplegics, i.e. after medical examination and successful completion of a training program in a rehabilitation center.

Different from *eLegs* and *ReWalk*, **REX**, produced by REX Bionics (Auckland, New Zealand), is an anthropomorphic lower body orthosis designed for sit-to-stand, stair ascend and overground walking, without the use of crutches (see Fig. 2.5-c). The system does not use sensor to sense the intention of the user but uses joystick for the user to control the exoskeleton. Users should have a height comprised from 1.46 m to 1.95 m, with a weight less than 100 kg and a hip width of maximum 380 mm. The system has been demonstrated with healthy subjects, and for sit-to-stand of wheelchair users. It is currently being sold in New Zealand for 150,000 \$.

Mina [34], Fig. 2.5-d, is a second generation of lower extremity robotic gait orthosis designed and built by researchers at the Institute for Human and Machine Cognition (IHMC), already developer of the IHMC mobility assist exoskeleton [35]. It has two actuated DOFs per leg, hip and knee flexion/extension, for a total of four identical actuators. The actuators are capable of performing both position control and torque control. Each actuator consists of a DC brushless motor (Moog BN34-25EU-02) and a 160:1 Harmonic Drive (SHD-20) gear reduction. The actuators are instrumented with two incremental encoders. *Mina* does not provide any hip abduction/adduction or intra/extrarotation of the leg. The torso section of *Mina* consists of a rigid back plate which has a curvature to match that of the human spine. *Mina* is designed to accommodate a range of body sizes. By using nested aluminum tubing as the structural links, adjustments are made to fit the user. *Mina* attaches to the user at the torso and at three places on each leg: thigh, shank, and foot. At the torso, there are two shoulder straps and a pelvis strap which secure the users torso to the rigid back plate. *Mina* has been tested on two paraplegic evaluators and is capable of providing mobility for paraplegic users on flat ground at slow walking speed, while it is not yet capable of being used to enhance a persons quality of life in real world settings. The users required some amount of training and practice, and



that more training and practice was required for paraplegic users than able-bodied users.


Vanderbilt powered orthosis [36] is a powered lower-limb orthosis that is intended to provide gait assistance to spinal cord injured (SCI) individuals by providing assistive torques in the sagittal plane at both hip and knee joints (see Fig. 2.5-e). Respect to the other exoskeleton it neither includes a portion that is worn over the shoulders, nor a portion that is worn under the shoes. The orthosis has a mass of 12 kg and is capable of providing torques at hip and knee joint level with hip and knee joint ROMs from 105 deg flexion to 30 deg extension and 105 deg flexion to 10 deg hyperextension, respectively. Each joint is powered by a brushless DC motor through a 24:1 gear reduction, which provides each joint with a maximum continuous joint torque of 12 N·m, and shorter duration maximum torques of approximately 40 N·m. The orthosis is intended to be worn in conjunction with a standard ankle foot orthosis (AFO), which provides support at the ankle and prevents foot drop during swing. The structure of the orthosis is a composite of thermoplastic reinforced and supplemented with aluminum inserts. Sensors in the orthosis include potentiometers in both hip and knee joints, in addition to accelerometers located in each thigh link. A custom distributed embedded system controls the orthosis with power being provided by a lithium polymer battery which provides power for one hour of continuous walking. The orthosis controller consists of a state-flow system with four states, where each state is defined by a set of joint angle trajectories, which are enforced by high-gain proportional-derivative (PD) control loops. Joints angles trajectories were pre-programmed for each motion based on normal biomechanical walking trajectories, obtained from a recording of the joint angle trajectories generated by a healthy subject while wearing the orthosis. In order to demonstrate the ability of the orthosis to assist walking, the orthosis was experimentally tested on a paraplegic subject. Experimental results indicate that the orthosis is capable of providing a repeatable gait with knee and hip joint amplitudes that are similar to those observed during non-SCI walking. Electrical power measurements with the current battery pack and control algorithms indicate a battery life of approximately



a hour, and a corresponding walking range of approximately 0.8 km.

The **Wearable Walking Helper (WWH)**, shown in Fig. 2.5-f, is a prototype developed by the group of professor Kosuge at the Department of Bioengineering and Robotics of Tohoku University in Japan. It is a lower extremity exoskeleton, covering both legs. The hip and ankle joints are both actuated in the sagittal plane with a rotatory actuator in the hip joint, and a long linear actuator connecting the hip and ankle to actuate the knee joint. The goal of the WWH is to support the operator during walking and standing by compensating some of the body weight. The required support is calculated by an inverse model without taking into account joint angle accelerations [37]. Joint angles of the hip, knee and ankle are measured and fed into a planar model of the operator consisting of a four link open chain. Experiments performed with the exoskeleton [37] showed that it could add support to the knee extension task. This was tested by standing on one foot, and measuring the force acting on a sensor installed between the non-supporting foot and the floor while maximally activating the knee extensor muscles. A second experiment showed that it was possible to perform significantly more knee bends when the support was activated. The control method has been improved in [38], taking into account ground reaction forces with force sensors to support walking. The system was investigated with stepping up and down, and while walking on a treadmill. The strain was measured through the heartbeat of the subject, and was shown to be reduced. In [39] the system was enhanced with dynamic terms, and experiments included the sit-to-stand and stand-to-sit movements without taking into account external contact forces from the chair. The experiments showed a significant decrease in muscle activation revealed by EMG signals.

Other medical exoskeletons that deserve to be mentioned are: the *ABLE* [40] system, which allows people with disabled lower limbs to have a standing posture even on uneven ground, a standing up motion from a chair, and climbing the stairs, the *Soft-actuated 10 DOF lower body exoskeleton* [41] that consists in an pneumatically actuated exoskeleton for force augmentation and active assistive walking training,




and the *Wearable Power-Assist Locomotor (WPAL)* [42] developed and tested on paraplegic participants. Like the REX exoskeleton it does not need crutches for the user balance.

2.2.2 “Treadmill-based” wearable robots

The main role of this rehabilitation therapeutic robotic platforms is to support partially the patient weight on one side and to generate symmetrical and periodic gait patterns on the other side. A technique known as “partial body weight support” usually forms the basis for lower limbs neurorehabilitation. Although not necessarily robotic, it simplifies many aspects of introducing robot-mediated neurorehabilitation for the lower limbs. Partial body weight support usually requires that the patient wear a parachute-type harness that is connected to an overhead gantry and allows the therapy to happen with only a percentage of the persons true weight appearing as a force on the treadmill. Data collected in [43] showed that after six weeks of exposure to partial body weight support therapy four times a week, subjects after a stroke performed better in their ability to balance, in their motor recovery, in their ability to walk, and in their endurance of walking. The disadvantage of partial body weight support is that it requires greater involvement of the therapist, often requiring two to three therapists to assist with the movement of the feet. Since these are repetitive and physically demanding tasks for the therapists, it is an opportunity to introduce robotic-based solutions. The potential for valuable robotic assistance is further enhanced when considering the safety of the patient in a partial body weight support mechanism and the fact that an inexperienced therapist may be applying greater forces and giving fewer opportunities for the task to be completed unaided. The robotic system must be designed so that it can assist on an *assistance-as-needed (AAN)* basis, much like highly skilled physical therapists perform when teaching a SCI patient to relearn to walk. When exposed to a constant and invariant movement strategy, the neural control circuitry accommodates by becoming non-responsive to the imposed motion.

When compared to upper limb retraining, gait retraining has more repeatable cyclic operations which favors simpler control concepts. In contrast, the engineer-



ing of lower limbs rehabilitation devices needs to be more considerate of the dynamics of gait, and the forces applied to the legs and feet need to be larger, although this engineering problem is simplified by using the partial body weight support mechanisms. Unfortunately, these devices are very large and they require the patient to be stationary while conducting the therapy. The versatility of these devices is also limited to only walking straight forward. This is very beneficial, but there are many more motions that a person performs in everyday life that could be improved upon with the same proficiency as walking with these devices.

Lokomat developed by Hocoma (Volketswil, Switzerland), see Fig. 2.6-a, has been the first mechatronic body weight support (BWS) system developed to provide precise body weight unloading for patients with neurological or other impairments during treadmill training [44]. To maximize the therapeutic outcome of human gait rehabilitation, a passive elastic spring element has used to take over the unloading body weight. The novel mechatronic design provides an active BWS, instead of traditional fixed BWS. In addition, a robotic exoskeleton system support hip and knee movement in the sagittal plane, while the ankle joint is not support. The system provides continuous torques limited at hip of 50 N·m and at knee of 30 N·m. DC motor and ball screw mechanism are chosen to build a linear actuator to drive the exoskeleton leg [45]. Initially, patient training in Lokomat is performed with a fixed gait pattern as the robot followed the predefined joint angle trajectories. However, this method does not take into account of peculiarities of each patient. Considering the patients who have residue voluntary locomotion abilities, AAN approach was proposed which states that the robotic intervention needs to be specifically tailored to the requirements posed on each subject and minimized to only the situations in which the subject really requires it [46]. Gait pattern adaptation algorithms were implemented in Lokomat to realize the AAN approach [47]. One algorithm is based on inverse-dynamics and uses the estimation of the interaction forces to adapt the angle trajectories so to minimize them. Additionally, also an impedance control scheme, based on the direct measurement of the interaction forces at the human-robot interface is presented and demonstrated. The results show that the





Figure 2.6: Treadmill-based exoskeletons for rehabilitative purposes. (a) Lokomat, (b) LOPES, (c) AutoAmbulator, (d) ALEX, (e) PAM-POGO.

Giorgio Carpino

impedance controller is the one which allows the best and more comfortable degree of subject adaptability in the gait pattern.

LOPES (Lower-extremity Powered ExoSkeleton) is a treadmill based wearable robotic device for gait training and assessment of motor function in stroke patients [48], developed at University of Twente by the group led by prof. Herman van der Kooij. The exoskeleton is shown in Fig. 2.6-b. It is comprised of two parts: the adjustable lightweight frame for pelvic control actuating the two horizontal pelvis translations and the exoskeleton leg with four actuated DOFs per each leg which assist hip flexion/extension, adduction/abduction, knee flexion/extension and ankle dorsi/plantarflexion. To fixate a subject in LOPES three cuffs per leg are used, one around the upper leg, one around the lower leg and one just above the ankle joint. Each fixation consists of a carbon shell and velcro strap as in Lokomat system. To ensure comfortable fixation the shells are available in different sizes. The position of the fixation points relative to the exoskeleton can be adjusted in two directions allowing a proper alignment of the subjects knee joint with the exoskeleton knee joint. All other actuated DOFs are based on a series elastic element, consisting of a servomotor, a flexible Bowden cable transmission and a force feedback controller. Placing the springs in series with the Bowden cable at the joint end side of the cable creates the series elastic element, which allows direct measurement of the applied force by measuring spring length (or relative spring length) and thus automatically compensates for friction in the Bowden cables and servo motor inertia. The use of series elastic actuators implies that the actuators are used as force (and torque) sources and allow impedance control of the robot. Impedance control with this kind of setup can be used in both high impedance control (resembling position control) and zero impedance control. Position control is also referred to as “robot in charge”, whereas zero-impedance control can be seen as the “patient in charge” mode. The latter is of special importance when supportive forces are provided during specific aspects of the gait cycle while other parts of the gait cycle are unsupported. The development of the device started in 2001 and since then has been used with healthy subjects as a neuroscientific tool to investigate motor learning and more recently



with chronic stroke patients to validate the device as a tool for neurorehabilitation. Preliminary studies were presented to demonstrate the ability of this rehabilitation tool to restore an improved kinematic walking pattern (improved foot clearance during swing) after a period of robot aided gait training [49].

The **AutoAmbulator** is a commercial system patented [50] and developed by HealthSouth Corp. (AL, USA), shown in Fig. 2.6-c. The Food and Drug Administration (FDA) granted HealthSouth permission to begin using its own innovation in 2002. Though including a different mechanical design of the weight support subsystem which reduces the weight and overall dimensions of the device, allowing also for faster don and doff times compared to the Lokomat, but it essentially consists of an electrically actuated anthropomorphic device supporting hip and knee movements in the sagittal plane. The AutoAmbulator has already proven itself a valuable tool in the rehabilitation of numerous patients. Patients with multiple sclerosis, Parkinsons Disease, a stroke, a brain or spinal cord injury or other neurological disorders may all be candidates for rehabilitation using this exoskeleton. Unfortunately, few details on the uses of this system could be retrieved in the peer-reviewed literature.

In [51] a pure mechanical exoskeleton taking advantage from a dynamics-oriented mechanical design was developed in the University of Delaware. It aims to reduce the effect of gravity on the patient's leg through a mechanism added with spring which makes the system gravity-balanced in every configuration. The results showed that the current implementation of the device, while not affecting required torques at the knee, reduced the average torque required from the patient's hip by 61%. Based on this previous experience, a treadmill-based rehabilitation robot was developed by the same group called **ALEX (Active Leg EXoskeleton)** [52], shown in Fig. 2.6-d. The system are actuated the hip and knee joints in sagittal plane while hip abduction/adduction and ankle are spring loaded. A force field controller is applied into the system which can display the force field acting on the foot to represent the physiological foot trajectory during overground locomotion.



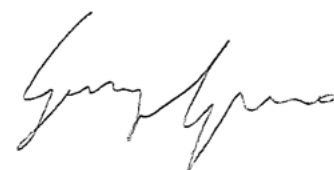
Test on an able body subject has been conducted in order to validate the goodness of the approach and tests on stroke patients are foreseen.

The **Pelvic Assist Manipulator (PAM)** and **Pneumatically Operated Gait Orthosis (POGO)** are pneumatic robots that compliantly assist in gait training, shown in Fig. 2.6-e. PAM can assist in 5 DOFs of pelvic motion, while POGO can assist the hip/knee flexion/extension [53]. The devices can be used in a back-drivable mode to record a desired stepping pattern that is manually specified by human trainers, then replay the pattern with compliant assistance. During compliant replay, the devices automatically synchronize the timing of the replayed motions to the inherent variations in the patients step timing, thereby maintaining an appropriate phase relationship with the patient. For spinal cord injuries the robot-assisted stepping assistance must occur bilaterally, whereas for strokes it is most likely to be needed unilaterally.

2.2.3 Hybrid solutions for wearable robots

A third class of wearable robots for assistance and rehabilitation of lower limbs can be envisaged where the capability of walking on the ground without the necessity of a treadmill and the portability of the system are combined. In this case a walker or a wheeled structure is coupled with a lower limbs orthosis in order to accommodate all the electronics, batteries and actuation units.

The first device, the **EXPOS (EXoskeleton for Patients and the Old by Sogang)**, has been developed by the researchers at Sogang University (Seoul, Korea) [54] and shown in Fig. 2.7-a. The device consists of a full lower limb orthosis paired with a specially designed walker (the *Smart Caster Walker*) that houses the battery, DC motors, and control computer, greatly reducing the weight of the worn structure. A cable drive transmits mechanical power to the joints of the wearer from the actuators in the walker. The orthosis actuates the hip/knee flexion/extension DOFs, and allows motion in the other DOFs of the leg, except the rotation of the ankle, which is fixed. User intent is sensed by a combination of joint angle sensors and a



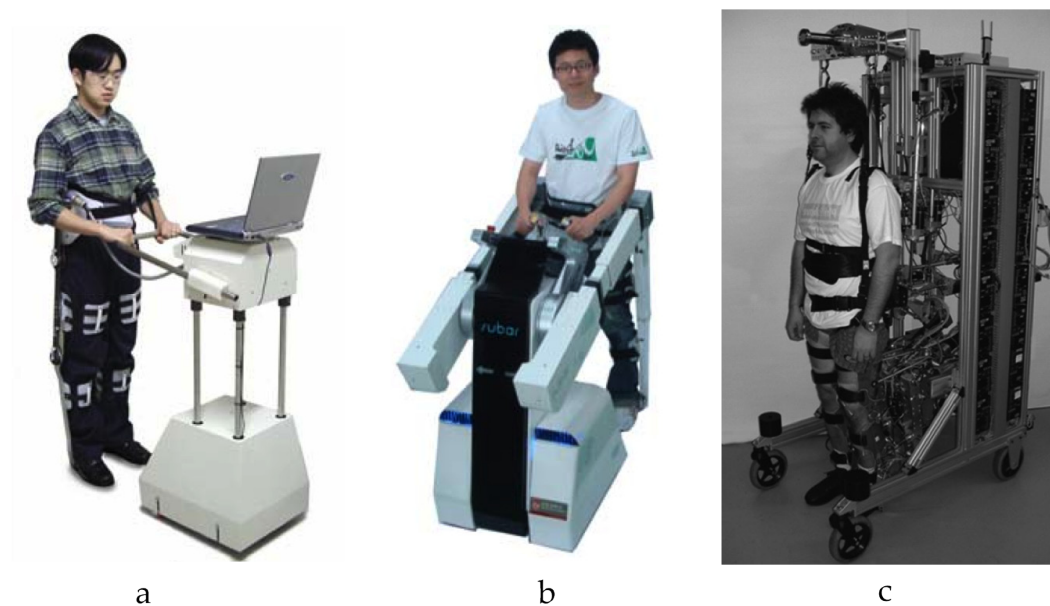


Figure 2.7: Hybrid solutions for wearable robots. (a) EXPOS, (b) SUBAR, (c) Walk-Trainer.

pressure sensor that gives a rough measure of force being applied by the quadriceps muscle. This design appears to exploit the consideration that most powered orthotic devices for physically impaired persons still require the use of crutches or other additional support methods, and finds a way to reduce the overall weight. Apparently, this system is limited to overground walking since both stairs ascending and sit-to-stand transitions are impeded by the demonstrated design. The same group has developed an advanced version of the robot named **SUBAR (Sogang University's Biomedical Assistive Robot)** [55] with an improved actuating power and a transmission mechanism for more effective assistance (Fig. 2.7-b).

The **WalkTrainer** [56], developed by the Laboratoire des Systemes Robotiques (LSRO) at the EPFL (Ecole Polytechnique Federale de Lausanne) under the Cyberthosis project funded by the "Fondation Suisse pour les Cyberthèses", is a rehabilitation device (see Fig. 2.7-c) enabling an active muscular participation of the subject in the walking reeducation process by the mean of closed-loop muscle stim-

ulation. The WalkTrainer is also equipped with a leg and pelvic orthosis, an active BWS, and motorized wheels to allow true over ground deambulation. From February to May 2008 six paraplegic subjects took part in the preliminary clinical trials with the WalkTrainer. This first short term preliminary clinical trial allowed to show the feasibility of getting paraplegic subjects to walk in the WalkTrainer. However, a reduction in spasticity was observed.

Other solutions of this family that deserve to be mentioned are: the *NaTUre-gaits* (*Natural and Tunable rehabilitation gait system*) [57] with the aim of improve walking capabilities of a subject in rehabilitation during overground training with pelvic control and active assistance to the lower limbs; the *KineAssist* [58] developed by the Northwestern University of Chicago (IL, USA) that allows the therapist to safely interact with and challenge a patient as they train in the whole body dynamic-balance tasks such as sit to stand or gait.

2.3 Structural intelligence-based design methodology for wearable robots

The objective is to go beyond the state of the art in the design of WRs for the lower limbs developing a novel design approach that can be used for active orthoses, prostheses and wearable robots for functional restoration or substitution, rehabilitation or human augmentation.

Robots described in the previous paragraphs have been designed around the human body, only complying with a set of detailed functional and technical specifications in order to obtain as safer as possible pHRI. Instead, the level of interaction between the WR and HB should be advantageously pushed ahead by designing the WR so that a *symbiotic interaction* occurs between it and the human body. The adjective “symbiotic” refers to the intimate physical interaction between the human body and the robotic artifact leading to *emergent dynamic behaviors* of the system comprised of “human body + robot”, as depicted in Fig. 2.8.

Designing for symbiosis is a kind of design for emergence aiming at producing



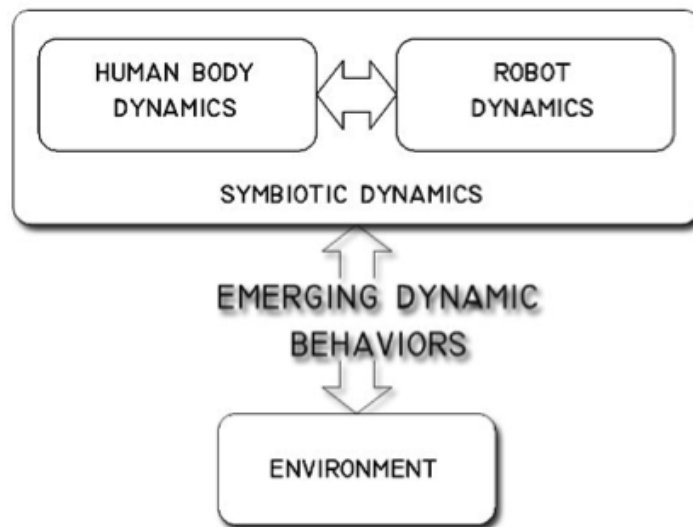


Figure 2.8: Emerging behaviours, arising from the coupled dynamics of human body and robotic structure interacting with the environment, help the performance of a complex task with lower computational efforts. Low-level adaptations to the environment are managed by the intrinsic properties of the mechanical structure of the WR (*preflexes*).

dynamic behaviors that are useful to a given purpose (e.g. restoring proper motor abilities in chronic subjects, of whom elderly people are the most socially relevant example). Since a WR interacts with the human body but also with the external environment, besides pursuing a design to achieve the emergence of useful dynamic behaviors, the mechanical structure of the WR is intended to intrinsically manage low level issues related to the interaction with the external environment by showing proper zero-delay, intrinsic responses (i.e. *preflexes*) to a perturbation [59]. The ability of a mechanical structure of producing useful emergent dynamic behaviors and of adapting itself to external perturbations through reflexes can be seen as whole as a form of **structural intelligence**, as an instantiation of *embodied intelligence*.

The concept of embodied intelligence highlights how intelligence benefits also from the physicality of an agent, where the term physicality is meant to catch as a whole the dynamic, kinematic and somesthetic properties of an organism and the typology of its possible interactions with the environment. Indeed, it is recognized

[60] that the embodiment of an agent has implications on the information theoretic processes (e.g. by effectively structuring the sensory inflow from the environment) and that morphology itself can perform computation through interactions of physical form (i.e. *morphological computation*). Robots designed to exploit embodied intelligence are frequently simpler, more robust and adaptive than those based on the classical control paradigm [61].

Over the past twenty years studies originally stemming out from the biological investigations on the locomotion of lower animal forms highlighted the intimate connections among intelligence, morphology and performance. As showed in [59], the lowest level of intelligence is actually completely physical, as it consists in the ability of neuro-musculoskeletal systems to present zero-delay, intrinsic responses to a perturbation [62]. Preflexes are useful for performing low-level tasks such as stabilization and feedforward locomotion control. As an example, the cockroach *Blaberus discoidalis* is able to scramble over randomly distributed obstacles up to three times its body height without significantly slowing down [63]. Such striking performance cannot be achieved by a feedback based, centralized sensory-motor control because of the required quick adaptation to the environment. On the contrary, robust locomotion is achieved mainly through a basic feedforward pattern applied to its properly tuned mechanical system. Such principles have been implemented in the development of a highly efficient hexapedal robot capable of sensorless robust locomotion at speeds up to 2.5 body lengths/sec [64].

On a higher level, recent studies on biped robots have shown that even complex tasks, such as walking, may arise from the intrinsic dynamics of a machine during its interaction with the environment. Studies on passive walking show that walking, normally obtained through computationally demanding algorithms requiring feedback from several sensors, can emerge from an accurate tuning of the dynamical properties of a purely mechanical system, without any feedback control [65, 66]. The performance obtained through this methodology produces a gait which appears to be more biomimetic under both the energetic and kinematic standpoints. In particular, it has been demonstrated that the energetic efficiency of such mechanisms resembles that of the human body, while existing bipedal walking robots are



about thirty times more energy demanding [19]. Moreover, experiments performed on physical simulation environments have shown that it is possible to optimize, via a coupled evolutionary process, both the morphological properties of a robot and its controller, with mutual benefits for both in terms of reduced complexity and enhanced efficiency [67].

The two examples mentioned above demonstrate that better performance, with lower computation cost and with simpler and lighter structures, can be achieved if the potentialities of structural intelligence are properly harvested and exploited. Till now, such concepts have been explored and applied to the development of robots inspired by a large variety of biological systems, such as mammals, fishes and insects. On the contrary, the human body has been poorly investigated from the structural intelligence standpoint, while this is a promising new route toward the development of useful machines intended for the strict interaction with humans, such as robots for rehabilitation, assistance and for the functional restoring for elderly and disabled people.

In the scenarios where the robot and the human body are strictly interacting, the design of the artificial system must take into account the dynamics of the biological counterpart, which is highly variable and actively tuned by the human sensory-motor system. When strict physical interaction occurs, the dynamics of the human body and that of the robotic artefact are strongly coupled. If the robotic artefact is meant to compensate for lost body functionalities, such as proper gait generation, the proposed approach consists in finding how the robotic system must be designed to take advantage of the variable biomechanical properties of the human body.

The objective is to design the robotic system in such a way that the dynamics of the human body, especially in the case of impaired or elderly subjects, and that of the robot during interaction, symbiotically benefit from each other, exhibiting emergent dynamic behaviours which favor the performance of the desired task. This can lead to a new generation of WRs helping HB, which are intrinsically better than those based on classical design and control paradigms.

The design approach differs from conventional methodology, in which a design is pursued that must comply with a set of detailed functional and technical



specifications defined a-priori, because it is based on **open-ended co-evolutionary approach** shaping both structure, sensory system and control. This process is performed in a simulation environment, in which the WR interacts constantly with HB, which is characterized by time-changing biomechanical properties and motor patterns, and with the external environment. The novel design approach follows the scheme depicted in Fig. 2.9 where the mechanical design stems out only after several optimization loops on robot kinematics, dynamics and control.

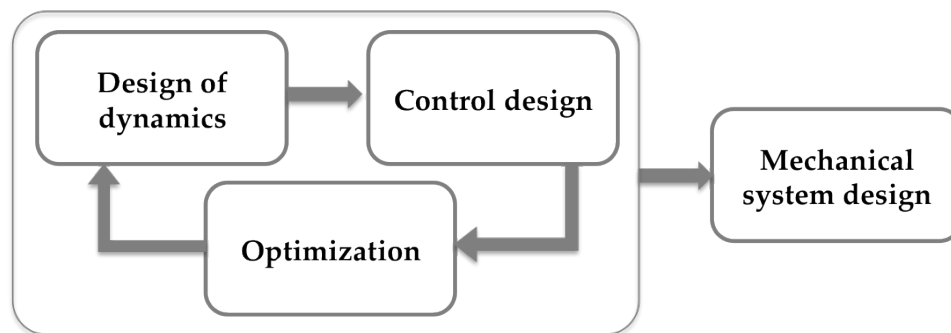


Figure 2.9: Block scheme of evolutionary design approach for wearable robots.

To achieve the highest level of structural intelligence, topology and morphology (i.e. number of links, types of joints, links length, etc.), the dynamic properties (joints stiffness and damping, inertial properties of links), sensors number and location and the control are *not defined a-priori*, as it usually happens when the design starts from application based specifications. On the contrary, all these aspects are left free to co-evolve, leading to robots with novel, possibly non anthropomorphic shapes and properties.

The chosen scenario to test the results coming from the novel evolutionary design approach is an active orthosis for the lower limbs, aimed at restoring proper walking in chronic subjects, such as aged people, because walking is a rather complex task suitable to be tackled by approaches taking advantages from structural intelligence.

In some systems developed in the last years the principles of structural intelligence can be glimpsed. In [68, 69, 70] **passive spring-based balancers** to sustain the

body weight during walking has been developed or modeled (see Fig. 2.10-a,b,c). In the development of the **MIT SkyWalker** [71] the inspiration to passive walkers is the basis to better exploit legs dynamics (see Fig. 2.10-d). Another example is the **Elastic exoskeleton** [72] developed at University of Michigan where leaf springs are used to provide intrinsic elastic properties to the structure and to optimize human-robot energy exchange during running. In **KNEXO** [73] (see Fig. 2.10-f) the principles of bioinspiration as a form of embodied intelligence has been exploited in the actuation system; the agonistic/antagonistic configuration of two pleated pneumatic artificial muscles has been adopted to actuate a knee orthosis for gait assistance.

2.4 Conclusions

The problem of assessing if, how and how much the findings achieved in the field of pseudo-passive bipedal walking can be transferred to the field of wearable robots for the lower limbs consists of a very tough challenge. Despite of that, the literature suggests that possible improvements of the performances of WRs can be provided by “opening” the design of the mechanical subcomponent, and not just focusing on novel control schemes or aspects related to actuators power efficiency or intrinsic safety.

These considerations suggest that wearable robots performances can benefit from a careful design of robot morphology, which is open in the case of non anthropomorphic WRs, and can allow to achieve a better dynamical interaction with the human body and with the environment.

The objective of this thesis is to develop concepts of WRs based on the principles of structural intelligence through a novel design methodology for WRs. This can be achieved through the design of novel compact compliant components to be implemented in the active and passive joints of WR to enhance a safer physical Human-Robot Interaction (pHRI). The novel design methodology can furthermore be employed in fore-coming research in order to answer to the scientific problem of quantifying which advantages to dynamical or ergonomics aspects can be introduced by an open-ended concurrent design of morphology in wearable robots.



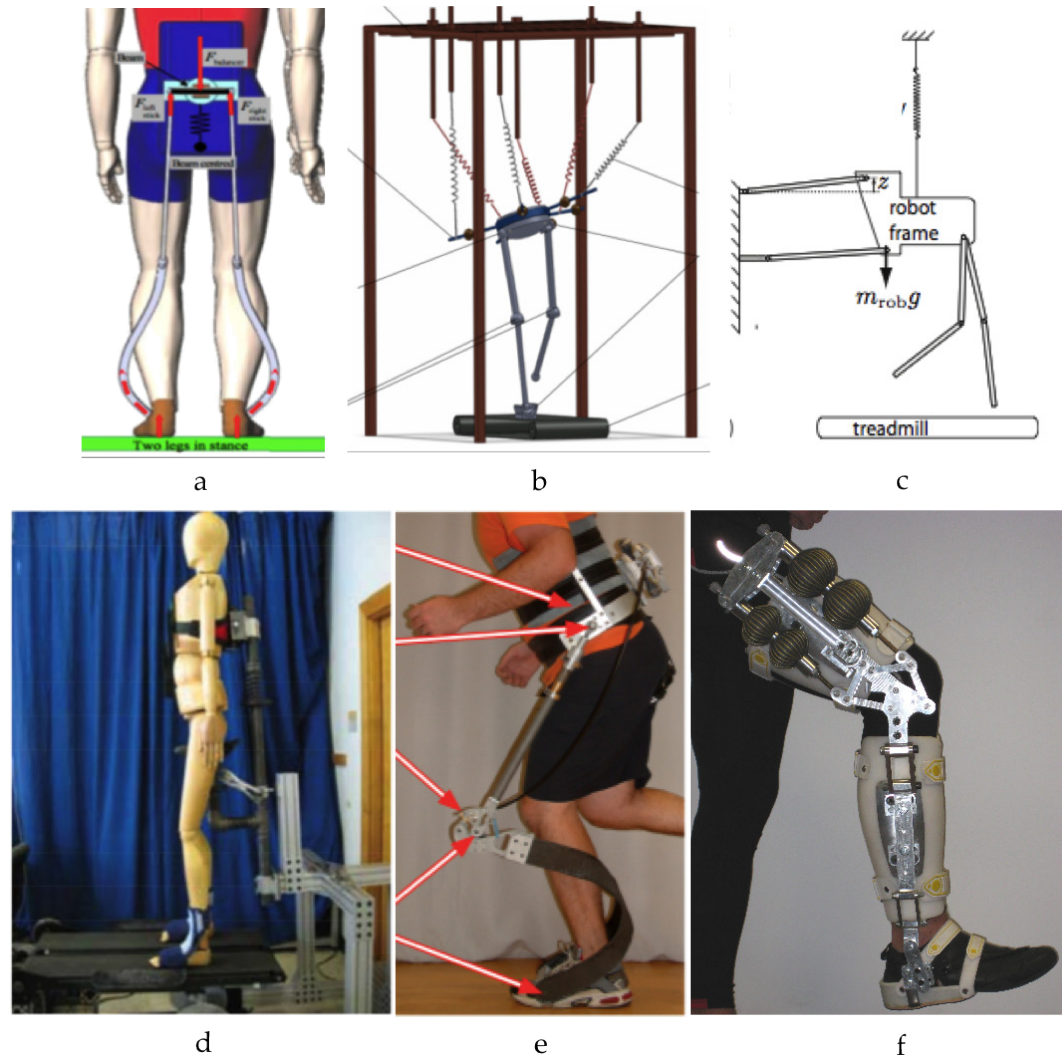
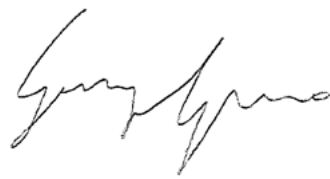


Figure 2.10: Examples of wearable robots exploiting embodied intelligence. (a) MoonWalker, (b-c) Spring-based passive pelvic supports for assistance during locomotion, (d) MIT SkyWalker, (e) Elastic exoskeleton, (f) KNEXO.

Giorgio Carpino

Tesi di dottorato in Ingegneria Biomedica, di Giorgio Carpino,
discussa presso l'Università Campus Bio-Medico di Roma in data 20/03/2012.
La disseminazione e la riproduzione di questo documento sono consentite per scopi di didattica e ricerca,
a condizione che ne venga citata la fonte

A handwritten signature in black ink, appearing to read "Giorgio Carpino". The signature is fluid and cursive, with the first name "Giorgio" and the last name "Carpino" clearly distinguishable.

Chapter 3

Active and passive joints for wearable robots for the lower limbs

The last twenty years witnessed a radical shift in the approach to the design of robots. In this new scenario, as already mentioned, pHRI represents one of the most important aspects to take into account in robot design. The need of a safe pHRI becomes crucial in robots interacting with humans for assistive or rehabilitation purposes; in this case the system should embed an intrinsic compliance, in order to improve the level of adaptability and safety. The assistance to human movements should be imparted by regulating interaction forces, thus avoiding to rigidly move subjects limbs through prescribed kinematic patterns. Robots physically interacting with humans for assistive and rehabilitation purposes are not required to simply move the limbs according to prescribed patterns, but should offer an amount of assistance adapted to the residual motor capabilities of the subjects [74, 4]. The need to stably and robustly regulate human-robot dynamic interaction, also on the basis of the variable level of assistance required by the subjects, entails the use of actuators operating in an ideal force (or torque) mode control. This implies theoretical zero output impedance (i.e. perfect backdrivability) and high force (torque) control fidelity.



Common knowledge in the legged robot community is that inclusion of springs in robotics can effectively reduce both the power and energy requirements demanded of an actuator [75, 76]. This is because a spring can store and release energy efficiently during cyclic repetitive tasks and the power released from a spring is limited only by the natural frequency and stiffness of the system. In other literature, van den Bogert describes a theoretical, passive mechanism that reduces peak power for human gait by more than 70% [77]. The passive device uses a series of elastic cords and pulleys around multiple anatomical joints to accomplish reduced power requirements. As written, the specific implementation described would not likely be practical, but the point of including springs in the design of wearable robotic systems is beneficial. In order to meet the demanding requirements stated above, a wearable robot should include lightweight, energy conservative, power reducing springs to be inherently safe and to lower the WR actuation requirements.

3.1 Active joint for wearable robots: Series Elastic Actuator 90W

Several actuation solutions have been proposed to meet requirements described above [78]. Series Elastic Actuator (SEA) [79, 80] is a simple and effective solution, which basically consists of a gearmotor in series to a spring connected to the load. This allows to decouple motor inertia and other nonlinearities from the output and to obtain a high fidelity in force control by only measuring the deflection of the elastic element. The intrinsic compliance guarantees low impedance across the whole frequency spectrum: for external perturbations at frequencies above the actuator controllable bandwidth, the impedance of the system reduces to the stiffness of the spring thus avoiding unsafe behaviors due to sensors failure and/or control bandwidth limitation. It can be demonstrated [80] that a higher compliance in the torque control loop allows increasing the control gains for some fixed stability margins, which results in a reduction of the effects of internal stiction and other transmission nonlinearities (friction and backlash) and in an improvement of the torque tracking performance. In [81] it has also been proved that the adequate selection of spring



stiffness, according to a specific application, can lead to an energetic optimization of the system, allowing the transfer of peak power values greater than the power limit of the source motor. The major drawback introduced by the series elastic element is the reduction of the actuator bandwidth [76]. Improving the compliance of the actuator reduces the saturation frequency for a given torque, thus decreasing the overall performances of the system. A direct drawback of this behavior is that, given some target torque control specifications, a SEA can require extra power requirements with respect to a traditional stiff motor. Moreover, when the system is stiffness-controlled, i.e. it mimics an elastic behavior, the maximum stiffness which can be virtually rendered is limited by the elastic element, if conservative demands for stability are to be met [82].

SEAs were originally employed in bipedal walking and running robots [83] where unavoidable high frequency disturbances due to impacts with the ground must be rejected. SEAs are now widely adopted also in wearable robotics for gait assistance [84, 85]. In this application, where a typical actuation cycle consists of a sequence of concentric (positive power transfer from the actuator to the load) and eccentric (negative power transfer) phases, the property of compliant elements to serve as energy buffers can be exploited to reduce actuator power demands. The system proposed in [79, 80] is a linear actuator but a number of rotary prototypes have been recently developed for different applications [84, 85, 86, 87, 88, 89, 90, 91]. SEAs are typically torque-controlled, using the control scheme depicted in Fig. 3.1.

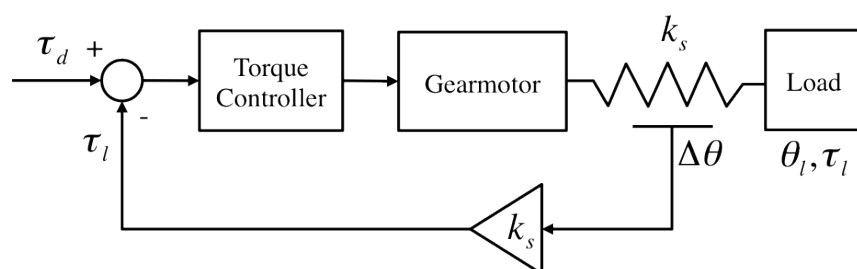


Figure 3.1: Torque control scheme for a rotary SEA. τ_d represents the desired torque, k_s the spring stiffness, $\Delta\theta$ the spring deflection, τ_l the output torque and θ_l the output angle.

In this general scheme, the measurement of spring deflection $\Delta\theta$ provides an estimate of the torque exerted by the actuator τ_i ; this measure is used as feedback signal for torque control thus converting the torque control problem in a simpler position control one. The equilibrium position of the spring is thus continuously varied for torque regulation. The stiffness of the series elastic element must be carefully selected in order to trade-off between performances, adaptability and safety, as it will be presented in the next paragraphs. Moreover, dimensions and weight must be reduced as much as possible, especially for wearable robotics applications. In order to be included in such torque control scheme, a compliant element for a SEA is then required to be verified against the maximum output torque supplied by the actuator and to provide a linear torque vs. rotation relationship both in static and dynamic conditions. However, the elastic element should be directly connected to the load, so to avoid the effect of force-fidelity reduction caused by transmission non-linearities. Moreover, typical applications in assistive robotics impose torque requirements in the order of 10-50 N·m. Unfortunately, no commercially available, sufficiently compact rotary component is able to fulfill all of the above-mentioned requirements.

3.1.1 SEA 90W design requirements

The SEA 90W is designed to provide partial support to knee flexion/extension during gait in elderly subjects with an age-related decay of motor performances.

A number of gait features are influenced by aging, such as decreased gait velocity, caused by decreased step length [92] and increased stance time [93]. Elderly people have generally a more conservative gait pattern than normals (i.e. a lower preferred walking speed [94] and shorter steps [95]). Considering the slow-walking data set described in [96], the maximum instantaneous power exerted by the knee joint is about 40 W with a maximum torque of 29 N·m and an RMS value equal to 20 N·m. In order to provide an assistive torque equal to the 30% of the peak torque required during overground walking, a target of 10 N·m for actuator torque is imposed as design requirement. However, the reduction in the duration of the swing phase also imposes torque regulation to be fast enough to provide rapidly



3.1. ACTIVE JOINT FOR WEARABLE ROBOTS: SERIES ELASTIC ACTUATOR 90W 43

changing assistance levels during walking. To this aim, considering that more than 90% of the power spectral density of knee torque is in the frequency range between 0 and 4 Hz (as obtainable from data in [96]), a minimum bandwidth of 4 Hz is set as a requirement to torque control.

As mentioned above, SEA torque regulation can be achieved, for example, by employing position control of the motor [97]. In order to avoid the use of complex non-linear control schemes and to allow homogeneous regulation capability above the whole range of deliverable torques, a linear torque vs. angle characteristic is desirable. Indeed, non-linear relationships would imply an increased sensitivity to motor positioning inaccuracies thus possibly implying high torques regulation errors. Moreover, the elastic component should be connected to the load in a direct drive configuration, so to avoid the reduction of force fidelity caused by transmissions non-linearities.

The target stiffness value needs to be selected after a careful trade-off between the requirement of providing a sufficiently high intrinsic compliance and that of obtaining an accurate torque control in a given frequency bandwidth (see also Section 3.1.2.2). The maximum spring deflection angle (θ) is calculated from the maximum torque required to the actuator (M_t) and the desired torsional stiffness (K_t): $\theta = M_t / K_t$. A larger θ (i.e. smaller K_t) would allow the use of a smaller reduction ratio, but in turns it would also reduce the maximum stiffness which can be rendered at high frequencies. Moreover, a smaller stiffness would negatively impact the bandwidth of the large force control [80]. Finally, the reduction ratio has to be selected to reach the required output torque, without increasing the mass/size of the DC motor (see Section 3.1.2).

Furthermore, the desirable physical stiffness values of SEAs for locomotion assistance, as retrieved from a literature analysis may range from 100 to 300 Nm/rad [84, 85, 89, 90]. Suitability of stiffness values within this range has been demonstrated also in theoretical analyses [80] and recent simulation studies [98], on the basis of realistic velocity and current limitations for DC motors.

Combining the previous considerations, a stiffness value of 150 N·m/rad and a peak admissible torque of 10 N·m are taken as target for the presented design.




TABLE 3.1: SEA 90W REQUIREMENTS.

Characteristics	Values
Output Stiffness	150 N·m·rad ⁻¹
Max admissible torque	10 N·m
Max dimensions	150 × 150 × 200 mm ³
Max weight	2 kg
Minimum bandwidth	4 Hz

The elastic element also requires an accurate measurement of its deflection. This can be achieved by mounting two encoders on the input and output shafts of the springs pack, thus estimating the elastic element deformation by subtracting the two independent measurements. This allows to implement the basic torque control scheme described in Fig. 3.1. Under this regard, it is important to define the basic requirements for the angle sensors, whose measurements will be used to infer the instantaneous torque applied to the load. Said K the equivalent output stiffness of the springs block put in series between the actuator and the load ($K = f(k)$, with f being the function defined by the connection topology of basic elements with stiffness k), and n the number of bits of the (single-turn) absolute encoders placed to measure the angle of the input and output shafts of the spring, the torque measurement quantization $\Delta\tau_{meas}$ is given by:

$$\Delta\tau_{meas} = \frac{(K \cdot 2\pi)}{2^n} \quad (3.1)$$

Inverting Eq. 3.1, and considering a minimum resolution of torque measurement of 0.1 N·m for wearable robotics applications [90], the minimum resolution required to the considered encoders ranges from 13 to 15 bit, hypothesizing for K a value comprised between 100 and 300 N·m·rad⁻¹.

Moreover, actuator dimensions and weight must be reduced as much as possible, especially for wearable robotics applications. It is reasonable to require the actuator to have a weight lower than 2 kg and to be contained in a volume of 150×100×100 mm³ in order to reduce the encumbrance in the sagittal plane.

For the sake of clarity, in Tab. 3.1 the SEA 90W requirements are listed.



3.1.2 SEA 90W design

This section describes the SEA 90W components (motor, reduction gear, torsional spring, sensors) and the related design choices. In Fig. 3.2 a picture of the prototype is reported.

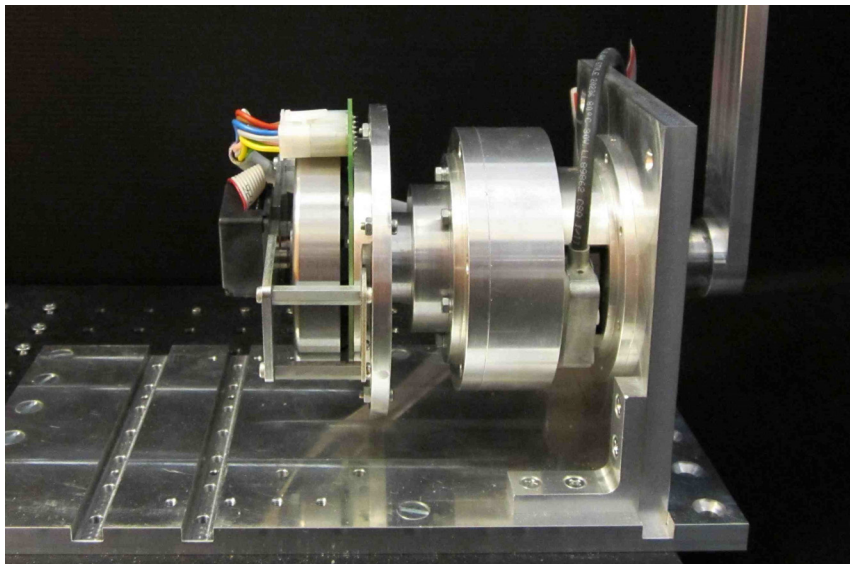


Figure 3.2: Picture of the assembled SEA 90W prototype: the frame is fixed to an aluminum support, while the actuator output shaft is connected to a link.

In Fig. 3.3 a block scheme of the actuator is depicted highlighting the serial configuration of the different components.

The design architecture of the developed SEA 90W has been conceived in order to obtain the highest possible level of modularity. Mechanical parts have been designed to be easily substituted in order to obtain different possible configurations and performances.

Flat DC motors have been selected since they show a good compromise between high torque/power and low volume/mass. The selected motor is a 90 W brushless DC motor (Maxon EC90-flat) with a weight of 648 g, and a maximum continuous torque of 494 mN·m. Maxon flat motor also includes Hall sensors for current commutation and a 500 counts per turn (cpt) optical incremental encoder Avago HEDL5540, to measure motor rotation with a resolution of 0.18 deg when using

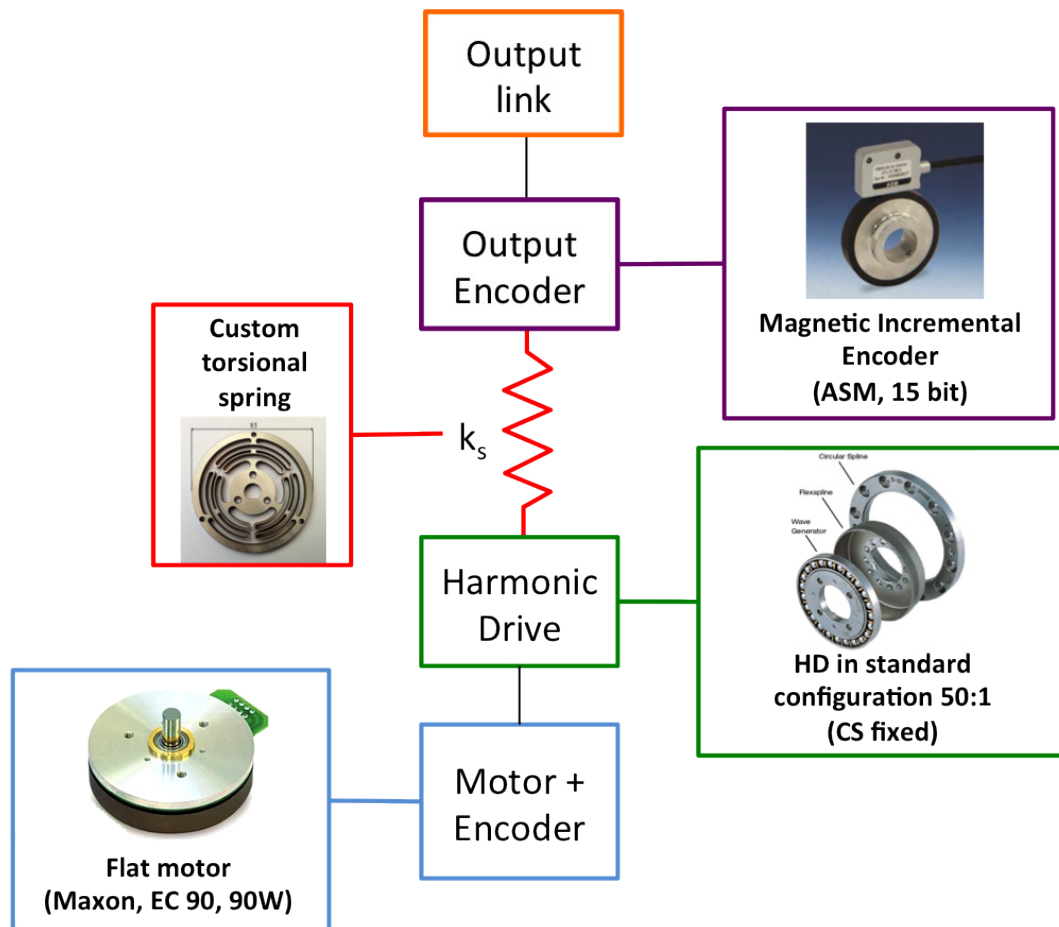


Figure 3.3: Block scheme of SEA 90W.

quadrature reading. It is worth mentioning that the motor is also disposable, once fixed the geometrical dimensions, with different electrical characteristics (two 90 W motors of the same families are available). A Harmonic Drive gear has been selected as reduction gear for its compactness, low weight, high positioning accuracy and high efficiency. The selected gearing is the CSD-20-100-2A-GR, with a reduction ratio of 50:1, a weight of 130 g, a thickness of 14 mm and a diameter of 70 mm. Also in this case, fixed the geometrical properties, three possible reduction ratio are available: 50, 100 and 160. A 15 bit ASM magnetic incremental encoder, composed by a PMIS4 reading sensor head and a PMIR4 magnetic code wheel, is included to measure the actuator output and allows to estimate spring deflection, used for SEA

Giorgio Carpino

3.1. ACTIVE JOINT FOR WEARABLE ROBOTS: SERIES ELASTIC ACTUATOR 90W 47

torque control. Actuator output measurement has a resolution of 32768 cpt ($3 \cdot 10^{-3}$ deg when using quadrature reading).

Figure 3.4 depicts a cross section of the obtained design. The actuator, as described above, is composed by: EC-flat 90W Maxon motor (Fig. 3.4-2) equipped with optical incremental encoder (Fig. 3.4-1); a Harmonic Drive reduction gear 50:1 in standard configuration (circular spline fixed to the frame, (Fig. 3.4- 3); custom torsional spring (Fig. 3.4-4); an output magnetic incremental encoder (Fig. 3.4-5); an output shaft (Fig. 3.4-6). The overall dimensions are: 120 mm (diameter) \times 165 mm (axial length) and the overall actuator mass is 1.8 kg, thus fulfilling the requirements reported in the previous paragraph.

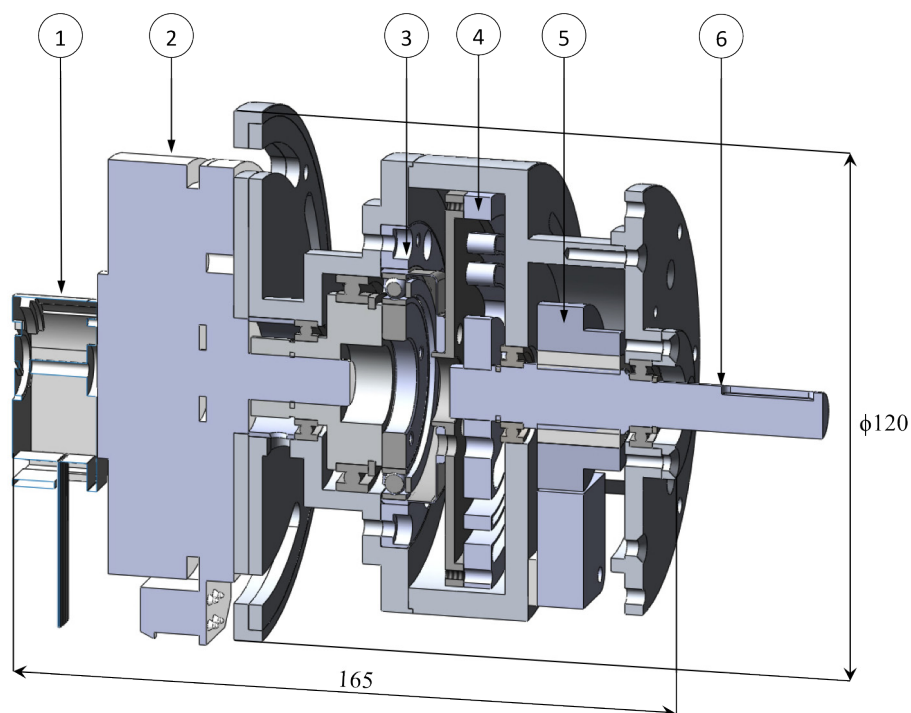


Figure 3.4: Cross section of rotary SEA 90W. 1: optical incremental encoder, 2: flat DC motor, 3: Harmonic Drive, 4: custom torsional spring, 5: magnetic incremental encoder, 6: output shaft. Dimensions: 120 mm (diameter) \times 165 mm (axial length). Total mass is 1.8 kg.

3.1.2.1 SEA 90W custom torsional spring

The introduction of intrinsic compliance in the actuation system of assistive robots is motivated by the necessity of improving safety and dynamical adaptability. Furthermore, in wearable robots for gait assistance, the exploitation of conservative compliant elements as energy buffers mimics the intrinsic dynamical properties of legs. However, commercially available compliant components do not generally allow to obtain the desired requirements in terms of admissible peak loading demanded by gait assistance, while guaranteeing a compact and lightweight design.

A considerable amount of research in SEA design has gone in the direction of designing custom components or systems, suitable to match the specific requirements of a given application. It can be useful to group the compliant components of SEAs in two different classes depending on the kind of solutions adopted to implement the desired output torsional stiffness. The first class comprises compliant systems adopting linear compression springs arranged so to produce a torsional stiffness [84, 86, 87, 88]. The springs arrangement generates a centering elastic torque against an external rotation of the joint shaft. The second class includes compliant systems employing torsional springs embedded in the transmission train [85] or custom torsional springs directly connected to the load [89, 90, 91].

Considering the first class of springs, a system with a three spoke output component, a circular input pulley and six linear springs was presented in [86] (see Fig. 3.5–A). The springs are made of 2.2 mm C85 carbon steel wire with stiffness of 62 N/mm, a free length of 18 mm and a maximum allowable deflection of 6 mm. A similar approach using six linear springs to achieve a torsional stiffness is pursued in [87] (Fig. 3.5–B). In [88, 100] four springs have been used so to develop a velocity sourced SEA intended for use in human-robot interaction applications. The series elastic system is 120 mm in diameter and 36 mm in thickness. Each spring stiffness is 19 N/mm while the four springs arranged in the module provide a rotational spring constant of 138 N·m/rad. In the SEA developed in [84, 99], the torsional elastic behavior is due to the agonistic-antagonistic configuration of two linear compression springs connected to the actuator disk with a cable so that a torsional spring is created (Fig. 3.5–C); the two compression springs are pre-tensioned



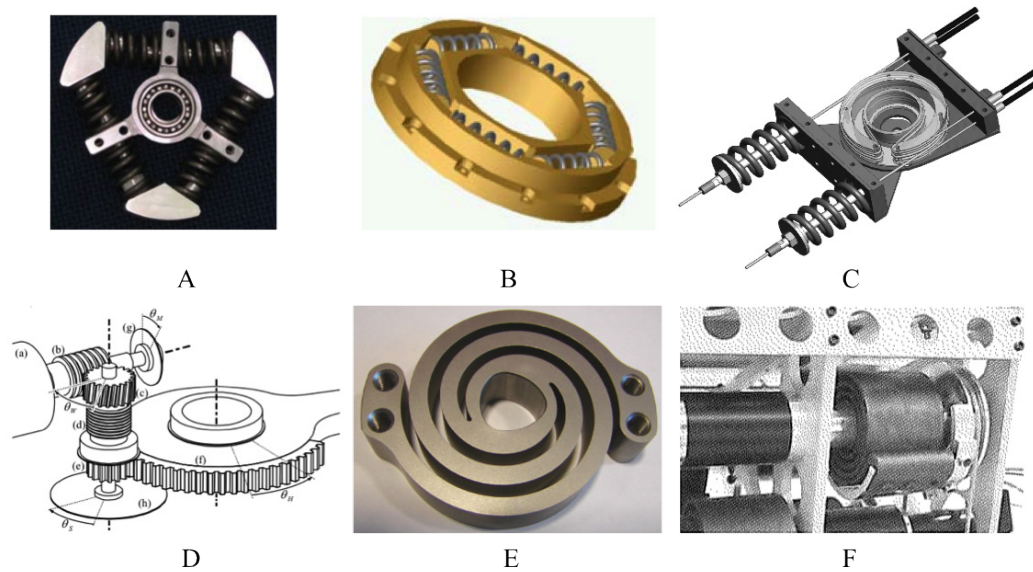


Figure 3.5: Compliant components for rotary SEA prototypes: [86] (A), [87] (B), [99] (C), [85] (D), [89] (E), [91] (F).

with the maximally desired force, so that the connecting cable will always be under tension during operation. The actuator has an approximate peak torque output of 30 N·m. Three different sets of springs were used as series elastic element so to achieve three different resultant stiffness values: 63.6 N·m/rad using high compliance springs, 156 N·m/rad with medium compliance springs and 393.6 N·m/rad with low compliance springs.

Compliant systems belonging to the second class can be either commercial or custom. In the first case the spring can be embedded in the power transmission stage so to satisfy the demanding peak torque requirements of pHRI applications, as in [85] (Fig. 3.5–D), where the spring is installed between the worm gear and output gears. In this configuration, the presence of a spring in the transmission stage allows achieving a good fidelity in transferring motion between the motor and the output link. However, the presence of output gears causes a loss of force transfer fidelity. A possible solution allowing to overcome these limitations is to directly place the spring between the gearmotor and the load; to investigate this option some authors have designed custom elastic components. In [89] a custom-made



double spiral spring in series to a frameless motor is presented (Fig. 3.5–E), based on previous experience [90] with a hydraulically-actuated SEA. The double spiral design has the advantage to cancel out undesired radial forces acting on the spring center when the spring is wrapping or unwrapping. Maraging steel (AISI grade 18Ni, 350) is employed, with a resulting mass of 235 g, a thickness of 15 mm and a diameter of 75 mm. A linear torque vs. rotation characteristic is demonstrated up to 100 N·m, with a resulting torsional stiffness of 219 N·m/rad, with an error of 38% from the value obtained through FEM optimization (353 N·m/rad). Another possible solution is shown in [91] (Fig. 3.5–F) where a custom spiral shaped unidirectional torsional spring has been implemented in the biped robot Kurmet. The spring, made of AISI 1095 steel, has an outside diameter of 72.14 mm and a thickness of 50.8 mm. It has been designed to have a torsional stiffness of 30 N·m/rad and a maximum allowable torque of 65 N·m.

The goal is to develop a compact, monolithic, torsionally compliant element, that can be included in the actuation architecture of a wearable robot for knee assistance. The application field demands for a design focused on the simultaneous achievement of the ability of providing the assistive power and torques necessary to support human locomotion and the minimization of the resulting weight and dimensions.

3.1.2.2 Spring design requirements

The selection of the physical stiffness of the series elastic component has an impact on performance and safety characteristics of the actuator [80]. In particular, an optimal stiffness value can be determined as a tradeoff between two objectives: *i*) increasing the Large Force Bandwidth (LFB) and *ii*) reducing the intrinsic mechanical impedance. Additionally, since the applied torque is inferred from the spring deflection measurement, spring stiffness has also an impact on the torque measurement resolution. For a given resolution of the measurement elements, a more compliant component allows a smaller quantization of the torque signal, thus improving the accuracy of torque estimation. Moreover, a high linearity in the torque vs. angle relationship is desirable in order to guarantee an accurate torque estimation



and consequent control performance. For this same reason, also residual deflection (at zero delivered torque) and hysteresis should be avoided.

It is particularly difficult to define an optimal value of physical elasticity for a SEA of a wearable robot for gait assistance. Both an analysis of the relevant wearable robotics literature [84, 85, 89, 90] and of biomechanics studies addressing the measurement of the intrinsic viscoelastic properties of lower limbs joints [101, 102] show heterogeneous results for each addressed joint of the lower limbs. Given this lack of evidence, the subsystem providing the desired series elasticity should be demanded to be highly modular, so to render a variety of desired stiffness values. This desired variability of physical stiffness can then be obtained by designing a single basic elastic element, and devising the proper set of interconnections between these building blocks, able to provide the specific required physical stiffness properties (e.g. series or parallel). It can be seen in Fig. 3.6 that several different output stiffness values can be obtained by interconnecting this element in different parallel and series configurations.

Considering these assumptions (see also Appendix 1), as already anticipated in Section 3.1.1, a stiffness value of $150 \text{ N}\cdot\text{m}\cdot\text{rad}^{-1}$ will be taken as specification for the basic torsional spring element. Furthermore, a peak torque of $10 \text{ N}\cdot\text{m}$ has been considered as target for the design of the elastic element of SEA 90W as suitable to assist motion of human knee joint of subjects with moderate disabilities (e.g. elderly people).

Furthermore, in order to minimize weight and dimensions, a monolithic disc-shaped design is pursued, since it allows minimizing the bulk in the axial direction, still maintaining an acceptable total thickness in the several springs arrangements as shown in Fig. 3.6. This shape implies that the transfer of torsional torque is between an outer ring (diameter of 100 mm) and an inner ring (diameter of 12 mm). Compliance is obtained by interposing flexible elements between the two rings. The shape and dimensions of such flexible elements are defined through an iterative Finite Element Method (FEM) simulations-based design and optimization process in the next paragraph. The minimum width of the flexible elements is 0.1 mm due to the manufacturing limitations. In the following, the design of the basic element



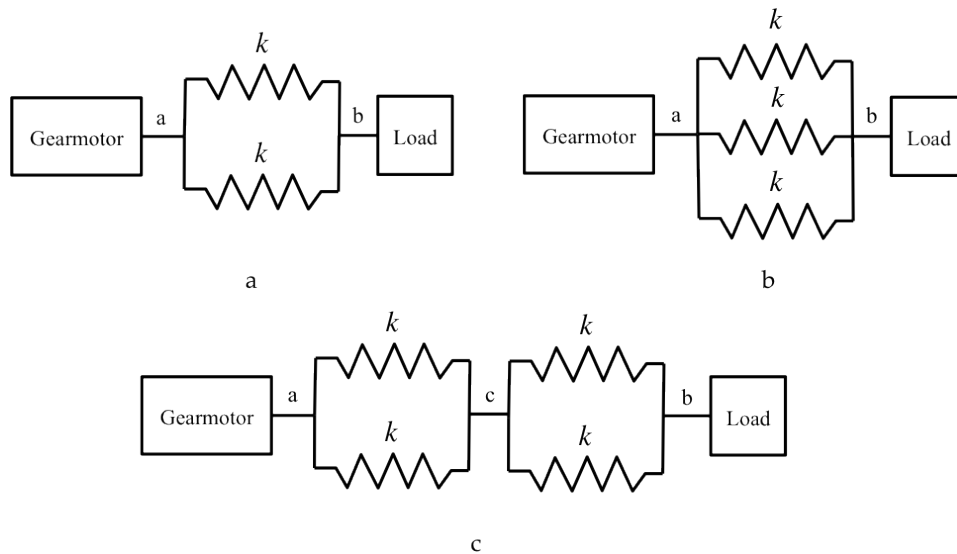


Figure 3.6: Schematic representation of springs possible arrangements. (a) Parallel configuration of two equal springs, each with a stiffness of $150 \text{ N}\cdot\text{m}\cdot\text{rad}^{-1}$ under a peak load of $10 \text{ N}\cdot\text{m}$. The total stiffness of the equivalent system, as seen between ports a and b , equals to $300 \text{ N}\cdot\text{m}\cdot\text{rad}^{-1}$ while the maximum admissible torque is $20 \text{ N}\cdot\text{m}$. (b) Parallel configuration of three springs. The total stiffness of the equivalent system is $450 \text{ N}\cdot\text{m}\cdot\text{rad}^{-1}$ while the maximum admissible torque is $30 \text{ N}\cdot\text{m}$. The connection of the gearmotor and the load to the elastic system is equivalent to case A. (c) Serial configuration of two parallel springs arrangement. The total stiffness of the equivalent elastic system is $150 \text{ N}\cdot\text{m}\cdot\text{rad}^{-1}$ while the maximum admissible torque is $20 \text{ N}\cdot\text{m}$.

of the architecture will be described, taking into account the requirements reported in Tab. 3.2.

3.1.2.3 Spring design methodology

The design of the series elastic element is conducted by means of an iterative Finite Element Method (FEM) simulations-based design and optimization process, as described by the flowchart in Fig. 3.7. The method basically consists in an optimization process, oriented to satisfy the following design criteria:

- to obtain a desired ratio between applied torque and rotation (stiffness);

TABLE 3.2: SEA 90W TORSIONAL SPRING REQUIREMENTS.

Characteristics	Values
Stiffness	150 N·m·rad ⁻¹
Max admissible torque	10 N·m
Max deflection	0.067 rad
Max outer diameter	100 mm
Max thickness	6 mm
Max weight	150 g
Fatigue life	≥ 10 ⁶ stress cycles

- to guarantee the structural integrity of the component in the maximum loading conditions.

The first step of the process consists in choosing an adequate basic topological structure for the elastic component. Each topology is in one-to-one correspondence with the set of parameters necessary to define a certain morphological implementation. For each topology, some parameters were fixed while others were considered open to be optimized. Said n the number of variable parameters, and (x_i^{MIN}, x_i^{MAX}) the range of admissible values for the i^{th} parameter, a n -dimensional search space is thus defined. Within this range, an initial value is assigned to each parameter based on a preliminary concept of the morphology, thus completely defining the 3D design of the compliant element. The model is then imported in a FEM analysis software to evaluate the response of the structure in the maximum loading condition and, in particular, to check if the design criteria are satisfied.

In the negative case two possibilities arise:

1. to change the parameters values within the range defined for the considered topology, in particular by adding and removing material until most of the structure has similar stress conditions subject to the desired displacement and output rotation;
2. to change topology and reiterate the process, if the search space for the selected topology is considered to be explored with sufficient depth.



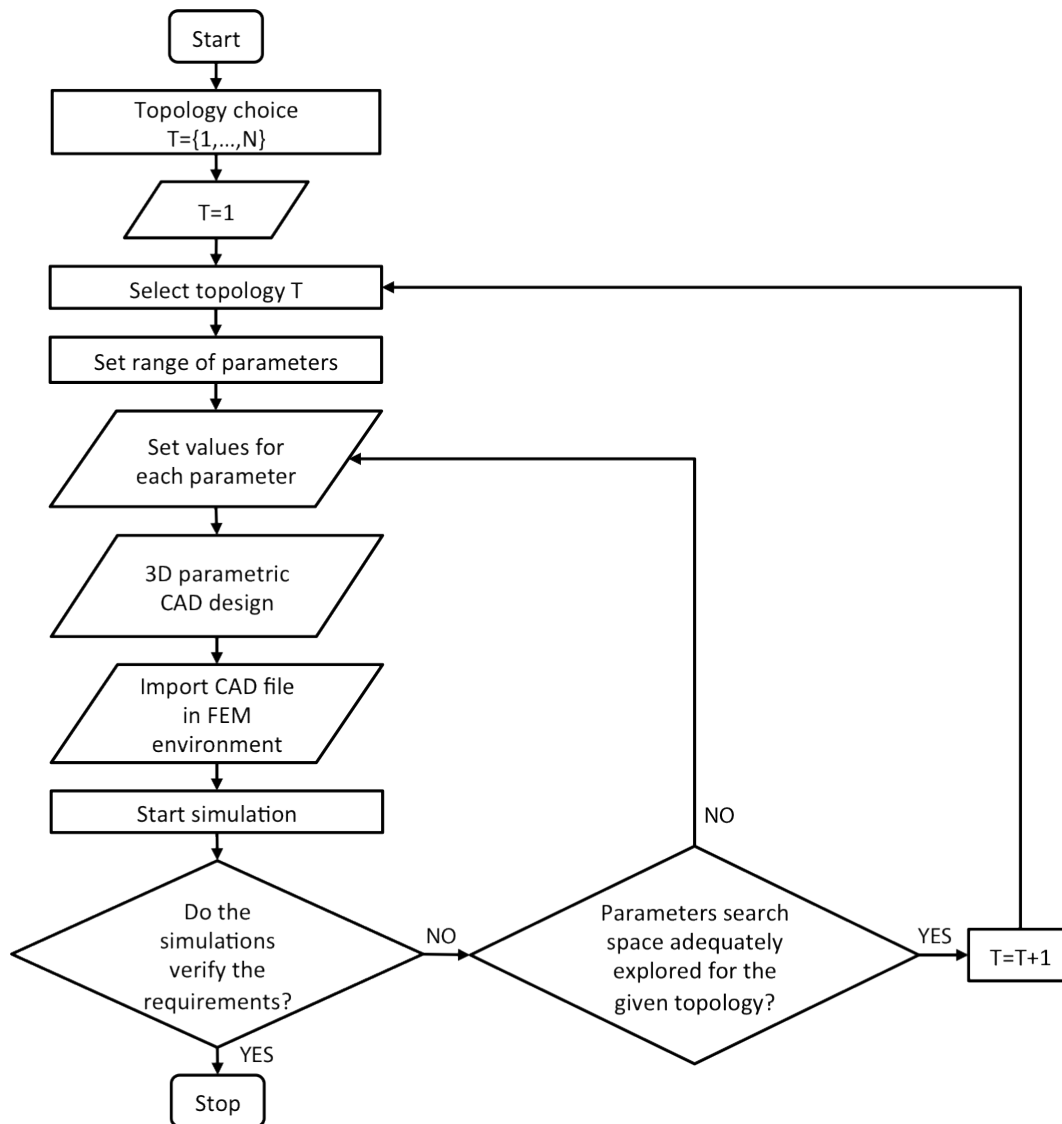


Figure 3.7: Flowchart of the spring design methodology.

In the positive case the optimization phase ends for the specified topology, and the chosen morphology is considered as a feasible design.

It is worth noting that the described methodology does not allow to exhaustively span the whole n -dimensional search space defined, but it is driven by heuristics and can be ended once the design objectives described above are satisfied.

Different evaluation criteria are employed in order to compare representative results pertaining to different topologies. A topology is discarded if the design criteria described in Section 2 could not be satisfied after a certain number of design iterations (twenty in our case). Moreover, a scalar value that allows to compare different basic elements is the specific energy stored in the spring in safe stress conditions. The specific energy (e_{el}) stored in the spring is defined as:

$$e_{el} = \frac{1}{2} \frac{k \Delta \theta^2}{M} \quad (3.2)$$

where k is the spring torsional stiffness, $\Delta \theta$ is the rotation angle and M is the spring mass. The torsional stiffness is calculated as ratio between the applied torque and the consequent spring deformation angle calculated from FEM simulations.

In Fig. 3.8 three representative examples of spring topologies under optimization are reported. The solid circles represent the inner and the outer rings, whose diameters values are fixed. The dotted ellipses represent the flexible elements whose morphology is optimized.

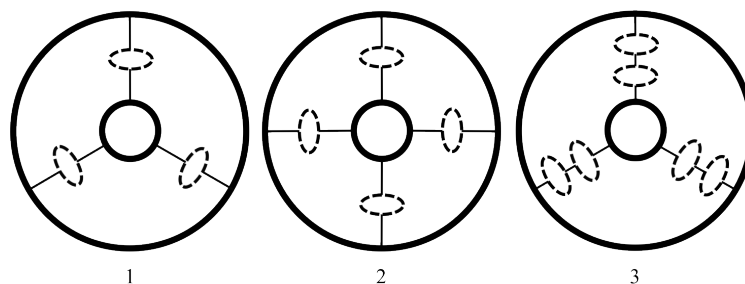


Figure 3.8: Three analyzed springs topologies. The solid circle represent the internal hole and external diameter of the spring while the dotted ellipses represent the flexible elements.

3.1.2.4 SEA 90W spring design

The first step in the design is to define the shape of the flexible elements represented in Fig. 3.8. The selected elements are flexible arched lamellae disposed in a closed loop acting as curved thin beam. Such shape can be then parameter-

ized into different designs, based on the particular value of a specified set of open parameters.

Considering each angular replication of lamellae blocks (as shown in Fig. 3.9), the distance of the m lamellae from the center are labeled with R_j ($j = 1 \dots m$) and the width of the lamellae with s_j ($j = 1 \dots m$). The width of the interconnections between lamellae and between lamellae and inner/outer rings are indicated with w_j ($j = 1 \dots m/2 + 1$), the width of the arches joining two different lamellae with p_j ($j = 1 \dots m/2$) and the aperture angle of the lamellae blocks with α . D_j ($j = 1, 2$) define the width of the inner and outer rings. Table 3.3 reports an example (i.e. topology 3) of the description of the design parameters with the definition of the lower and upper bounds and the minimum increment adopted to explore the search space. Fixed parameters comprise the diameter of the inner hole, the outer diameter of the external ring and the thickness of the torsional spring (not shown in Fig. 3.9).

Figure 3.10 reports the maximum e_{el} for the best morphology obtained after the optimization process described in the previous section, for each of the three analyzed topologies. Table 3.4 provides an overview of the best representative morphologies obtained after the optimization phase implementing the three considered topologies.

Considering this metrics, and considering also that no valid design could be produced by optimization of topology 1 after the specified number of design iterations, it is assumed that the fittest solution can be obtained through a parameter optimization based on topology 3. Such configuration includes three replications of two couples of lamellae, arranged at 120 deg as shown in Fig. 3.9, where optimized variables are labeled using letters, while fixed parameters are indicated using their numerical value.

The optimized spring, shown in Fig. 3.11, has been manufactured by WEDM and then ground; it is made of Bohler W720 (maraging steel 300, Young modulus of 186 GPa, yield stress of 1.91 GPa and ultimate tensile strength of 1.96 GPa after an aging treatment of 3 hours at 500°C). In the fourth column of Tab. 3.3 the optimized spring dimensions are reported. Holes on the outer and inner rings are used for the connections with the gearmotor axis and the output shaft respectively, thus



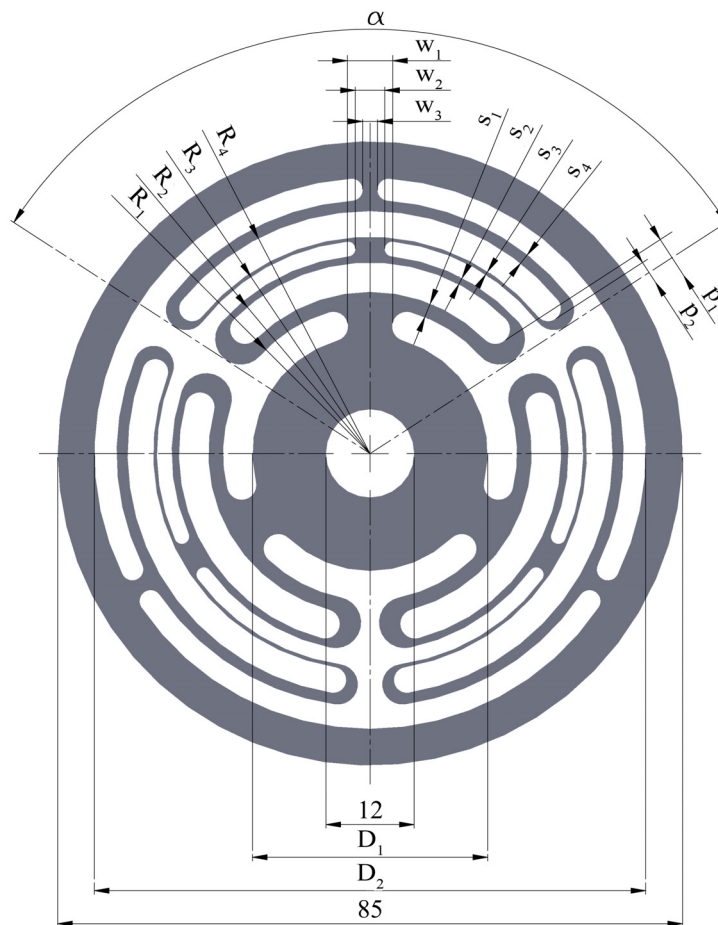


Figure 3.9: Sketch of an arbitrary morphology based on topology 3, in order to describe design parameters. Letters are used for optimized parameters while numbers indicate fixed dimensions in [mm]. Spring thickness is a design constraint and is set to 3 mm. Radii of arches connecting two different lamellae are not reported since are not independent variables.

embodying the Series Elastic Actuation architecture.

3.1.2.5 FEM simulations

FEM static stress-strain analyses (COMSOL Multiphysics 3.5, Comsol AB) have been performed in order to optimize the mechanical design to satisfy the reported design objectives. In the static analysis, the boundary conditions include the fixa-

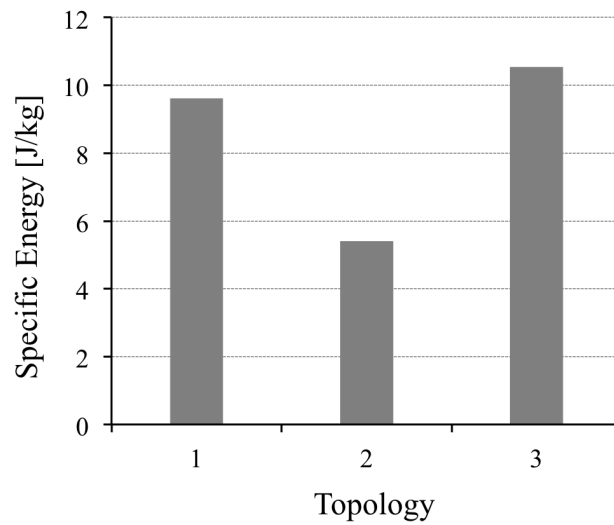


Figure 3.10: Specific energy for the three investigated topologies. For each topology the best morphological implementation obtained through the optimization is considered. No individual deriving from topology 2 reached the design objectives after the specified threshold number of design iterations.

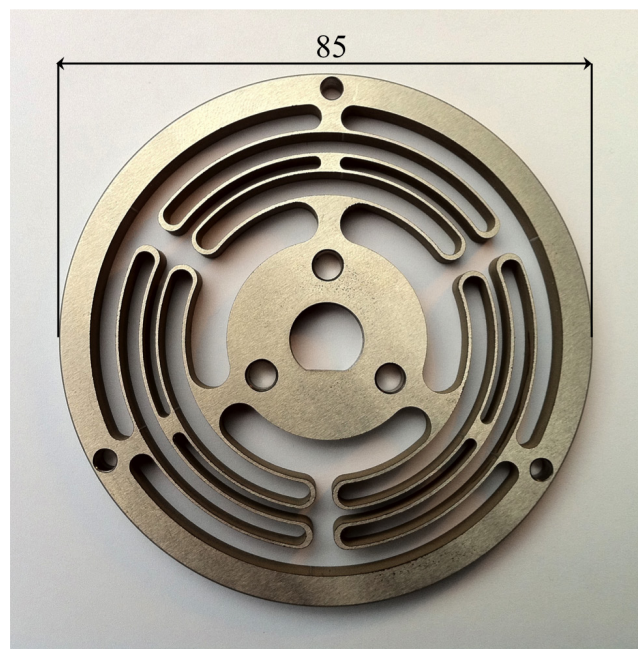


Figure 3.11: Frontal view of the custom made torsional spring. Diameter: 85 mm. Thickness: 3 mm. Weight: 61.5 g.

Giorgio Carpino

TABLE 3.3: DEFINITION OF THE SEARCH SPACE FOR THE OPTIMIZATION PROBLEM OF TOPOLOGY 3. FOR EACH PARAMETER, ITS DOMAIN OF VARIABILITY IS DEFINED, BASED ON THE UPPER AND LOWER BOUND AND MINIMUM INCREMENT ADOPTED IN THE OPTIMIZATION PROCESS. R_j , s_j , w_j , p_j AND D_j ARE IN [MM], α IS IN [DEG].

Parameters	Min.	Max.	Min. increment
R_1	20	24	0.5
R_2	23	27	0.5
R_3	26	30	0.5
R_4	29	33	0.5
s_1	0.1	2	0.1
s_2	0.1	2	0.1
s_3	0.1	2	0.1
s_4	0.1	2	0.1
w_1	3	10	0.5
w_2	2	8	0.5
w_3	2	8	0.5
p_1	0.1	2	0.1
p_2	0.1	2	0.1
D_1	30	35	1
D_2	70	75	1
α	50	57	1

tion of the inner annulus to ground (red arrows in Fig. 3.12) and loading the lateral surface of the outer annulus with a tangential distributed force (blue arrows in Fig. 3.12), representing the equivalent applied torsional moment. The tangential distributed force f is calculated starting from the torsional moment M applied to the external surface. Knowing that $d\tau = dF \cdot R = f \cdot R^2 \cdot d\phi$, where $d\tau$ is the infinitesimal moment, dF is the infinitesimal equivalent force, R is the outer annulus radius and $d\phi$ is the infinitesimal rotation angle, it is possible to express the total tangential distributed force as:

$$f = \frac{M}{2\pi \cdot \Delta z \cdot R^2} \quad (3.3)$$

where Δz is the spring thickness.




TABLE 3.4: PARAMETERS DEFINING THE BEST MORPHOLOGIES PRODUCED BY THE OPTIMIZATION, FOR EACH OF THE THREE CONSIDERED TOPOLOGIES. R_j , s_j , w_j , p_j AND D_j ARE IN [MM], α IS IN [DEG]. N IS THE NUMBER OF ANGULAR REPLICATION OF COMPLIANT BLOCKS, m IS THE NUMBER OF LAMELLAE (2 FOR EACH BLOCK).

Parameters	Topology 1	Topology 2	Topology 3
R_1	18	18	23
R_2	26.5	26.5	27
R_3	N/A	N/A	29.5
R_4	N/A	N/A	33
s_1	1.1	1	0.6
s_2	0.9	0.8	0.5
s_3	N/A	N/A	0.6
s_4	N/A	N/A	0.5
w_1	5	5	5
w_2	N/A	N/A	3
w_3	4	4	4
p_1	1.1	1	0.6
p_2	N/A	N/A	0.6
D_1	32	32	32
D_2	75	75	75
α	116	86	116
N	3	4	3
m	2	2	4

A one layer swept tetrahedral mesh has been used (Fig. 3.12); in this way the 3D subdomain has been meshed starting from a source face and then sweeping the resulting face mesh along the subdomain to an opposite target face. The distribution method is linear with an element ratio equal to 1. The adopted sweep path is straight. The mesh is refined around higher curvature elements (e.g. lamellae and holes), while it is coarser in correspondence of the external ring, where lower stresses are expected.

A stationary non linear solver (SPOOLES) with a relative tolerance of 10^{-6} has been used. Large deformations have been implemented in the simulations. In Fig. 3.13, 1:1 spring deformation and von Mises stress as obtained by the FEM simulation are reported under an applied torsional moment of 10 N·m. The maximum



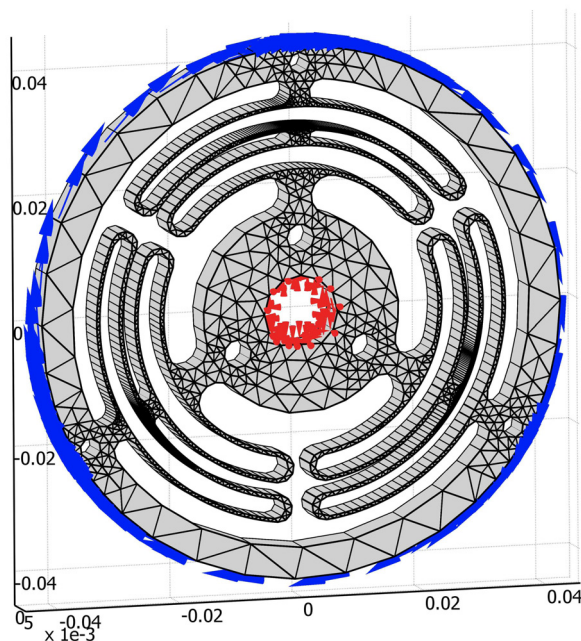


Figure 3.12: Boundary conditions and swept mesh for torsional spring FEM simulations. Axes dimensions are [m].

resultant von Mises stress is 0.93 GPa. Considering that the yield stress of the selected material (σ_y) is 2 GPa and knowing that $SF = \sigma_y / \sigma_{max}$, a safety factor (SF) of 2.3 is achieved. The resultant external ring rotation is 0.061 rad so obtaining a spring torsional stiffness of $164 \text{ N}\cdot\text{m}\cdot\text{rad}^{-1}$, as predicted by FEM simulations.

The specific energy stored in the component, considering the chosen material and a total weight of 123 g, is equal to 4.92 J/kg.

The inner and outer rings, having a large width compared to the flexural elements, can be approximated to rigid bodies. The stress they experience is negligible compared to the von Mises stress in the flexural elements. Therefore, the stress intensification effect caused by the holes (between 3 and 5) increases the small nominal stresses to values which are still largely below those measured in the flexural elements. Being rigid bodies, the external loads can be applied anywhere on them, provided static consistency is assured.

Furthermore, in general the shear stress distribution depends from the geome-

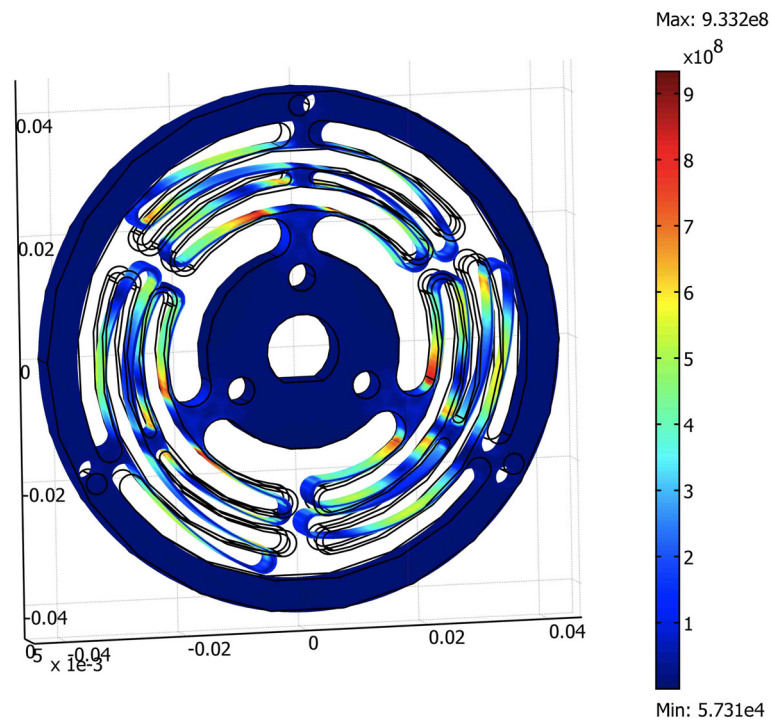


Figure 3.13: von Mises stress in [Pa] and 1:1 spring deformation. Axes dimensions are [m].

try, the boundary conditions and the specific loads applied. For instance, in the case of concentric rigid rings, connected by radial beams and subjected to torsional moments, each beam, being loaded by equal shear forces at the extremities, experiences a constant shear stress, corresponding to a linear bending moment. In the specific design, shear stresses are negligible compared to normal and stresses, because each beam has a thickness (0.5 or 0.6 mm) which is very small compared to its length (from 40 to 60 mm). The geometry has been adapted resorting to FEM analysis for the evaluation of von Mises equivalent stress. The most loaded regions have been thickened to keep the maximum von Mises stress below the yielding point with an acceptable safety factor ($SF = 2.3$).

3.1.2.6 Characterization of the torsional spring

The experimental characterization of the spring was performed directly including the spring in the SEA assembly, and connecting the SEA 90W output shaft to a torque sensor (Lorenz Messtechnik GmbH DR-2, nominal measurable torque 50 N·m), fixed to the test-bed frame. To avoid spurious forces deriving from radial misalignments between SEA and sensor shafts, a flexible coupling (Rodoflex ATMK60L77, nominal torque 60 N·m) was used. In Fig. 3.14 the SEA connected to the test bed is shown.

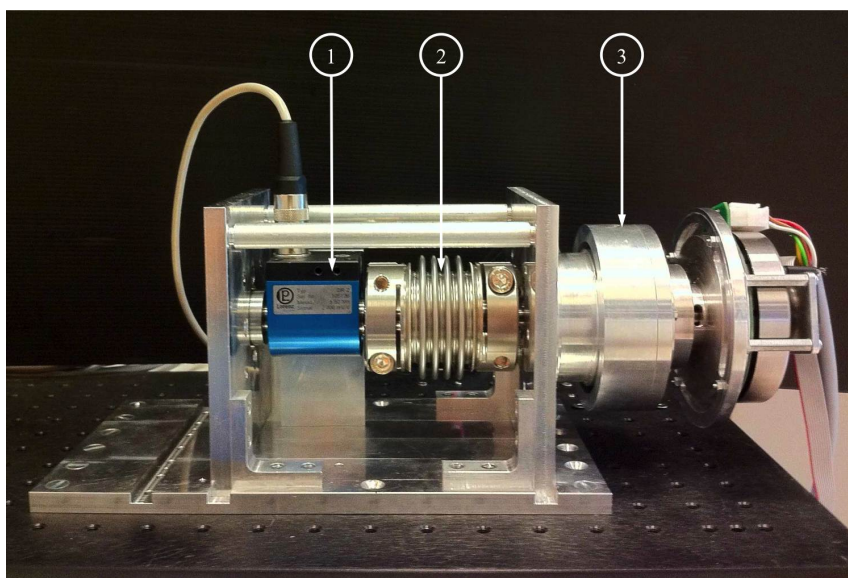


Figure 3.14: Custom dynamometric test-bed used for spring and SEA 90W characterization. 1: torque sensor, 2: flexible coupling, 3: SEA 90W.

The SEA was commanded to track a position profile consisting in a sequence of steps (amplitude 0.2 deg, duration 2 s), including both loading and unloading directions, and the torque necessary to impose a certain spring deflection was measured via the torque sensor, resulting in the plot shown in Fig. 3.15.

Two one-coefficient linear regressions, for positive and negative spring deflections, were performed imposing crossing of the origin. The two regression coefficients calculated differed in less than 0.5% in amplitude and allowed to calculate a global stiffness value as their average, providing an estimation of spring stiffness

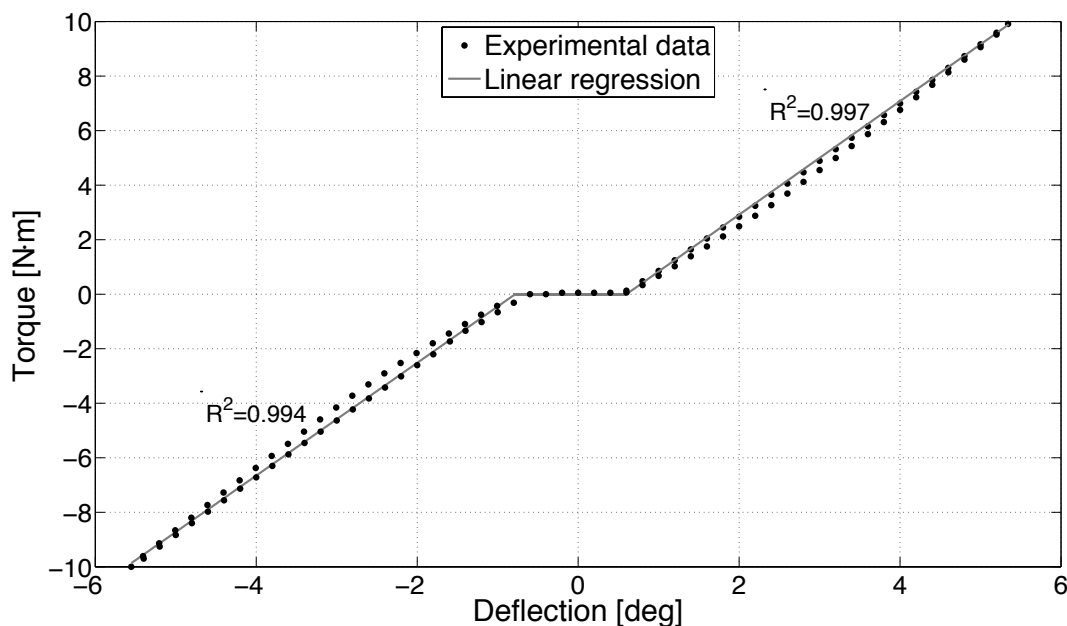


Figure 3.15: Characterization of the torsional spring. Loading and unloading phases are reported, both for positive and negative deflection. R^2 coefficients refer to the fitting of both positive and negative torque vs. deflection curves to the global stiffness curve, reported in solid line.

equal to $119 \text{ N}\cdot\text{m}\cdot\text{rad}^{-1}$. Backwards regression was then implemented on the so-determined profile (measured stiffness of $119 \text{ N}\cdot\text{m}\cdot\text{rad}^{-1}$), giving R^2 coefficients higher than 0.99 for both positive and negative deflections (0.997 and 0.994 respectively).

It is possible to observe the presence of a non-negligible backlash (amplitude of 1 deg), determined by the shaped shaft/hub coupling of the elastic element. This clearance between the shaft and the internal ring of the spring has allowed an easier assembly and disassembly of the torsional spring in the frame of SEA 90W during the characterization phase but in the next prototype an interference coupling between shaft and spring hub will be implemented.

The value of K_s determined experimentally is 25% lower than the one predicted by FEM simulations. A bigger discrepancy (38%) between simulated and experimental data was previously reported by other researchers using different FEM methods and different geometries [89]. It is worth to note that this discrepancy can-

TABLE 3.5: SEA 90W TORSIONAL SPRING PROPERTIES.

Characteristics	Values
Stiffness	119 N·m·rad ⁻¹
Max torque	10 N·m
Max deflection	0.084 rad
Outer diameter	85 mm
Thickness	6 mm
Weight	123 g
Specific energy	4.92 J/kg
Estimated fatigue life	10 ⁶ stress cycles

not be inputed to the series compliance of the characterization setup because, based on components datasheets, the torque sensor stiffness is 4796 N·m·rad⁻¹ while the flexible coupling stiffness is 41998 N·m·rad⁻¹. Hence, the equivalent series stiffness introduced by the test bed is an order of magnitude (about 30 times) higher than the one to be tested.

A fatigue analysis has also been performed following the indications in [103] considering a sinusoidal load with a peak value of 10 N·m. The fatigue strength σ_f , considering more than 10⁶ working cycles, can be expressed as:

$$\sigma_f = 0.5 \sigma_R \cdot C_L \cdot C_G \cdot C_S \quad (3.4)$$

where σ_R is the ultimate tensile strength of the spring material ($\sigma_R=2.1$ GPa), C_L is the load coefficient ($C_L = 1$), C_G is the stress gradient coefficient ($C_G = 0.9$) and C_S is the surface finish coefficient ($C_S = 0.9$) due to the manufacturing process (i.e. WEDM plus grinding process leading to a final surface roughness equal to 0.8). Under these conditions, the fatigue strength is equal to 851 MPa. The maximum stress, as described above, is equal to 933 MPa for an applied torque of 10 N·m and it is comparable to the value of calculated fatigue strength thus verifying the infinite life of the component.

In Tab. 3.5, the relevant mechanical properties of the torsional spring are reported, as experimentally characterized.

The designed elastic element can be conceived as the basic building block of a



modular architecture involving serial and parallel interconnections, so to match the particular requirements of a given application. As an example, it is possible to connect in parallel two equal torsional springs such as the one presented, thereby providing an equivalent stiffness of $238 \text{ N}\cdot\text{m}\cdot\text{rad}^{-1}$ and a maximum torque of $20 \text{ N}\cdot\text{m}$ (twice the peak torque admissible for each spring). Figure 3.16-a depicts a cross section of the mentioned parallel configuration. Also springs interconnections in series can be achieved as depicted in Fig. 3.16-b. In this case two springs parallel configurations are connected in series providing an equivalent stiffness of $119 \text{ N}\cdot\text{m}\cdot\text{rad}^{-1}$ and a maximum torque of $20 \text{ N}\cdot\text{m}$. In this configuration, each springs parallel configuration is loaded with an equal maximum torque of $20 \text{ N}\cdot\text{m}$ and subject to an equal maximum deflection of 0.168 rad .

3.1.3 SEA 90W experimental characterization

SEA torque regulation is performed by measuring the deflection of the elastic element (i.e. the difference between the SEA output angle θ_{out} and the gearmotor rotation θ_m). Said K_s spring stiffness and supposing that the torque vs. deformation relation of the elastic element is well fitted by a linear characteristic, the torque delivered by the actuator can be estimated as $\tau = K_s(\theta_m - \theta_{out})$.

The SEA control scheme follows the approach proposed in [82, 100]. A block diagram describing SEA torque control is reported in Fig. 3.17. The desired velocity command generated by the torque and impedance controllers, implemented on the National Instrument CompactRIO, is transmitted to the velocity controller, implemented on the Maxon Motor EPOS device, through the CAN bus (CANopen protocol). Both control loops run at 1 kHz . An outer loop, closed on the load angle measurement, implements the impedance control in order to render virtual stiffness K_v and damping c_v .

As a preliminary validation of the described design, the actuator was position-controlled to track a typical knee angle profile during locomotion, as retrieved from the slow walking dataset in [96], for a gait cycle duration of 1.6 s , with the actuator output unloaded. Fig. 3.18 shows a position regulation performance in the described conditions, where an RMS error of 2.7 deg is obtained.



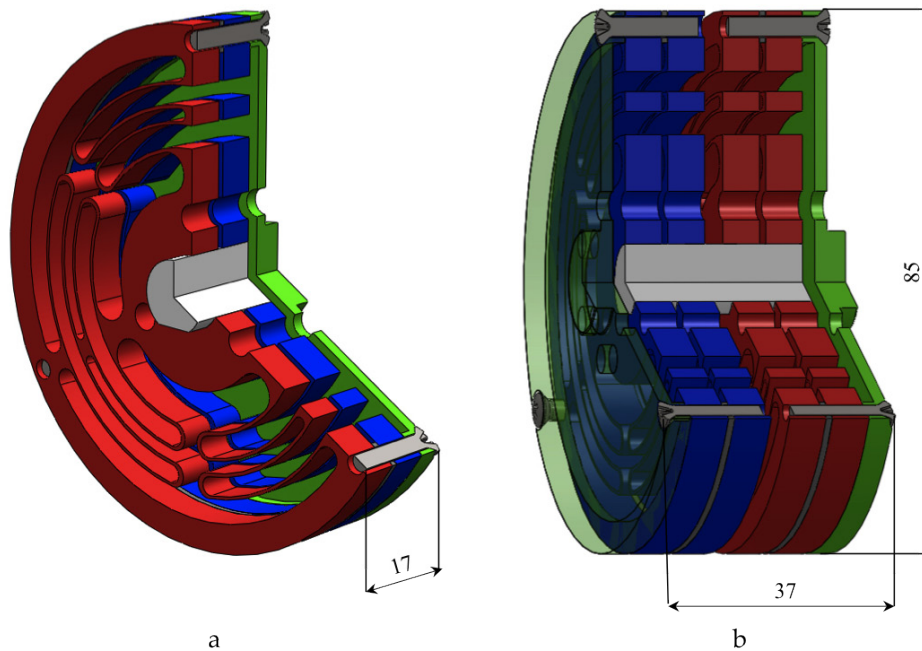


Figure 3.16: Series and parallel springs arrangements. (a) Section view of a design embedding the parallel configuration of two basic elastic elements (Fig. 3.6-a). The springs are shown in red and in blue, the output shaft connecting the internal rings of the springs with the load is shown in white, and the flange connecting the external rings of the springs and the gearmotor are reported in green. Using the basic element designed in the previous sections (specs reported in Tab. 3.5), the equivalent output stiffness is 238 Nm/rad and the max supported torque 20 Nm. (b) Section view of a design including the series connection of two parallel spring blocks (shown in blue and in red). The white shaft connects the internal rings of the two springs blocks while the green flanges, acting as input and output ports of the elastic system, connect the external rings of the two springs blocks. The equivalent stiffness between input and output is 119 Nm/rad and the maximum supported torque 20 Nm. Dimensions are in [mm].

Torque control performances of the developed SEA were characterized using the method proposed in [80], which involves the connection of the actuator output shaft to the ground frame (blocked output conditions). In this configuration, different metrics were considered to measure the performances of the torque controller.

PI torque controller gains were regulated based on the system response to a step commanded torque, in order to have an overshoot lower than 5% of the setpoint and a rise time lower than 10 ms. Fig. 3.19 shows the response of the system to commanded steps with different amplitudes: 3 and 10 N·m. The system responds with a 4% overshoot and with a maximum rise time of 6 ms, for the largest commanded input. Actuator non-linearities (motor velocity saturation) in the response to the largest input imply a 2 ms lag between the rise time calculated at 3 and 10 N·m and a difference in the overshoot in these two situations. Torque measurement has a theoretical quantization introduced by the resolution of the encoders used to measure spring deflection, equal to $3 \cdot 10^{-3}$ deg, implying a quantization of 5 mN·m. However, the step responses measured in the real system had a higher maximum regime error, of 0.1 N·m. This was caused by motor positioning inaccuracy introduced by velocity control, and by the backlash of the set-up. However, a torque control resolution of 0.1 N·m is considered adequate for applications involving human assistance [90].

In order to measure the performances of the system and to assess the followed biomechatronic design, a further test was performed, by imposing a sinusoidal ref-

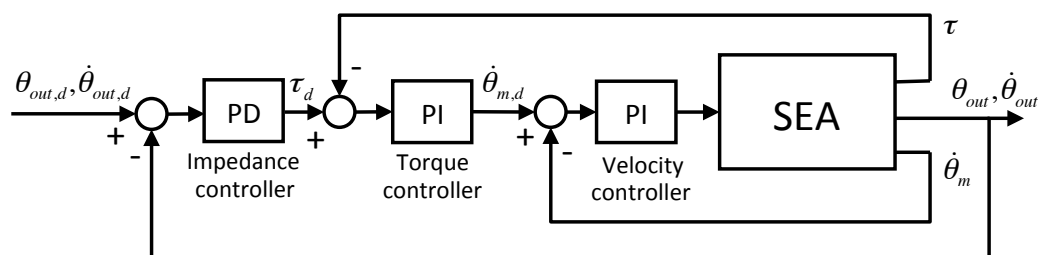


Figure 3.17: SEA torque control scheme. The delivered torque is measured as $\tau = K_s(\theta_m - \theta_{out})$, being θ_{out} the SEA output angle and θ_m the gear motor rotation. $\theta_{m,d}$ is the desired motor velocity as generated by the torque controller.

Giorgio Carpino

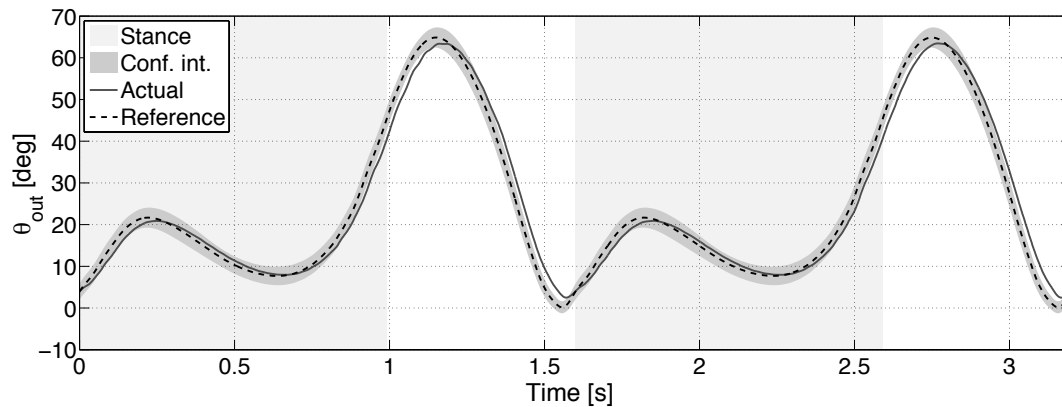


Figure 3.18: SEA 90W position tracking for a typical knee profile during over-ground walking (gait cycle duration: 1.6 s), with superimposed confidence intervals ($p < 0.05$). RMS error is 2.7 deg.

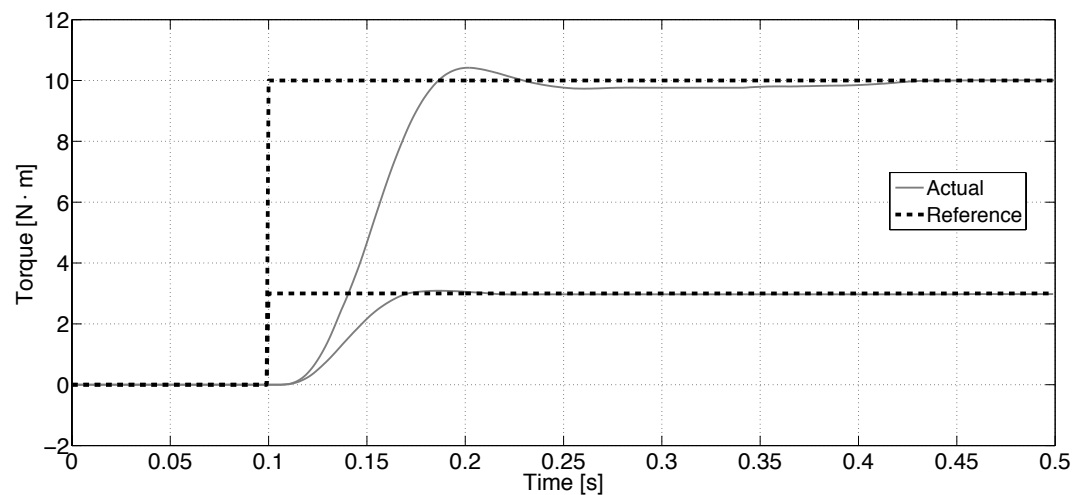


Figure 3.19: Response of the system to torque step commands (amplitude 3 N·m and 10 N·m, with blocked actuator output).

reference torque signal, with amplitude equal to 10 N·m and frequency 5 Hz, to assess whether the torque controller is capable of providing the required peak torque at 5 Hz. The result is shown in Figure 3.20, showing that the torque bandwidth is effectively equal to 5 Hz, for a reference torque signal of 10 N·m.

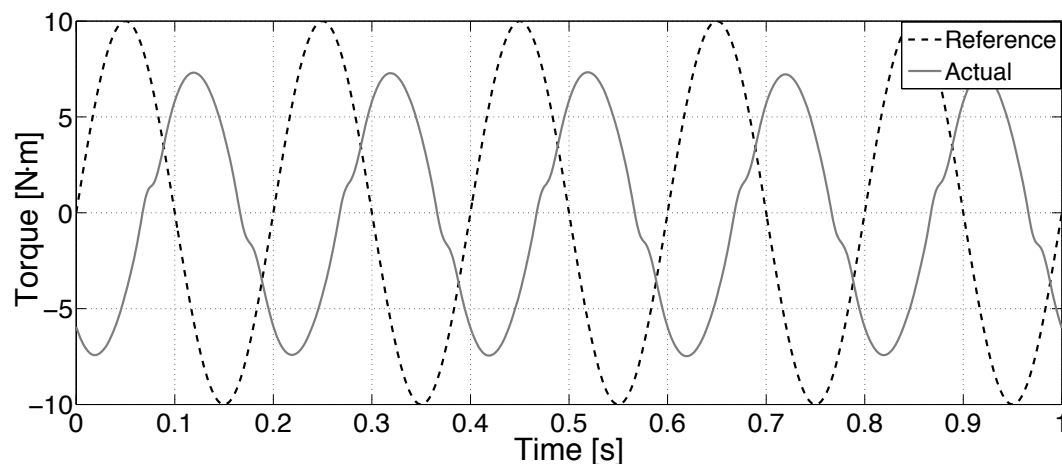


Figure 3.20: Steady-state response of the system to a torque reference sinusoid, amplitude of 10 N·m, corresponding to a RMS value of 7.07 N·m. Signal drop at this frequency is 3.1 dB, with a phase lag of 126 deg.

3.1.4 Conclusions and future works

The chosen application field poses significant challenges to the design of an actuator, since it requires high performances in terms of both amplitude and bandwidth of torque regulation, and also the addition of limited mass and inertia in order to minimally perturb the wearer's knee natural movements. SEA architecture introduces an important advantage in wearable robotics, since it provides intrinsic compliance in the transfer of mechanical energy between actuators and human limbs. However, such compliance is obtained at the cost of reducing torque regulation capabilities at high frequencies.

The presented design is developed with the aim of fulfilling a set of requirements defined on the basis of gait analysis data of target users. A major element of the pursued design is the torsional spring, which was purposively optimized and fabricated, since no commercial component would have been able to provide the desired torque and stiffness properties in such a compact and lightweight configuration. The manufactured component has a significantly lower stiffness than the one required ($119 \text{ N}\cdot\text{m}\cdot\text{rad}^{-1}$ instead of $150 \text{ N}\cdot\text{m}\cdot\text{rad}^{-1}$). Probably the type of stationary FEM analysis carried on is not the most appropriate to solve this type of

3.1. ACTIVE JOINT FOR WEARABLE ROBOTS: SERIES ELASTIC ACTUATOR 90W 71

problem; a time-dependent analysis will be implemented in order to verify the correspondence of simulated and measured stiffness characteristics. Also fabrication inaccuracies expectedly contributed to such discrepancy, given the sensitivity of the torsional stiffness with regards to lamellae thickness.

The SEA 90W weights 1.8 kg and it makes possible to directly include the actuator on the frame of a wearable knee orthosis. In Fig. 3.21 a concept of a knee orthosis actuated by the SEA 90W has been depicted. The actuator is aligned with the center of rotation of the knee joint; the SEA 90W frame is connected to the orthosis link in correspondence of the thigh and the actuator output link is connected to the orthosis link in correspondence of the calf. The orthosis is connected to the human limbs through apposite cuffs.



Figure 3.21: Knee orthosis concept.

A handwritten signature in black ink, appearing to read 'Giorgio Carpino'. The signature is written in a cursive, flowing style.

The performances of the developed prototype have been experimentally characterized using system identification techniques. A velocity-source type torque control scheme allows to regulate a continuous torque of 10 N·m with a bandwidth of 5 Hz. Impedance control was also implemented. Performances in response to externally applied perturbations were experimentally measured, demonstrating that the actuator is able to render virtual stiffness and damping fields in ranges potentially useful in human-robot interaction schemes for gait assistance.

A new version of SEA 90W is under development with the aim of reducing the total dimensions and to improve the performance in term of maximum admissible torque. The frame and the interconnection flanges have been redesigned in order to have a total diameter of 98 mm (reduction of 18% in diameter) and a total length of 127 mm (reduction of 27% in length). The new assembly is shown in Fig. 3.22; furthermore, the components assembly is easier than the first prototype. In order to meet higher requirements in terms of maximum admissible torque new spring design has to be considered also embedding mechanical hard stops to prevent spring failure. A possible spring that could be used to reach these goals is the spring designed for SEA 300W as described in the following paragraphs. The shaft-hub coupling has to be changed since it is probably not a perfect choice since it introduces an asymmetrical force transmission into a symmetrical system. An improvement in the sensors system is also desirable: an addition of a potentiometer between the Harmonic Drive and the spring or the use of two absolute encoders instead of the actual incremental ones can help to detect the rest position ("zero") of the spring and of the entire joint if embedded in a structure like a knee active orthosis.

3.2 Active joint for wearable robots: Series Elastic Actuator 300W

Following the same considerations done in the previous paragraphs, the objective was to develop a novel actuator to be integrated in a full lower limbs wearable robots able to provide assistance during gait.

In order to comply with the requirements of:



3.2. ACTIVE JOINT FOR WEARABLE ROBOTS: SERIES ELASTIC ACTUATOR 300W 73

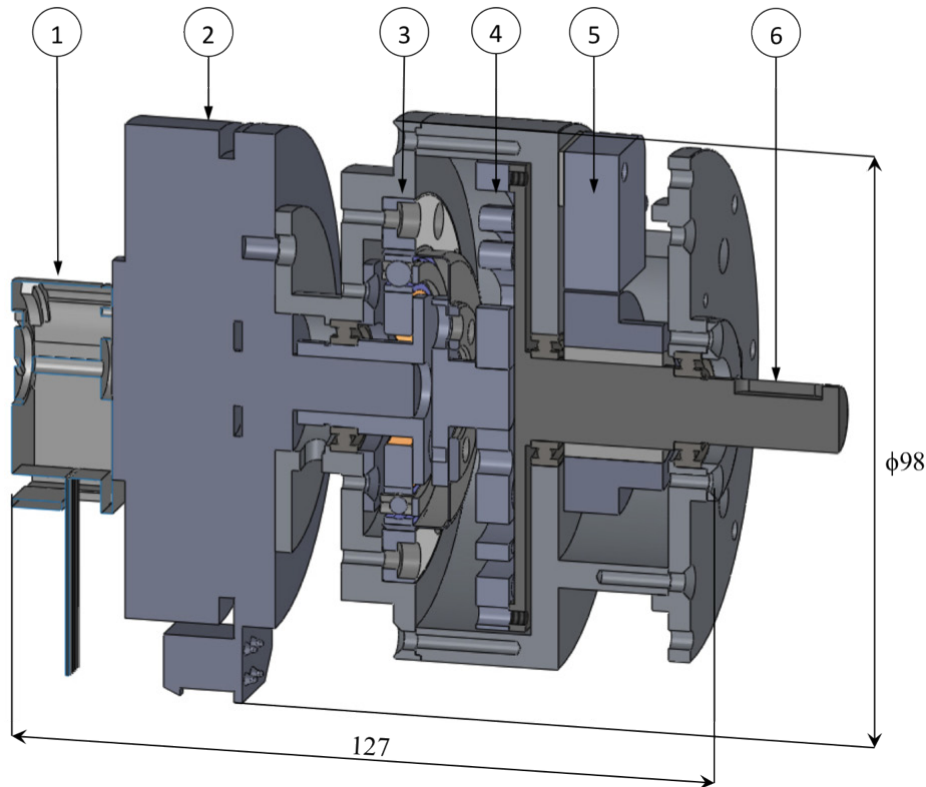


Figure 3.22: Cross section of the second version of SEA 90W. 1: optical incremental encoder, 2: flat DC motor, 3: Harmonic Drive, 4: torsional spring, 5: magnetic incremental encoder, 6: output shaft. Dimensions: 98 mm (diameter) \times 127 mm (axial length).

- tolerance to external shocks so to improve the intrinsic safety of the system;
- low intrinsic actuator output stiffness;
- reduced effects of stiction, friction and backlash;
- simple control of the system;

also in this case a series elastic configuration has been adopted.

3.2.1 SEA 300W requirements

The SEA 300W is designed for assisting hip or knee flexion/extension during gait. Considering the normal-walking data set described in [96] for a person of 75 kg, the maximum instantaneous power exerted by the hip during normal walking is about 53 W with a maximum torque of 45 N·m while the maximum instantaneous power exerted by the knee during normal walking is about 56 W with a maximum torque of 46 N·m. In order to provide a full assistance to both human joints required during overground walking, a target of 40 N·m for actuator peak output torque has been selected as design requirement for the actuator. However, the reduction in the duration of the swing phase also imposes that torque regulation needs to be fast enough to provide rapidly changing assistance levels during walking.

The stiffness of the series elastic element also in this case needs to be carefully selected in order to trade-off between performances, adaptability and safety. As already described for the SEA 90W, in order to be included in a torque control scheme, the compliant element is required to be verified against the maximum output torque supplied by the actuator and to possibly provide a linear torque vs. rotation relationship both in static and dynamic conditions directly connecting the spring to the load, so to avoid the effect of force fidelity reduction caused by transmissions non-linearities. The physical stiffness values of SEAs for locomotion assistance, as retrieved from a literature analysis may range from 100 to 300 N·m·rad⁻¹ [84, 85, 89, 90]. Considering this assumption a stiffness value of 200 N·m·rad⁻¹ will be taken as specification for the spring. A peak torque of 40 N·m has been considered as target for the design of the elastic element of the actuator as suitable to assist motion of human hip and knee joints.

Moreover, actuator dimensions and weight must be reduced as much as possible. The requirements in terms of torque and power have been increased respect to the SEA 90W and the requirements for the total weight and dimensions of the actuator have been consequently increased. It is reasonable to require the actuator to have a weight lower than 4 kg and to be contained in a volume of 100 × 200 × 350 mm³.

For the sake of clarity, in Tab. 3.6 the SEA300W requirements are listed.



3.2.2 SEA 300W design

This paragraph describes the SEA 300W components (motor, reduction gear, torsional spring, sensors) and the related design choices. The design architecture of the developed SEA 300W has been conceived in order to dislocate the actuator center of mass respect to the actuated human joint. This choice has been made in order to reduce the encumbrance of the actuator, caused by the presence of a non-flat motor in the SEA architecture, when integrated in a lower limbs WR. In this way the gearmotor can be placed parallel to the limb to be actuated lowering the encumbrance in the sagittal plane. In Fig. 3.23 a picture of the prototype is reported.

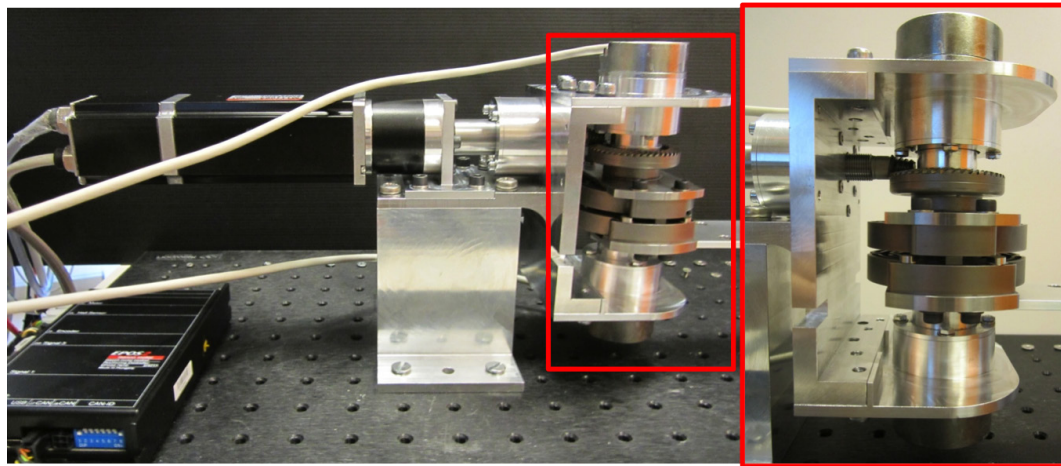


Figure 3.23: Picture of the assembled SEA 300W prototype: the frame is fixed to an aluminum support, while the output link is free. On the right a zoom view of the components inside the fork-shaped frame.

TABLE 3.6: SEA 300W REQUIREMENTS.

Characteristics	Values
Output Stiffness	$200 \text{ N}\cdot\text{m}\cdot\text{rad}^{-1}$
Peak torque	$40 \text{ N}\cdot\text{m}$
Nominal velocity	$6.2 \text{ rad}\cdot\text{s}^{-1}$
Max dimensions	$100 \times 200 \times 350 \text{ mm}^3$
Max weight	4 kg
Minimum bandwidth	4 Hz

Giorgio Carpino

In Fig. 3.24 a block scheme of the actuator is depicted highlighting the serial configuration of the different components.

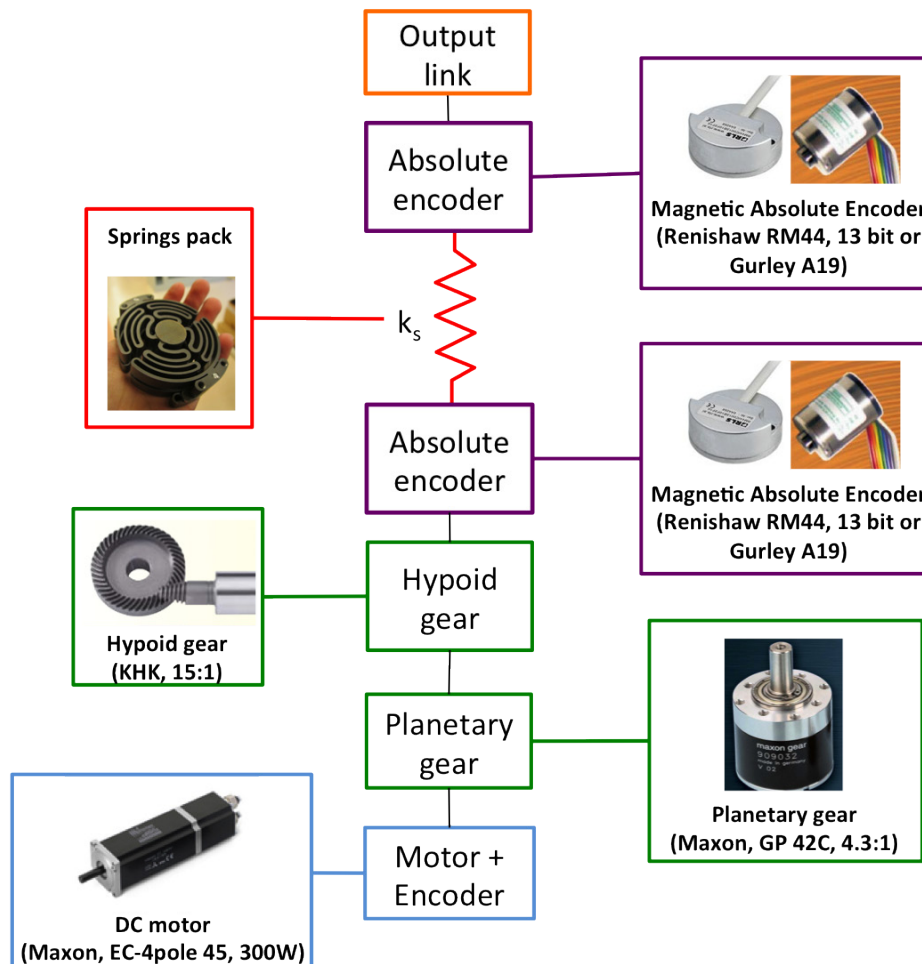


Figure 3.24: Block scheme of SEA 300W.

A 300 W brushless DC motor (Maxon EC-4pole 45, 300W) with a weight of 1130 g, and a maximum continuous torque of 635 mN·m has been selected. The motor also integrates a 2048 cpt optical incremental encoder (R35i) to measure motor rotation with a resolution of 0.044 deg when using quadrature reading.

The reduction gear has composed by two different reduction stages in series. The first reduction stage is composed by a Maxon planetary gear GP 42C with a reduction ratio 4.3:1 directly connected to the motor with an efficiency of 90%. For

Giorgio Carpino

3.2. ACTIVE JOINT FOR WEARABLE ROBOTS: SERIES ELASTIC ACTUATOR 300W 77

the second reduction stage a hypoid gear has been selected because of its high efficiency. A KHK hypoid gear with reduction ratio 15:1 has been implemented rendering an efficiency of 85%. The efficiency of the actuator, as product of the efficiency of the two reduction stages in series, is equal to 76.5%, still guaranteeing the backdrivability of the actuator. The hypoid gear is thus connected to the same shaft where the input port of the custom made springs pack, described in the next paragraph, engages.

On the input and on the output shafts of the springs pack two absolute encoders have been placed to measure the total deflection of the springs pack, used as parameter for SEA torque control. The sensorization scheme of SEA 300W follows the scheme depicted in Fig. 3.25. The SEA 300W prototype has the possibility to connect two type of absolute encoders with two different resolution: 13 bit absolute encoders Renishaw Magnetic RM44 (allowing a torque quantization of 0.15 N·m) or 15 bit absolute encoders Gurley A19 (allowing a torque quantization of 0.03 N·m).

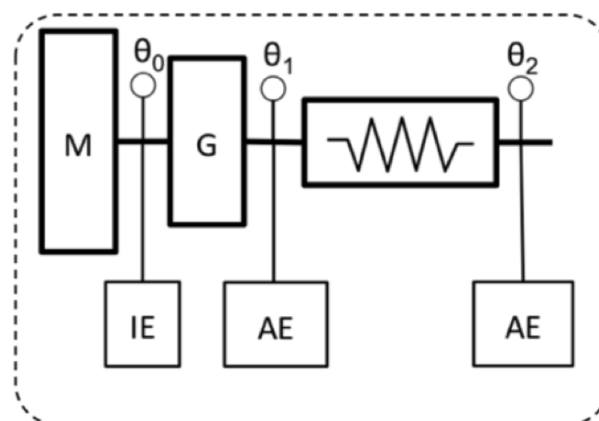


Figure 3.25: Sensorization block scheme of SEA 300W. *M* is the motor, *IE* is the incremental encoder on the motor side measuring the angle θ_0 , *G* are the reduction gear stages, *AE* represent the absolute encoders measuring the angles θ_1 and θ_2 on the input and the output ports of the springs pack.

Figure 3.26 depicts a 3D view of the obtained design. The actuator, as described above, is composed by: Maxon EC-4pole 45 300W (Fig. 3.26-1) with an integrated optical incremental encoder; Maxon planetary gear 4.3:1 (Fig. 3.26- 2); abso-

lute encoder on the input port of the springs pack (Fig. 3.26-3); fork-shaped frame (Fig. 3.26-4); KHK hypoid gear 15:1 (Fig. 3.26-5); custom springs pack (Fig. 3.26-6); output link (Fig. 3.26-7); absolute encoder on the output port of the springs pack (Fig. 3.26-8). The overall dimensions are: 335 mm (length) \times 164 mm (thickness) and the overall actuator mass is 3.5 kg, thus fulfilling the requirements reported in the previous paragraph.

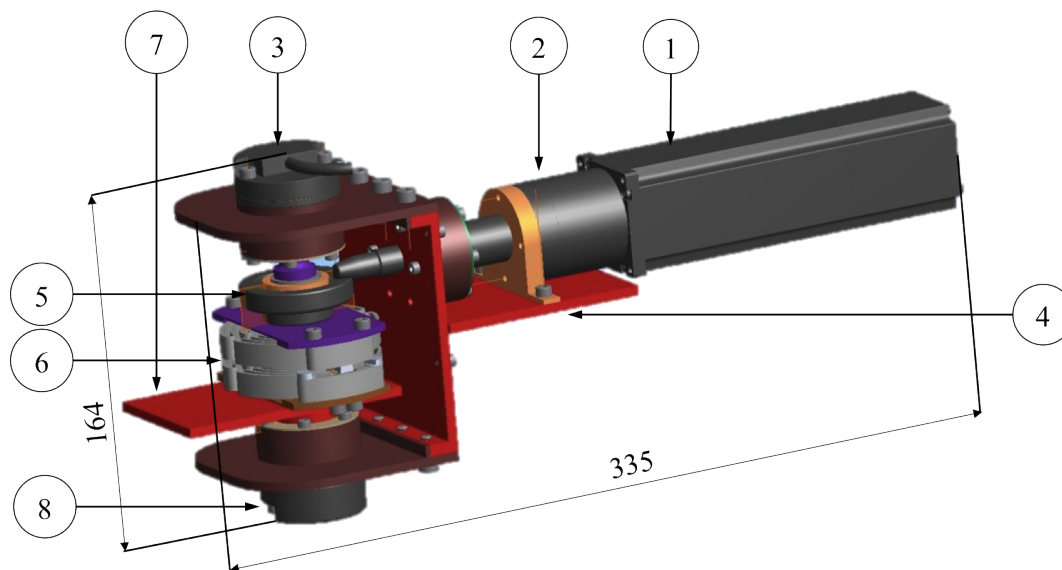


Figure 3.26: 3D CAD view of rotary SEA 300W. 1: Maxon EC-4pole 45, 300W equipped with an integrated incremental encoder, 2: Maxon planetary gear, 3: absolute encoder, 4: fork-shaped frame, 5: KHK hypoid gear, 6: springs pack, 7: output link, 8: absolute encoder. Dimensions: 164 mm (thickness) \times 335 mm (axial length). Total mass is 3.5 kg.

3.2.2.1 SEA 300W springs pack

The same considerations made for SEA 90W about the necessity of introducing an intrinsic compliance in the actuation system of assistive robots to improve the system intrinsic safety and dynamical adaptability can be extended also in the case of SEA 300W. Commercially available compliant components are still not able to guarantee to obtain the desired requirements in terms of admissible peak load-

ing demanded by gait assistance, while guaranteeing a compact and lightweight design.

The aim has been to develop a compact, monolithic, torsionally compliant system, which can be included in the SEA 300W. The dimensioning of the physical stiffness of the spring emerges, as already said, from tradeoff between two objectives: (i) increasing the Large Force Bandwidth (LFB) and (ii) reducing the intrinsic mechanical impedance. The desirable physical stiffness values of SEAs for locomotion assistance, as retrieved from a literature analysis may range from 100 to 300 $\text{N}\cdot\text{m}\cdot\text{rad}^{-1}$ [84, 85, 89, 90]. Considering this assumption, a stiffness value of 200 $\text{N}\cdot\text{m}\cdot\text{rad}^{-1}$ will be taken as specification for the torsional springs pack. A peak torque of 40 $\text{N}\cdot\text{m}$ has been considered as target for the design of the elastic element of the WR SEA as suitable to assist motion of the human hip and knee joints. In order to satisfy these requirements of stiffness and admissible peak torque, a serial configuration of two equal custom torsional springs has been pursued, as it is shown in Fig. 3.27-a. In this serial configuration, each spring is loaded with a maximum torque of 40 $\text{N}\cdot\text{m}$ rendering a stiffness of 400 $\text{N}\cdot\text{m}\cdot\text{rad}^{-1}$ and deflecting half of the total deflection of the springs pack. The two internal rings of the springs are connected through the same shaft, while the torque is transmitted between the external springs rings through the input and the output ports, as depicted in Fig. 3.27-c. Furthermore, the serial configuration allows to implement mechanical hard stops connected in parallel to the springs in order to prevent failure due by applied torques bigger than 40 $\text{N}\cdot\text{m}$ (see Fig. 3.27-b). The mechanical hard stops for applied torques bigger than 40 $\text{N}\cdot\text{m}$ contact each other thus preventing the overdeflection of the two springs and consequently guaranteeing the intrinsic safety of the system.

In Tab. 3.7 the requirements for the springs pack are summarized.

3.2.2.2 SEA 300W custom torsional spring

In order to minimize weight and dimensions, a monolithic disc-shaped design is pursued as in the case of SEA 90W, since it allows minimizing the bulk in the axial direction, still maintaining an acceptable total thickness. This shape implies that



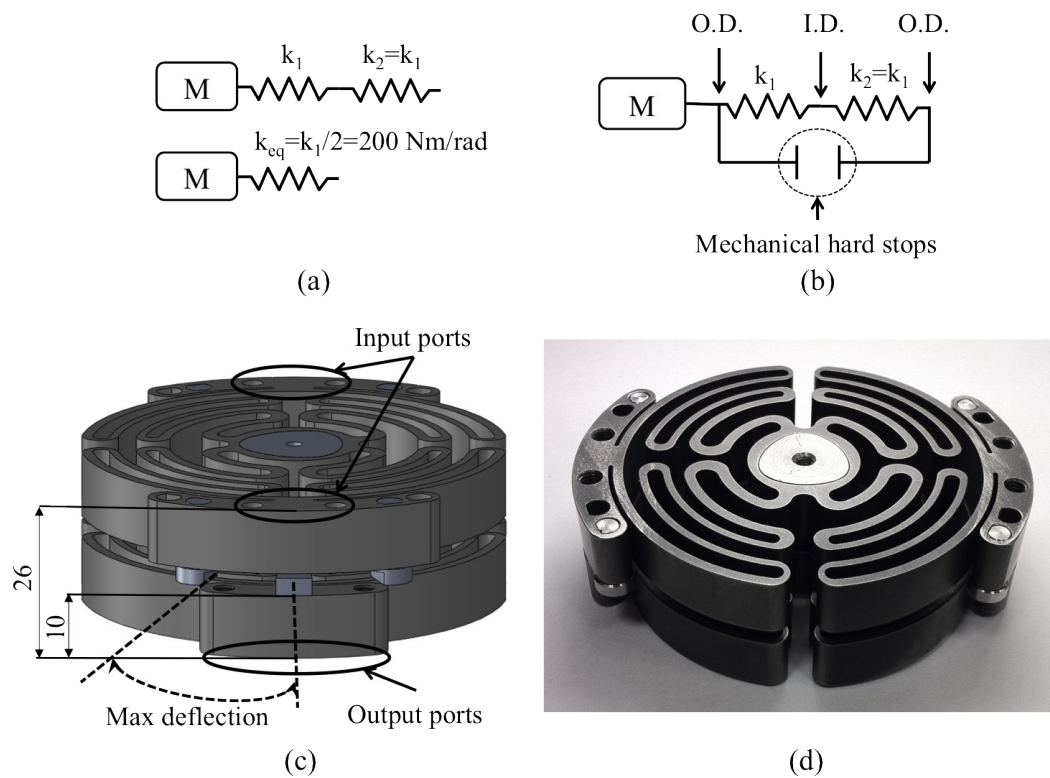


Figure 3.27: Springs pack: serial configuration of two equal torsional springs. (a) Block scheme of the serial configuration of two springs with equal stiffness, $k_1=k_2$. The k_{eq} is half of the stiffness of each springs, in this case $200 \text{ N}\cdot\text{m}\cdot\text{rad}^{-1}$. (b) Block scheme of the parallel connection of mechanical hard stops and springs pack to prevent system failure. (c) 3D view of the springs pack; input and output ports and maximum deflection allowed by the mechanical hard stops are highlighted. Dimensions of the springs pack: 80 mm (external diameter) and $\times 26 \text{ mm}$ (thickness). (d) Picture of the springs pack.

Giorgio Carpino

TABLE 3.7: SEA 300W SPRINGS PACK REQUIREMENTS.

Characteristics	Values
Stiffness	200 N·m·rad ⁻¹
Max torque	40 N·m
Max deflection	0.2 rad
Max outer diameter	100 mm
Max thickness	30 mm
Max weight	300 g
Fatigue life	≥ 10 ⁶ stress cycles

the transfer of torsional torque is between an outer ring (diameter of 80 mm) and an inner ring (diameter of 16 mm). Compliance is obtained by interposing flexible elements between the two rings. The shape and dimensions of such flexible elements are defined through an iterative Finite Element Method (FEM) simulations-based design and optimization process.

The optimization algorithm described in Fig. 3.7 does not produce absolute optimal solutions. Rather, it depicts a search strategy which halts as soon as a solution compatible with the requirements is found. The geometry, which halted the search for the SEA 90W model, does not satisfy the requirements of the 300W model. Therefore, a new search was initiated for the SEA 300W model. The search seeds are manually selected, using a heuristic approach. The resulting geometry is quite different from the previous one.

The topology chosen for the spring of SEA 90W is thus not adequate for the new requirements, listed in Tab. 3.8. A different topology has been chosen able to store more elastic energy and to render a stiffness of 400 N·m·rad⁻¹ under a load up to 40 N·m still guaranteeing an infinite life of the component.

The design of the torsional spring has been conducted following the same iterative Finite Element Method (FEM) simulations-based design and optimization process described by the flowchart in Fig. 3.7. The corresponding selected morphology includes four replications of worm-shaped lamellae. Lamellae provide the necessary compliance, acting as curved thin beam.

As in the case of SEA 90W, Bohler W720 (maraging steel 300, Young modulus of



TABLE 3.8: SEA 300W TORSIONAL SPRING REQUIREMENTS.

Characteristics	Values
Stiffness	400 N·m·rad ⁻¹
Max torque	40 N·m
Max deflection	0.1 rad
Max outer diameter	100 mm
Max thickness	10 mm
Max weight	150 g
Fatigue life	≥ 10 ⁶ stress cycles

193 GPa) was the material selected for the strength analysis, due to his high nominal yield stress of 2 GPa and ultimate tensile strength of 2.1 GPa after an aging treatment of 3 hours at 500°C). Figure 3.28 shows the resultant springs (female on the left and male on the right) manufactured by Wired Electrical Discharge Machining (WEDM) and then ground; springs total dimensions are 80 mm for the outer diameter and 10 mm for the thickness. A shaped shaft/hub coupling (P3G polygone) has been adopted as connection between the two springs internal rings; this choice has been implemented in order to reduce the backlash between the shaft connecting the two springs and the springs themselves and to reduce the fretting surface fatigue due to the coupling.

FEM static stress-strain analyses (COMSOL Multiphysics 3.5, Comsol AB) have been performed in order to optimize the mechanical design to satisfy the reported design objectives. In the static analysis, the boundary conditions include the fixation of the internal surfaces of the tapped holes on the external arcs to ground (red arrows in Fig. 3.29) and loading the internal surface of the inner annulus (approximated for simplicity with a circle of 16 mm in diameter) with a tangential distributed force (blue arrows in Fig. 3.29), representing the equivalent applied torsional moment, calculated as in the case of SEA 90W spring.

A one layer swept tetrahedral mesh has been used (Fig. 3.29); the distribution method is linear with an element ratio equal to 1. The adopted sweep path is straight. The mesh is refined about higher curvature elements (e.g. lamellae and holes), while it is coarser in correspondence of the external ring, where lower



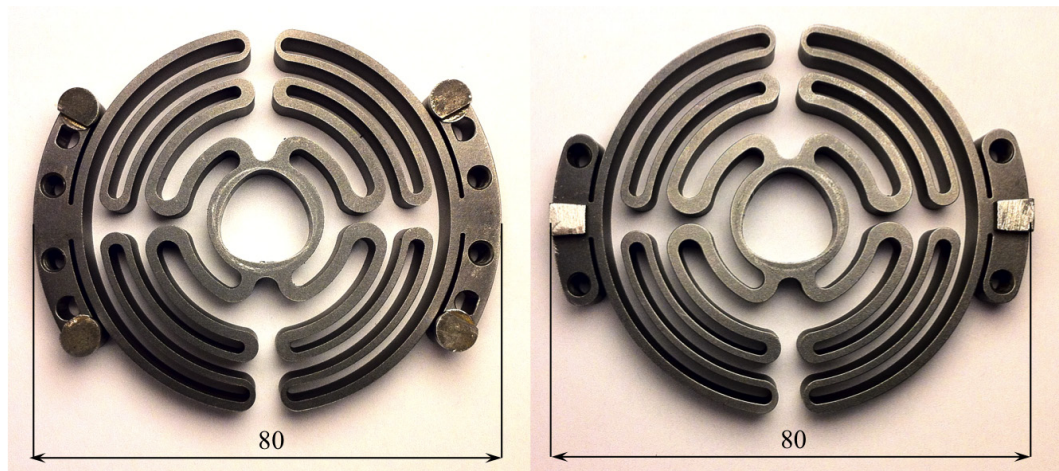


Figure 3.28: Pictures of the custom torsional springs for SEA 300W. On the left the female spring (input side of the springs pack) and on the right the male spring (output side of the springs pack). The springs morphology are equal but they only differ on the holes present on the outer arcs. A shaped shaft/hub coupling (P3G polygone) has been adopted as connection between the two springs internal rings. Dimensions: 80 mm (external diameter) and $\times 10$ mm (thickness).

stresses are expected.

A stationary non linear solver (SPOOLES) with a relative tolerance of 10^{-6} has been used. Large deformations have been implemented in the simulations. In Fig. 3.30, 1:1 spring deformation and von Mises stress as obtained by the FEM simulation are reported under an applied torsional moment of 40 N·m. The maximum resultant von Mises stress is 0.87 GPa. Considering that the yield stress of the selected material (σ_y) is 2 GPa and knowing that $SF = \sigma_y / \sigma_{max}$, a SF of 2.3 is achieved. The resultant external ring rotation is 0.094 rad so obtaining a spring torsional stiffness of $435 \text{ N}\cdot\text{m}\cdot\text{rad}^{-1}$, as predicted by FEM simulations.

The specific energy stored in the component, considering the chosen material and a total weight of 141 g, is equal to 70.3 J/kg.

As it is clear in Fig. 3.28, tapped holes on the outer arcs allow connecting the springs to the input or output shafts acting on the springs pack. The “female” spring is connected to the input shaft and transmit the torque from the gearmotor to the springs pack while the “male” spring is connected to the output shaft and trans-

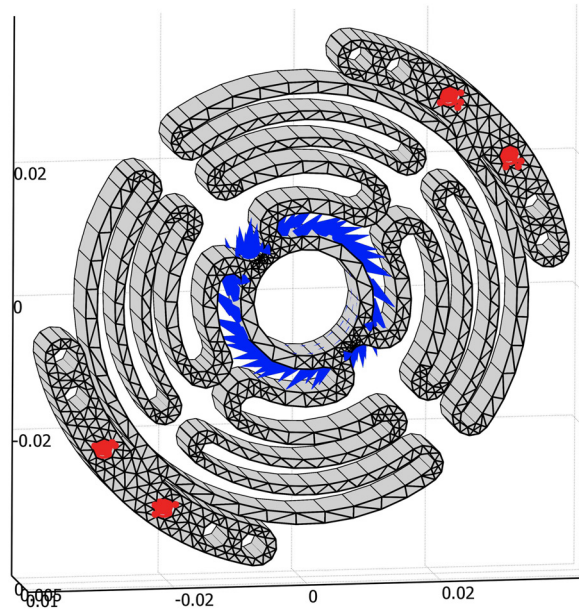


Figure 3.29: Boundary conditions and swept mesh for FEM simulations of torsional SEA 300W spring. Axes dimensions are [m].

mit the torque from the springs pack to the load. The other shaped holes present on the external arcs serve to connect the mechanical hard stops to the springs. On the female spring there are two pairs of four holes allowing the connection of the “female” mechanical hard stops in two ways depending on the real stiffness of the spring. As learned from the characterization of the SEA 90W spring, there could be a discrepancy between the spring stiffness calculated in simulation and the spring stiffness obtained by the spring characterization. In this way it is possible to easily modify the position of the mechanical hard stops correcting the possible discrepancy. The supposed discrepancy between simulated and characterized data has been set equal to 30%. On the male spring, instead, there are only two shaped holes to connect the “male” mechanical hard stops.

3.2.2.3 Characterization of SEA 300W torsional spring

The experimental characterization of the SEA 300W spring was performed using the same custom dynamometric test-bed used for the characterization of the

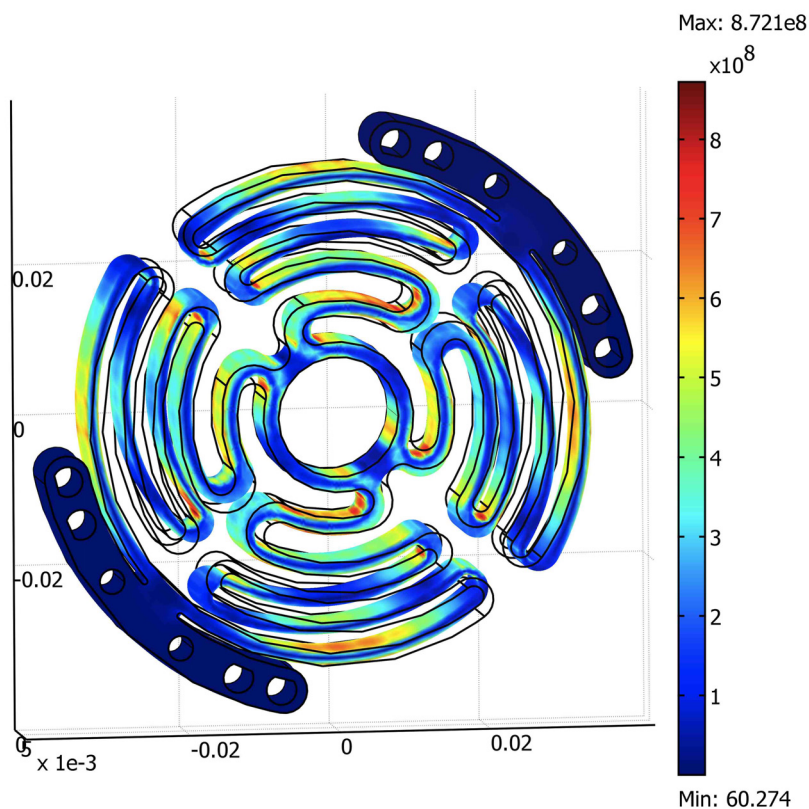


Figure 3.30: von Mises stress in [Pa] and 1:1 spring deformation. Axes dimensions are [m].

SEA 90W. In this case a test motor has been included to drive the spring deflection. The external ring of the spring has been fixed to the test bed frame while the inner ring has been connected to the test gearmotor through a torque sensor (Lorenz Messtechnik GmbH DR-2, nominal measurable torque 50 N·m). The test gearmotor comprises a Maxon EC45 250 W brushless DC motor and a Maxon GP 52C planetary gear (126:1). The gearmotor is equipped with an optical incremental encoder Avago HEDL 9140 (resolution: 0.18 deg). To avoid radial misalignments between the spring and torque sensor shafts, a flexible coupling (Rodoflex ATMK60L77, nominal torque 60 N·m) is used. As already mentioned, the series elasticity introduced by the test bed does not affect the measurements of the spring stiffness. To measure the deflection of the torsional spring a 15 bit encoder has been placed on the

output. An ASM magnetic incremental encoder (reading sensor PMIS4, magnetic wheel PMIR4; resolution of 32768 counts per turn, 0.003 deg with quadrature reading) has been utilized, with the reading sensor fixed to the test bed frame and the magnetic wheel coupled to the internal ring of the spring through the output shaft. In Fig. 3.31 the spring characterization platform has shown.

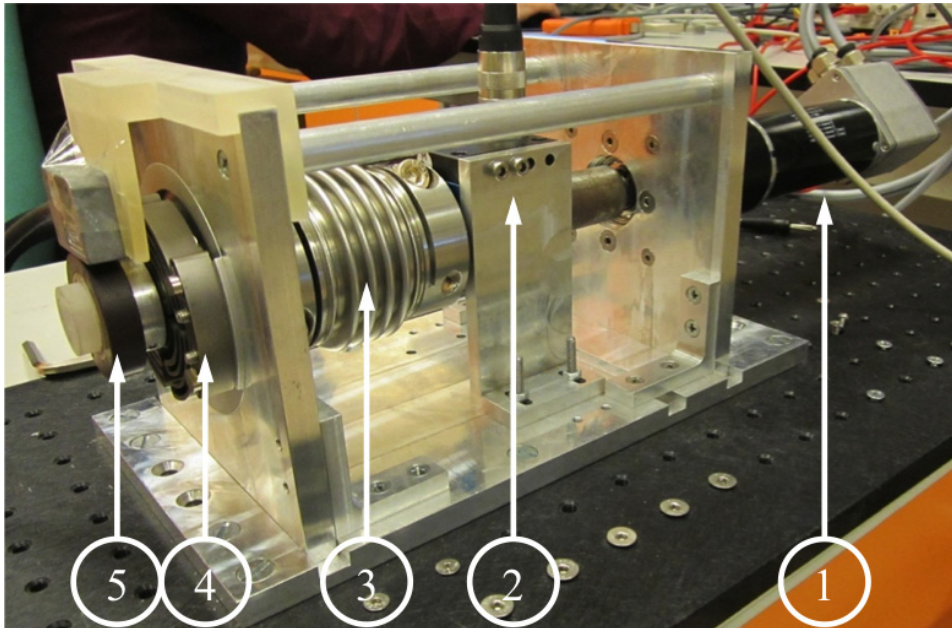
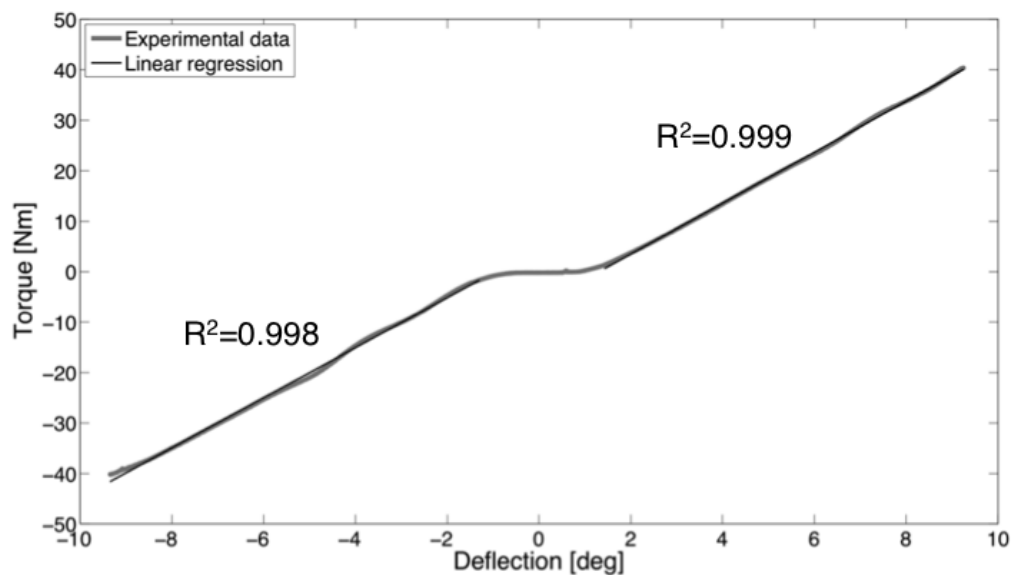


Figure 3.31: Custom dynamometric test-bed used for SEA 300W spring. 1: test motor, 2: torque sensor, 3: flexible coupling, 4: SEA 300W torsional spring, 5: output encoder.

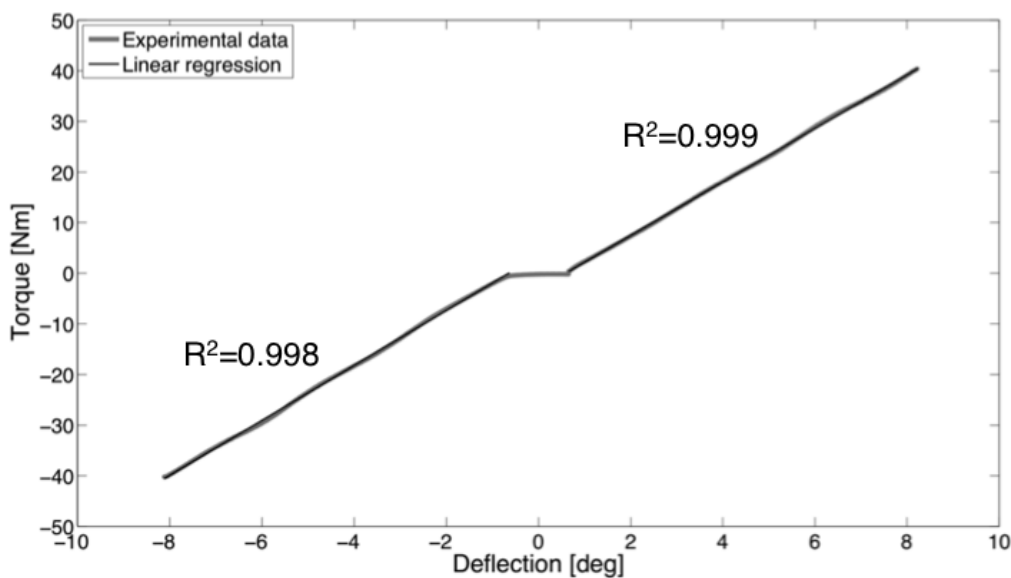
The two springs included in SEA 300W springs pack have been tested. The test motor was commanded with a position ramp (1 deg/s) reversing when 40 Nm torque was reached and the torque necessary to impose a certain spring deflection was measured via the torque sensor, resulting in the two plots shown in Fig. 3.32.

It is possible to observe the presence of a non-negligible backlash (amplitude of 2 deg for the female spring and amplitude of 1 deg for the male spring), determined by the clearance between the shaft and hub coupled by a P3G polygone profile. This clearance has allowed an easier assembly and disassembly of the springs pack for the first tests on the SEA 300W but in the next prototype an interference coupling

A handwritten signature in black ink, appearing to read 'Giorgio Carpino'.



(a)



(b)

Figure 3.32: Characterization of the torsional springs of SEA 300W springs pack (a: female spring, b: male spring). Loading and unloading phases are reported, both for positive and negative deflection. R^2 coefficients refer to the fitting of both positive and negative torque vs. deflection curves to the global stiffness curve.

between shaft and spring hub will be implemented.

Two one-coefficient linear regressions, for positive and negative springs deflection were performed, imposing crossing of the origin. The R^2 coefficients are higher than 0.99 for both positive and negative springs deflections (in both cases 0.999 and 0.998 respectively). The two regression coefficients calculated differed in less than 0.5% in amplitude and allowed to calculate a global stiffness value as their average, providing an estimation of springs stiffness. For the female spring (Fig. 3.32-a) for positive deflections the measured stiffness is $284 \text{ N}\cdot\text{m}\cdot\text{rad}^{-1}$ while for negative deflections is $289 \text{ N}\cdot\text{m}\cdot\text{rad}^{-1}$, with a mean stiffness of $286.5 \text{ N}\cdot\text{m}\cdot\text{rad}^{-1}$. For the male spring, instead, (Fig. 3.32-b) for positive deflections the measured stiffness is $303 \text{ N}\cdot\text{m}\cdot\text{rad}^{-1}$ while for negative deflections is $311 \text{ N}\cdot\text{m}\cdot\text{rad}^{-1}$, with a mean stiffness of $307 \text{ N}\cdot\text{m}\cdot\text{rad}^{-1}$. The differences between the stiffness values measured for the two springs (7% of discrepancy) are probably due to fabrication inaccuracies, given the sensitivity of the torsional stiffness with regards to lamellae thickness, reflecting in a slight variation between springs stiffness.

Also in this case as for SEA 90W spring, the value of K_s determined experimentally is 34% and 29% lower than the one predicted by FEM simulations for the female and male springs respectively. As already mentioned, it is worth to note that this discrepancy cannot be inputted to the series compliance of the characterization setup. Probably the type of stationary FEM analysis carried on is not the most appropriate to solve this type of problem; a time-dependent analysis will be implemented in order to verify the correspondence of simulated and measured stiffness characteristics.

A fatigue analysis has also been performed following the indications in [103] considering a sinusoidal load with a peak value of $40 \text{ N}\cdot\text{m}$. The fatigue strength σ_f , considering more than 10^6 working cycles, can be expressed as:

$$\sigma_f = 0.5 \sigma_R \cdot C_L \cdot C_G \cdot C_S \quad (3.5)$$

where σ_R is the ultimate tensile strength of the spring material ($\sigma_R=2.1 \text{ GPa}$), C_L is the load coefficient ($C_L = 1$), C_G is the stress gradient coefficient ($C_G = 0.9$) and C_S is the surface finish coefficient ($C_S = 0.95$) due to the manufacturing process




TABLE 3.9: SEA 300W TORSIONAL SPRINGS AND SPRINGS PACK PROPERTIES.

	Female spring	Male spring	Springs pack
Stiffness	286.5 N·m·rad ⁻¹	307 N·m·rad ⁻¹	142.2 N·m·rad ⁻¹
Max torque	40	40	40
Max deflection	0.14 rad	0.13 rad	0.28 rad
Outer diameter	80 mm	80 mm	80 mm
Thickness	10 mm	10 mm	26 mm
Weight	141 g	141 g	322 g
Specific energy	70.3 J/kg	70.3 J/kg	70.3 J/kg
Estimated fatigue life	> 10 ⁶ stress cycles	> 10 ⁶ stress cycles	> 10 ⁶ stress cycles

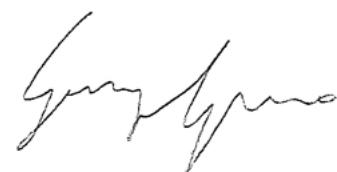
(i.e. WEDM plus grinding process leading to a final surface roughness equal to 0.8). Under these conditions, the fatigue strength is equal to 898 MPa. The maximum stress, as described above, is equal to 872 MPa for an applied torque of 40 N·m and it is lower than the value of calculated fatigue strength thus verifying the infinite life of the component.

In Tab. 3.9, the relevant mechanical properties of the two torsional springs and the consequent properties of the springs pack are reported, as experimentally characterized.

3.2.3 Conclusions and future works

The augmentation in design requirements for SEA 300W respect to SEA 90W in terms of output torque and power has led to different architectures of the two actuators. On one hand, in the case of SEA 90W, the actuator architecture has been designed so to co-locate the actuator center of mass within the actuated joint; on the other hand, due to its encumbrance and augmented weight, the SEA 300W architecture has been conceived in order to de-locate the center of mass of the actuator within the actuated joint in order to allow an easier integration of the same actuator in the frame of a WR.

The performances of the springs pack have been experimentally characterized. SEA 300W prototype is currently in its characterization phase through system identification techniques. A velocity-source type torque control scheme and impedance control will be implemented. Performances in response to externally applied per-



turbations will be experimentally measured, demonstrating that the actuator is able to render virtual stiffness and damping fields in ranges potentially useful in human-robot interaction schemes for gait assistance.

A new version of SEA 300W is under development with the aim of reducing the thickness of the fork-shaped frame and to improve the performances in term of maximum output torque. To reduce the total thickness, the 15 bits absolute encoders have been brought inside the fork implementing a non-colocated measurement of springs pack deflection using gears with reduction ratio of 2:1. The output resolution is increased to 65536 cpt because of the presence of the reduction stage acting as multiplier stage for the absolute encoders. The gears module has been chosen equal to 0.2 in order to minimize the possible backlash introduced by the gear itself. This new arrangement of the two encoders allows to place the output link outside the fork enabling its 360 deg motion and thus facilitating its use as a robot actuator.

To improve the SEA 300W performances, a new springs pack has been designed. The upper limit of the torque delivered by the first SEA 300W prototype (40 N·m) was indeed given by the springs maximum admissible torque. The objective is to reach an output peak torque of 60 N·m. The new springs pack is still constituted by a serial configuration of two equal springs. The morphology of the springs is the same but the springs have to be verified against a peak torque of 60 N·m still guaranteeing an infinite life. To fulfill these new requirements slight modifications in the springs shape have been done in order to increase the elastic energy storable in the torsional springs; in particular, the diameter of each spring has increased from 80 mm to 90 mm and the thickness has increased from 10 mm to 11 mm. Moreover, the coupling between the two springs is not obtained by a P3G polygone shaft as for the first version; now, the whole springs pack is manufactured as a single block avoiding all the problems related with the backlash in the shaft/hub couplings. The internal cavity and the shape of the springs is obtained by WEDM. The springs are connected with the input and output shafts by a shaped shaft/hub coupling through apposite flanges present at the end of the shafts. Although the thickness of each spring is increased of 1 mm, a new configuration of the mechanical hard



stops, still positioned in parallel to the springs, allows a reduction in springs pack thickness of 2.5 mm respect to the springs pack of SEA 300W first prototype; the springs pack diameter, instead, will increase from 80 mm to 90 mm. In Fig. 3.33 the new springs pack is shown.

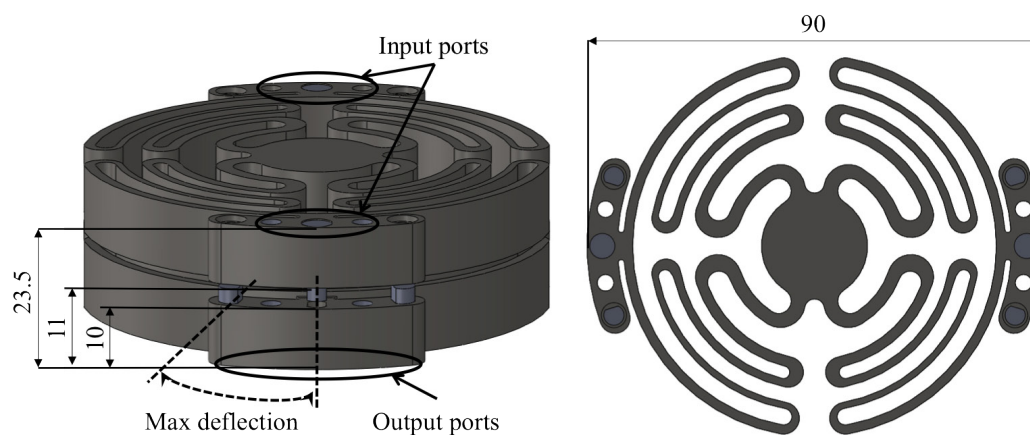


Figure 3.33: 3D and frontal views of the second version of the springs pack implementing a serial configuration of two equal torsional springs. Input and output ports and maximum deflection allowed by the mechanical hard stops are highlighted. Dimensions of the springs pack: 90 mm (external diameter) and \times 23.5 mm (thickness).

Furthermore, the fork has been reinforced with a C-shaped support with the aim of closing the fork-shaped frame thus preventing the possible undesired deflection of the frame which can affect the alignment of the pinion and gear.

These design optimization will lead to a reduction in the total thickness of SEA 300W of about 33% (164 mm against 110 mm of the second version of SEA 300W). In Fig. 3.34 the 3D CAD of the new version of SEA 300W is shown.

3.3 Passive joint for wearable robots: passive viscoelastic joint

In the design of WRs that strictly interact with HB and, in general, in any robotics application that involves the human component, the possibility of having modular

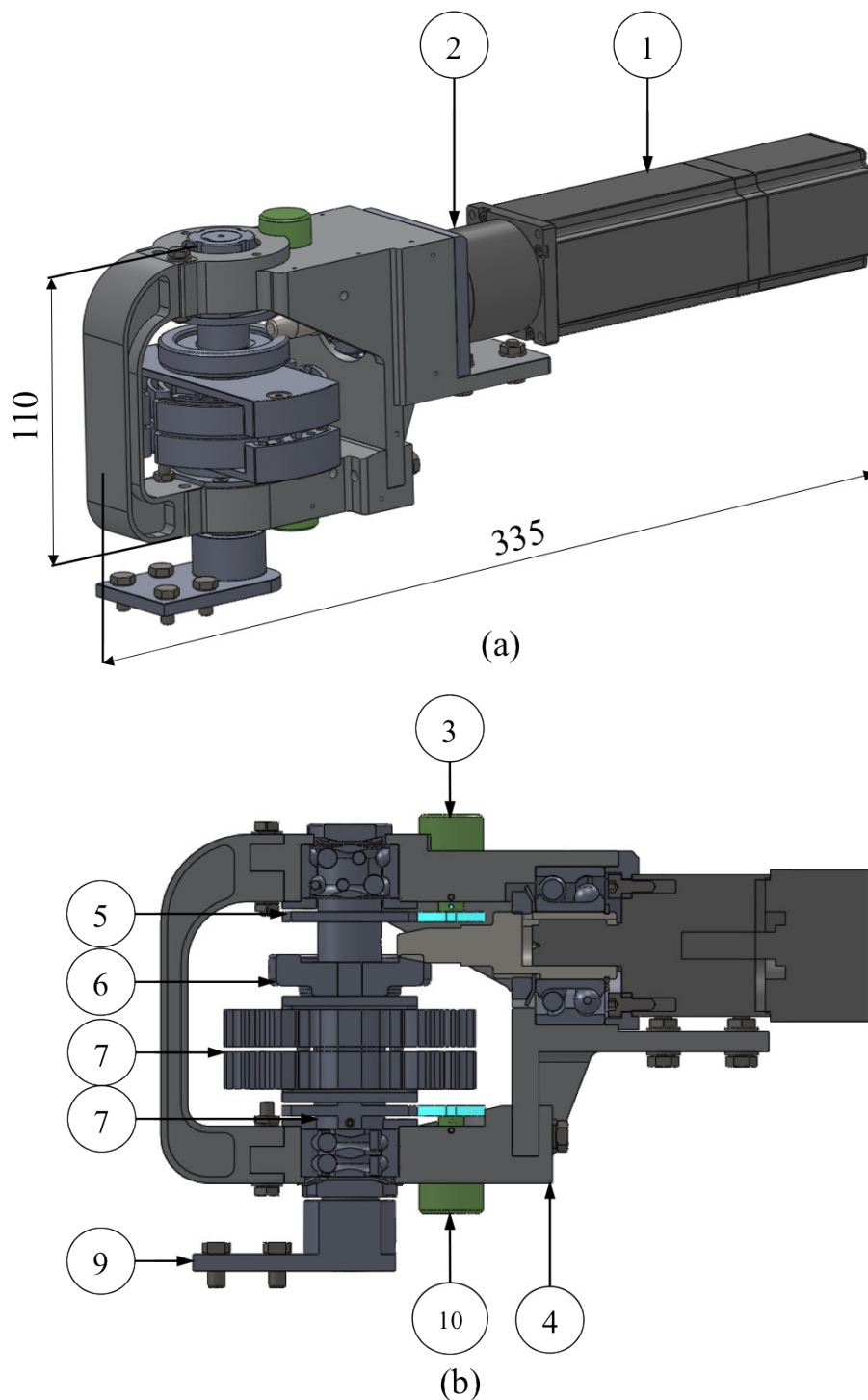


Figure 3.34: (a) 3D CAD view of the second version of SEA 300W; (b) Zoom of the cross section at hypoid gear level. 1: Maxon EC-4pole 45, 300W equipped with an integrated incremental encoder, 2: Maxon planetary gear, 3: absolute encoder, 4: fork-shaped frame, 5: absolute encoder gear; 6: KHK hypoid gear, 7: new springs pack, 8: absolute encoder gear, 9: output link, 10: absolute encoder. Dimensions: 110 mm (thickness) \times 336 mm (axial length). Total mass is 3.5 kg.

Giorgio Carpino

joints able to produce a viscoelastic behaviour is very useful to achieve an efficient and safe human-robot interaction and to give rise to emergent dynamical behaviors. In complex dynamical tasks human motor control notably exploits the possibility of regulating joints mechanical impedance, both for stability and for energetic optimization purposes. These biomechanical findings should translate in design requirements for wearable robotics joints, which are required to produce adaptable intrinsic viscoelastic behaviors. The development of robots that can establish dynamic interactions with the human body requires the use of joints and actuators which mechanical impedance can be adjusted (i.e. VIJ, Variable Impedance Joints and VIA, Variable Impedance Actuators). The tuning of the mechanical impedance, which is usefully exploited to perform different tasks, allows improving the dynamical performances of a joint, similarly to the variation of human joints stiffness [104].

Solutions where the stiffness of passive elements can be modulated allow achieving both high energetic efficiency and a safer pHRI. Regarding variable stiffness actuators a substantial number of designs have been developed [105, 106, 107, 108, 109, 110, 111, 112, 113].

Compared to solutions based on active control, the main disadvantage of regulating impedance by purely mechanical means consists in their complexity, which reverberates on increased mass and volume. A number of attempts have been made to overcome this limitation.

As it regards torsional springs, a classification has been already provided in the previous paragraphs. As it regards dampers, they are often developed so to exploit the tunable viscosity of electrorheological [114, 115] or magnetorheological [116, 117] fluids. In these systems, the rheological properties of the fluid, and the resultant damping, are controlled through an electric or magnetic field. The above-mentioned solutions show some drawbacks in terms of large volume, high weight and mechanical complexity. An alternative approach focuses on *frictional* dampers, where energy is dissipated in the contact between moving parts. In such devices, damping can be modulated by modifying the contact of two surfaces through piezoelectric actuators [118] or by compressing a stack of discs [119, 120]. These systems



have the advantage of being compact and lightweight, but they may be expectedly affected by surfaces wearing.

All the proposed approaches are not capable to tune via hardware both stiffness and damping of the joint; they rely on the control for what concerns damping regulation.

The objective was to design a compact rotary passive ViscoElastic Joint (pVEJ), comprising purely mechanical stiffness and damping modules acting in parallel on the output shaft where torque-rotation angle and torque-angular velocity characteristics can be manually set [121].

3.3.1 pVEJ requirements

The aim is to design a modular robotic joint with intrinsic viscoelastic properties, which components can be easily substituted, in order to comply with the requirements of different operative conditions. The system has to integrate two functionally distinct sub-modules: one to render a desired torsional stiffness profile and the other to provide a desired torsional damping.

The pVEJ has to be mounted on the passive (i.e. not actuated) joints of a lower limbs active orthosis, in order to establish an optimal dynamical coupling between the robot and the human body. For this reason, the target ranges of torsional stiffness and damping coefficients to be rendered by the pVEJ have been chosen to be of the same order of magnitude of those exhibited by the human lower limbs joints [101, 102]: stiffness varies from 0 to $1.7 \text{ N}\cdot\text{m}\cdot\text{deg}^{-1}$, the damping from 0 to $3.5 \cdot 10^{-2} \text{ N}\cdot\text{m}\cdot\text{s}\cdot\text{deg}^{-1}$. Moreover, in the intended application torsional stiffness should not be constrained to be constant, but it should also vary with joint angle (e.g. constant, linear and quadratic stiffness-angle behaviour). As it will be shown in the following, other stiffness-angle relations can be easily rendered, by purposely shaping an interchangeable cam. The stiffness of the pVEJ can thus be changed by accordingly changing the cam profile. The maximum input torque is set to $50 \text{ N}\cdot\text{m}$.

Since the joint has to be compact and lightweight because it is intended for assistive WRs applications, the dimensional constraints for the joint were 150 mm for the diameter and 100 mm for the thickness and a maximum of 1.5 kg for the weight.




TABLE 3.10: PVEJ REQUIREMENTS.

Characteristics	Values
Stiffness	0 to $1.7 \text{ N}\cdot\text{m}\cdot\text{deg}^{-1}$
Damping	0 to $3.5 \cdot 10^{-2} \text{ N}\cdot\text{m}\cdot\text{s}\cdot\text{deg}^{-1}$
Max input torque	50 N·m
Outer diameter	150 mm
Thickness	100 mm
Weight	1.5 kg

In Tab. 3.10 the requirements for the passive viscoelastic joint are summarized.

3.3.2 pVEJ concept and dimensioning

The joint has interchangeable modular components to provide different torque-displacement and torque-velocity characteristics, adaptable to a wide range of operative conditions. The two sub-modules for the torsional spring and damper will be described in the next sections.

3.3.2.1 Torsional stiffness

The torsional stiffness module is implemented using n linear compression springs connected between the joint shaft and n rollers sliding on cam profiles. This arrangement generates a centering elastic torque $M(\theta)$ against an external rotation of the joint shaft. A desired stiffness characteristic can be achieved by opportunely selecting the shape of the cam. In Fig. 3.35 a schematic representation of the stiffness module is depicted (only one spring k_m is represented).

The analytical expression for the cam profile $r(\theta)$ necessary to implement a generic torsional stiffness $k_\theta = f(\theta)$ has been derived. In particular, the cases of constant, linear and quadratic torsional stiffness have been analyzed. The following analysis will consider the radius of the cam follower rollers in contact with the cam profile negligible.

A joint rotation θ causes a compression $x(\theta)$ of each spring, characterized by a stiffness k_m . The relation between the cam profile and the spring deformation can



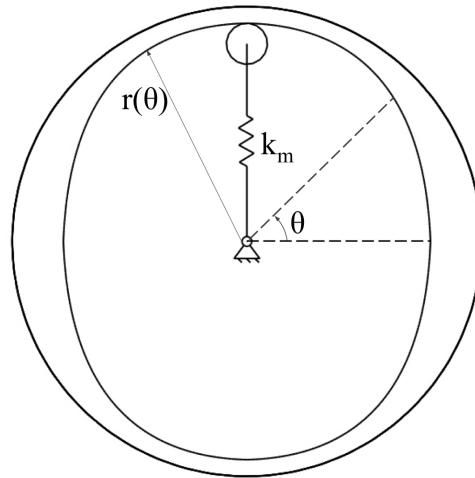


Figure 3.35: Schematic representation of the torsional spring module: k_m is the spring stiffness, θ the shaft rotation and $r(\theta)$ the cam profile.

be expressed as:

$$r(\theta) = r_0 - x(\theta), \quad -\frac{\pi}{n} < \theta < \frac{\pi}{n} \quad (3.6)$$

where r_0 is the spring rest position.

Noting that the angle-dependent torsional stiffness is defined as a differential quantity ($k_\theta(\theta) = dM/d\theta$), the total moment, required to achieve a finite angular deflection θ , is calculated using the following integral expression:

$$M(\theta) = \int_0^\theta k_\theta(\alpha) d\alpha \quad (3.7)$$

The infinitesimal external work is $dL = M(\theta)d\theta$ and the total work associated to the compression of a spring is:

$$L(\theta) = \int_0^\theta M(\alpha) d\alpha \quad (3.8)$$

Moreover, the variation in the elastic energy of the n springs can be calculated as:

$$E(\theta) = n \int_0^{x(\theta)} k_m x(\alpha) d\alpha \quad (3.9)$$

3.3. PASSIVE JOINT FOR WEARABLE ROBOTS: PASSIVE VISCOELASTIC JOINT 97

The energy balance $L(\theta)=E(\theta)$ leads to:

$$\int_0^\theta M(\alpha)d\alpha = n \int_0^{x(\theta)} k_m x(\alpha)dx \quad (3.10)$$

Equation (3.10) can be rewritten as:

$$\int_0^\theta M(\alpha)d\alpha = n \int_0^\theta k_m x(\alpha) \frac{dx}{d\alpha} d\alpha \quad (3.11)$$

Calculating the derivative of (3.11) with respect to θ and using the expression (3.7) for the total moment, it can be obtained:

$$\int_0^\theta k_\theta(\alpha)d\alpha = nk_m x(\theta) \frac{dx}{d\theta} \quad (3.12)$$

Equation (3.12) can be readapted as:

$$\frac{1}{2} \frac{d(x^2(\theta))}{d\theta} = \frac{\int_0^\theta k_\theta(\alpha)d\alpha}{nk_m} \quad (3.13)$$

From (3.13) the analytic relation between the torsional stiffness k_θ and the linear spring deflection can be derived as:

$$x(\theta) = \sqrt{\frac{2}{nk_m} \int_0^\theta d\alpha \int_0^\theta k_\theta(\alpha)d\alpha} \quad (3.14)$$

Constant, linear and quadratic stiffness-angle characteristics can be obtained respectively by setting $k_\theta(\theta) = K$, $k_\theta(\theta) = A\theta$ and $k_\theta(\theta) = B\theta^2$ in (3.14) with K , A and B constant values.

Considering a constant torsional stiffness k_θ , the resultant cam profile, taking into account (3.6), is:

$$r(\theta) = r_0 - \sqrt{\frac{k_\theta}{nk_m}} \theta \quad (3.15)$$

In case the torsional stiffness is $k_\theta(\theta) = A\theta$ (linear characteristic), the resultant cam profile is:

$$r(\theta) = r_0 - \sqrt{\frac{A}{3nk_m}} \theta^{1.5} \quad (3.16)$$



If the torsional stiffness is $k_\theta(\theta) = B\theta^2$ (quadratic characteristic), the resultant cam profile is:

$$r(\theta) = r_0 - \sqrt{\frac{B}{6nk_m}}\theta^2 \quad (3.17)$$

The corresponding cam profiles for the above mentioned characteristics are reported in the polar diagram of Fig. 3.36.

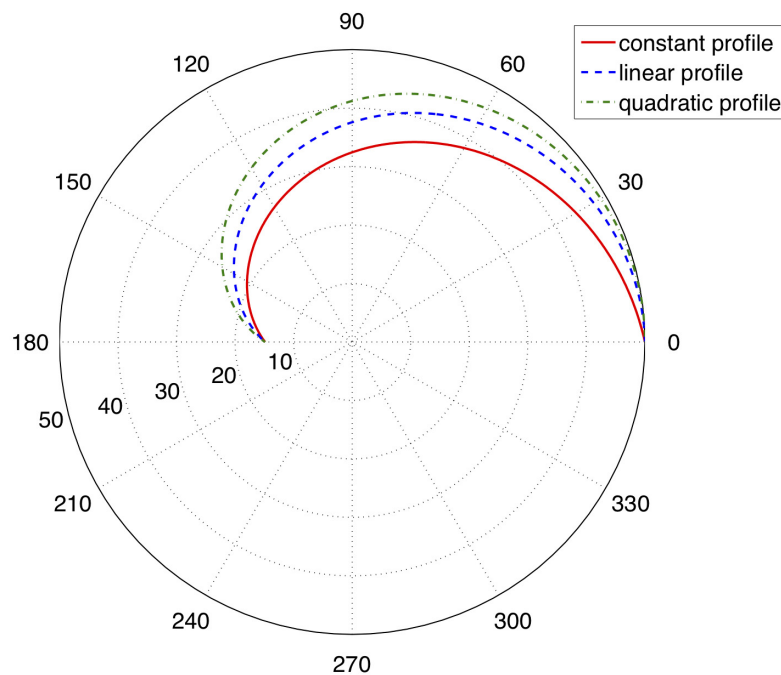


Figure 3.36: Cam profiles for constant (solid line), linear (dashed line) and quadratic (dash-dot line) torsional stiffness characteristics.

3.3.2.2 Torsional damping

The working principle is similar to a peristaltic pump: the torsional damping module is implemented connecting the joint shaft to a roller, which compresses a tube filled with a viscous fluid. The tube endings are connected together, to form a circular closed circuit. In this way, the rotation of the shaft forces the circulation of the fluid in the tube. Localized pressure drops, obtained by partially closing a

Giorgio Carpino

valve, cause viscous forces which result, if the flow inside the tube is laminar, in a torque proportional to the angular velocity on the joint shaft.

A schematic representation of this module is reported in Fig. 3.37. With this arrangement the viscous damping can be varied modifying the pressure drop (i.e. varying the lumen of the tube through a valve). With the valve fully opened (minimal localized pressure drop), the minimal value of the torsional damping can be achieved.

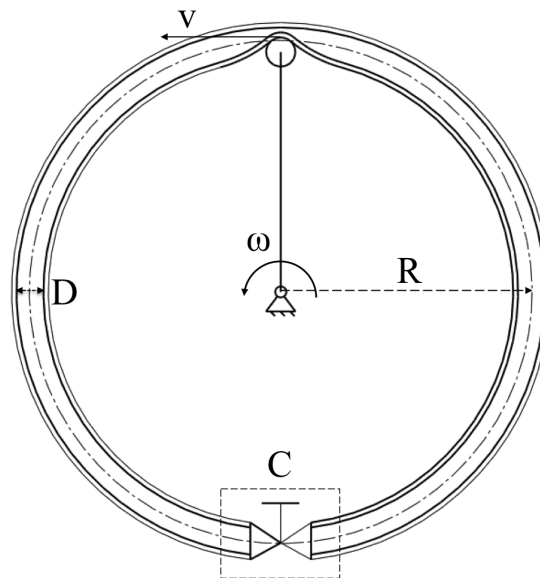


Figure 3.37: Schematic representation of the torsional damping module. ω is the angular velocity, R the radius, D the inner diameter of the tube and v the linear velocity. The valve is schematized in block C.

In this section the equivalent torsional damping, as a function of geometric parameters of the system and of the rheological fluid properties, will be derived in the hypothesis of no localized pressure drop.

Assuming a laminar flow in the tube, for Poiseuille law the volumetric flow rate q can be written as:

$$q = \frac{\pi}{128\mu} \frac{\Delta p}{L} D^4 \quad (3.18)$$

where Δp is the pressure drop, μ the dynamic viscosity of the fluid, D the tube inner

diameter, $L = 2\pi R$ the tube length with R the radius of curvature of the center line, as shown in Fig. 3.37.

The power dissipated by fluid internal friction can be expressed as:

$$P_f = q\Delta p \quad (3.19)$$

The power associated to the rotation of the joint is:

$$P_j = c_{min} \omega^2 \quad (3.20)$$

where c_{min} is the minimum viscous torsional damping and ω the joint angular velocity. For the energy conservation, $P_f = P_j$. From this equality it is possible to calculate the viscous damping as:

$$c_{min} = \frac{q\Delta p}{\omega^2} \quad (3.21)$$

Considering the fluid mean linear velocity v and the tube section S , the volumetric flow can be written as:

$$q = vS = \omega R \frac{\pi}{4} D^2 \quad (3.22)$$

and the angular velocity can be obtained:

$$\omega = \frac{4q}{\pi R D^2} \quad (3.23)$$

Substituting the quantity $\Delta p/q$ (calculated from (3.18)) and (3.23) in (3.21), the minimal torsional damping can be calculated as:

$$c_{min} = 16\pi^2 \mu R^3 \quad (3.24)$$

The obstruction of the tube, obtained by the action of the valve C in Fig. 3.37, increases the viscous drop in the system with a consequent increase of the value of the torsional damping c . Equation (3.24) accounts for fluid viscosity effects, but it neglects energy dissipation occurring during the hysteretic large deformations of the silicone tube. For this reason, (3.24) must be considered an under-estimation of the actual minimum value of the damping coefficient.



3.3.3 pVEJ design

Fig. 3.38 shows an exploded view of the pVEJ, which is depicted in Fig. 3.39 and Fig. 3.42. The system dimensions are 115 mm (diameter) \times 85 mm (axial length) while the overall joint mass is 1.4 kg, thus fulfilling the requirements listed in Tab. 3.10.

An ASM magnetic incremental encoder (reading sensor PMIS4, magnetic wheel PMIR4; resolution of 32768 counts per turn, 0.003 deg with quadrature reading) is mounted on the output shaft, with the reading part fixed to the joint frame and the magnetic wheel coupled to the rotating shaft.

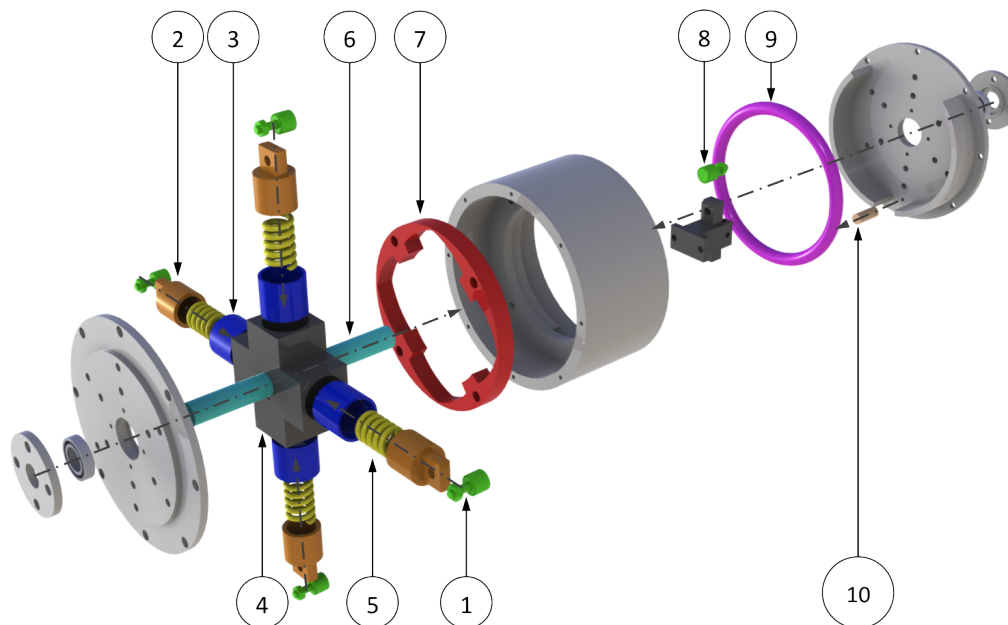


Figure 3.38: Exploded view of the pVEJ. 1: cam follower rollers, 2: roller-spring connectors, 3: bushings, 4: central hub, 5: linear compression springs, 6: joint shaft, 7: cam profiles, 8: fluid mover, 9: silicone tube, 10: pressure drop regulator.

3.3.3.1 Torsional stiffness module

The torsional spring is implemented using a roller with a spring support following a cam profile. The system, shown in Fig. 3.39, is comprised of a central hub (AISI 420) connected to shaft through a key, four self-lubricating bushings, four harmonic

A handwritten signature in black ink, appearing to read 'Giorgio Carpino'.

steel springs, four rollers-springs connectors, four cam follower rollers, and the cam profile (AISI 420). The shaft is simply supported by two radial ball bearings. The central hub has two holes to connect the fluid mover system of the torsional damping module. The self-lubricating bushings (MU - Boccole Italia Srl) have a twofold function: hosting the springs so to reduce the friction between the rollers-springs connectors and the central hub; avoiding bending moments on the spring which can produce undesired compression forces outside the axis of the springs. The rollers-springs connectors (AISI 420) support the cam follower rollers.

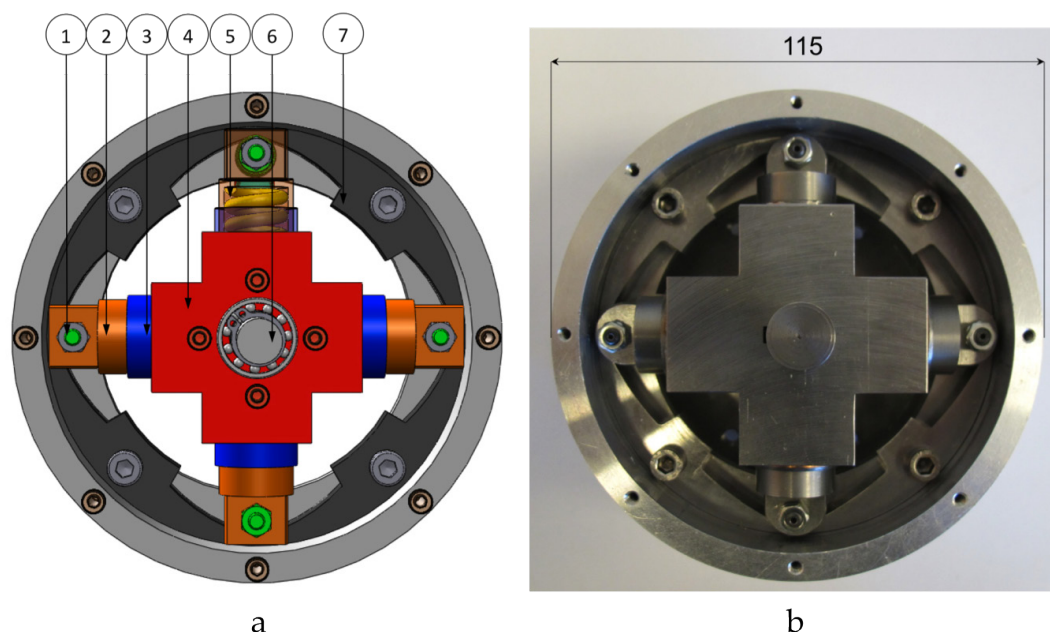


Figure 3.39: Stiffness module. (a) 3D CAD drawing of the torsional spring module (constant stiffness and 4-springs configuration is reported). 1: cam follower rollers, 2: rollers-springs connectors, 3: bushings, 4: central hub, 5: linear compression springs, 6: central shaft, 7: cam profiles. (b) Frontal view of the prototype highlighting the components of the torsional stiffness module with diameter dimension overlaid (mm).

The main characteristics of the springs are reported in Tab. 3.11. The cam profile is intended in this case for constant torsional stiffness but, as discussed above, it can be replaced with different cam profiles able to produce a linear or quadratic characteristic for the torsional stiffness.

TABLE 3.11: PVEJ SPRINGS MAIN CHARACTERISTICS.

Characteristics	Values
Outer diameter	15.5 mm
Inner diameter	9.1 mm
Wire diameter	3.1 mm
Length	25 mm
Pitch	5.37 mm
Weight	12.77 g
Number of coils	5.5
Stiffness	140.9 N·mm ⁻¹
Block length	18.6 mm
Material	DIN 172233, C1 class

TABLE 3.12: RESULTS FOR CONSTANT, LINEAR AND QUADRATIC TORSIONAL STIFFNESS CHARACTERISTICS.

	<i>Constant</i> $k_{\theta}(\theta)=K$	<i>Linear</i> $k_{\theta}(\theta)=A\theta$	<i>Quadratic</i> $k_{\theta}(\theta)=B\theta^2$
Stiffness	$K = 100 \text{ N}\cdot\text{m}\cdot\text{rad}^{-1}$	$A = 125 \text{ N}\cdot\text{m}\cdot\text{rad}^{-1}$	$B = 96.1 \text{ N}\cdot\text{m}\cdot\text{rad}^{-1}$
Springs number	4	4	3
Max. rotation	$\pm 28^{\circ}$	$\pm 45^{\circ}$	$\pm 60^{\circ}$
Max. torque	48 N·m	40 N·m	34 N·m
Max. total elastic energy	12 J	10.7 J	8.7 J

In Fig. 3.40 a plot for the three possible stiffness characteristics (constant, linear and quadratic) are reported. The maximum rotation is reached when the springs go in block. A maximum rotation of $\pm 60^{\circ}$ can be achieved for the case of quadratic stiffness in a 3-springs configuration, as it is clear in Fig. 3.40. Considering instead a 4-springs configuration, the resulting maximum rotation would be $\pm 45^{\circ}$.

Three cam discs have been fabricated, corresponding to constant, linear and quadratic stiffness-angle characteristics. The resultant profiles are shown in Fig. 3.41.

Table 3.12 summarizes all the results in terms of stiffness, number of springs, maximum rotation, maximum torque and maximum elastic energy for constant, linear and quadratic torsional stiffness characteristics.



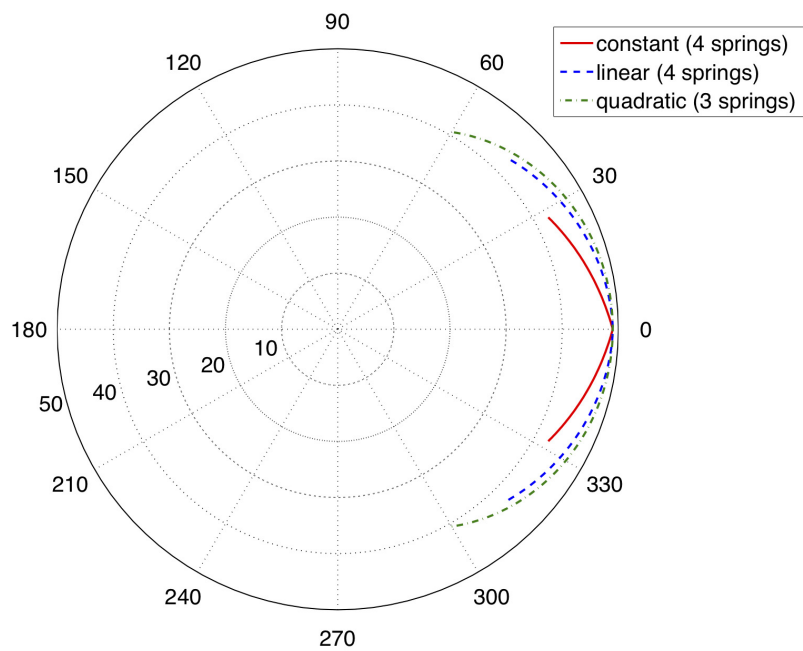


Figure 3.40: Resultant cam profile for constant (solid line), linear (dashed line) and quadratic (dash-dot line) torsional stiffness. All the numbers in the graph are in mm.



Figure 3.41: Cam discs with constant, linear and quadratic stiffness-angle characteristics (from left to right).

Giorgio Carpino

3.3.3.2 Torsional damping module

The damping module, depicted in Fig. 3.42, includes a silicone tube set in circular configuration (radius $R = 50$ mm) and fixed to the chassis (Anticorodal Al 6000). The tube is filled with silicone tube filled with mineral oil (grade SAE 80; dynamic viscosity range at room temperature: $1.0 - 1.3 \text{ kg}\cdot(\text{m}\cdot\text{s})^{-1}$ (Fig. 3.42-3). The tube has an outer diameter of 8 mm and an inner diameter of 5 mm. The valve is implemented using a screw (metric, M4, pitch: 0.7 mm), which pushes a teflon cylinder on the tube, thus locally reducing its lumen (Fig. 3.42-4). When the valve is fully open (minimum localized pressure drop, maximum tube lumen), the minimum value of the torsional damping is achieved. According to (3.24) the theoretical minimum damping, with the selected mineral oil, ranges from $2.8 \cdot 10^{-5} \text{ N}\cdot\text{m}\cdot\text{deg}^{-1}$ to $3.7 \cdot 10^{-5} \text{ N}\cdot\text{m}\cdot\text{deg}^{-1}$. The fluid mover (Anticorodal Al 6000, Fig. 3.42-2) has an adjustable arm (Fig. 3.42-1), which allows the shift of the roller for an easy insertion/substitution of the tube.

3.3.4 pVEJ characterization

To experimentally measure the stiffness and the damping of the pVEJ, the same custom dynamometric test-bed used for the characterization of the torsional spring of SEA 300W has been adopted (Fig. 3.43).

3.3.4.1 Stiffness module

Torque-angle plot for the constant, linear and quadratic stiffness cam profiles are shown in Fig. 3.44. For the constant profile, the linear regression provided a R^2 coefficient of 0.99 giving a stiffness value $\hat{K} = 2.105 \text{ N}\cdot\text{m}\cdot\text{deg}^{-1}$, which differs from the desired one (stiffness $K = 1.745 \text{ N}\cdot\text{m}\cdot\text{deg}^{-1}$) by 20%.

A quadratic regression for the linear cam profile was performed to determine the A coefficient introduced in section 3.3.2 (R^2 equal to 0.96). The estimated value $\hat{A} = 0.066 \text{ N}\cdot\text{m}\cdot\text{deg}^{-2}$ differs by only 3% from the desired value ($0.064 \text{ N}\cdot\text{m}\cdot\text{deg}^{-2}$).

A cubic regression for the quadratic stiffness profile estimated a parameter value $\hat{B} = 1.47 \cdot 10^{-3} \text{ N}\cdot\text{m}\cdot\text{deg}^{-3}$, which differs by around 50% from the desired value of $2.5 \cdot 10^{-3} \text{ N}\cdot\text{m}\cdot\text{deg}^{-3}$.



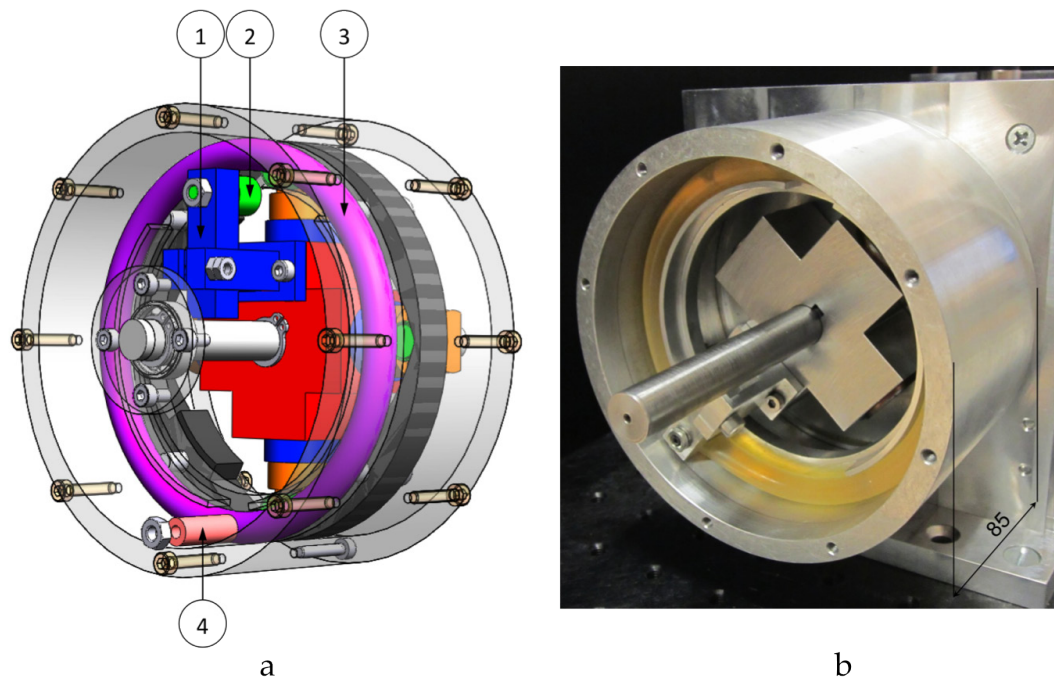


Figure 3.42: Damping module. (a) 3D CAD drawing of torsional damping module. 1: fluid mover, 2: cam follower roller, 3: silicone tube, 4: pressure drop regulator, (b) View of the prototype highlighting the components of the torsional damping module with thickness dimension overlaid (mm).

The stiffness values differed from the expected one from 3% to 50%. Such discrepancy is due to two main causes: (i) the approximation used in (3.14), where the radius of the roller is neglected; (ii) fabrication inaccuracies.

3.3.4.2 Damping module

The damping module was characterized with the linear springs unmounted, in order to exclude the elastic effect of the stiffness module. Characterization procedure consisted in rotating the pVEJ shaft with a constant velocity (from $5 \text{ deg}\cdot\text{s}^{-1}$ to $35 \text{ deg}\cdot\text{s}^{-1}$). A linear regression $\tau = \hat{c} \omega$, with $\omega = \dot{\theta}$, (torque vs. angular speed) was performed. This test was repeated at three valve positions. If δ indicates the linear displacement of the screw, $\delta = 0 \text{ mm}$ corresponds to the case when the valve is fully open, while $\delta = 1.4 \text{ mm}$ and $\delta = 2.1 \text{ mm}$ correspond to 2 and 3 turns of the

Giorgio Carpino

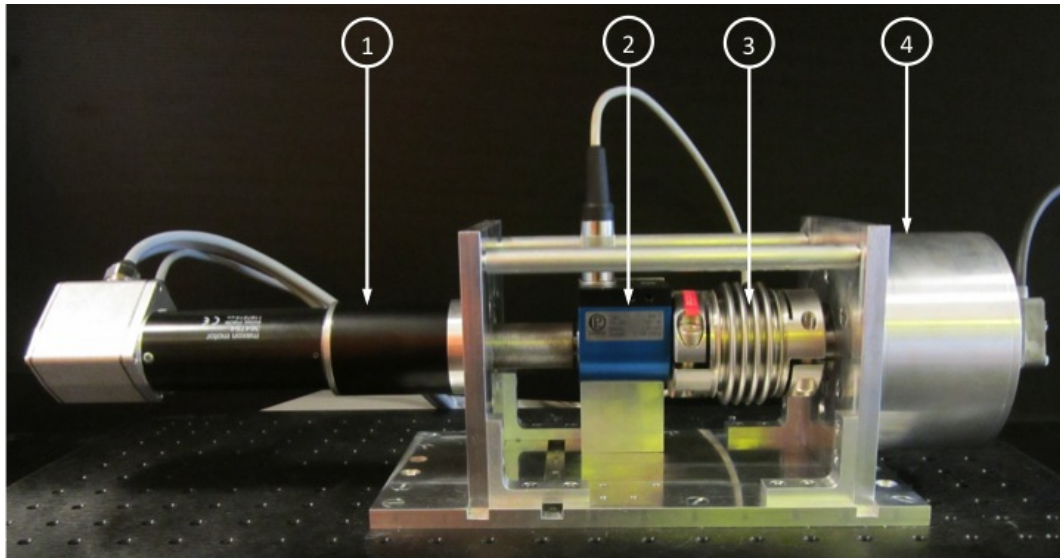


Figure 3.43: Custom dynamometric test-bed. 1: gearmotor, 2: torque sensor, 3: flexible coupling, 4: pVEJ with encoder.

screw, respectively.

In Fig. 3.45 torque-velocity fitting of the experimental data for these different conditions are reported; the slopes of the curves represent the damping coefficients.

The damping coefficient, measured when the valve is fully open, is one order of magnitude higher than the minimum theoretical value, evaluated using (3.24). The difference between the experimental and theoretical minimum values is likely due to simplifications introduced in the analytical calculation. In particular, in the prototype the damping is higher than the theoretical one because: (i) energy losses associated to tube compression increases the resultant damping action; (ii) a further localized pressure drop occurs at the connector between the two ends of the tube.

3.3.5 Conclusions and future works

The presented design is endowed with a high degree of modularity, which enables the regulation of the mechanical properties of the system by replacing single components. For example, the modification of the stiffness vs. angle characteristic can be achieved by using different cam profiles or by employing linear springs with

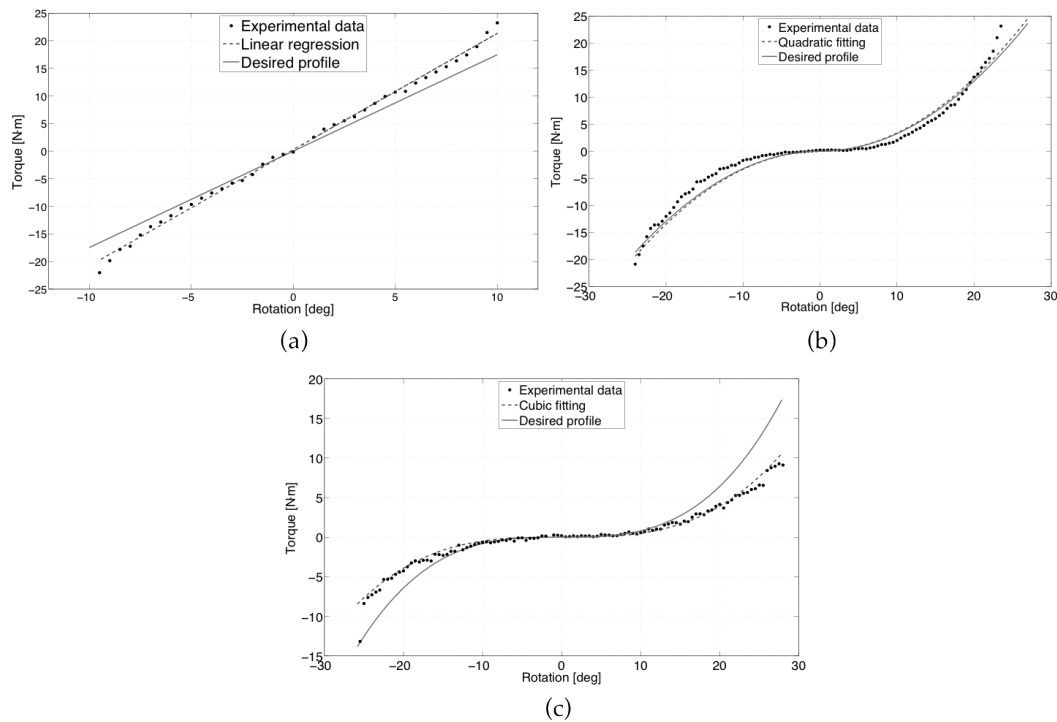


Figure 3.44: Torque vs. angle profiles. a: constant stiffness-angle characteristic ($\hat{K} = 2.105 \text{ N}\cdot\text{m}\cdot\text{deg}^{-1}$); b: linear stiffness-angle characteristic ($\hat{A} = 0.066 \text{ N}\cdot\text{m}\cdot\text{deg}^{-2}$); c: quadratic stiffness-angle characteristic ($\hat{B} = 1.47\cdot 10^{-3} \text{ N}\cdot\text{m}\cdot\text{deg}^{-3}$).

different elastic constants. Moreover, damping can be varied by using different fluids and/or by regulating the localized pressure drop in the tube.

As future work, an on-line damping regulation system will be introduced by connecting the screw, which regulates localized pressure drops, to a motor.

Finally, if the pVEJ is connected in series to a motor, a Series ViscoElastic Actuator (SVEA) can be obtained, where the mechanical impedance can be actively tuned.

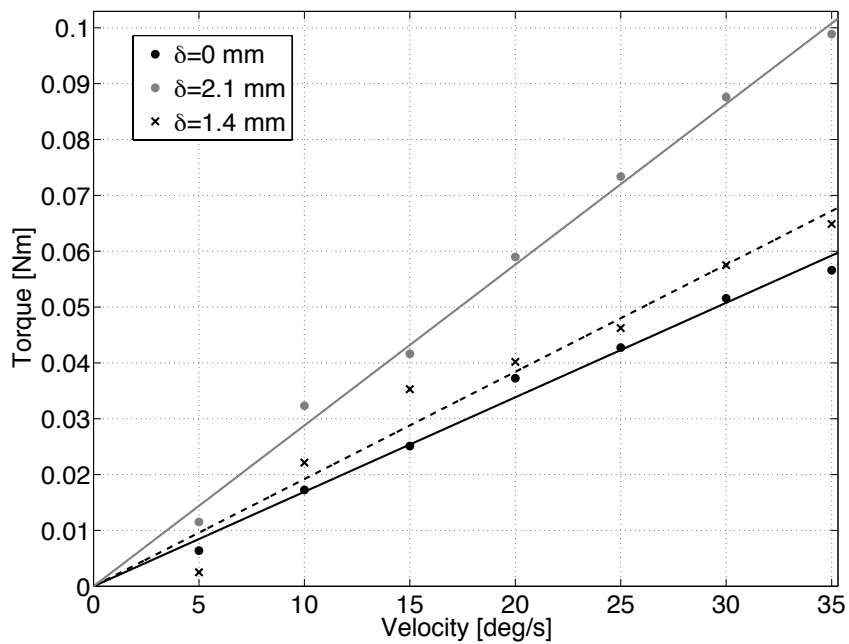



Figure 3.45: Torques vs. angular velocities for the damping module. The slopes of the curves represent the torsional damping coefficients for the three different valve regulations. For $\delta = 0$ mm, $\hat{c}_{min} = 1.69 \cdot 10^{-3}$ N·m s/deg ($R^2 = 0.99$); for $\delta = 1.4$ mm, $\hat{c} = 1.92 \cdot 10^{-3}$ N·m s/deg ($R^2 = 0.96$); for $\delta = 2.1$ mm, $\hat{c} = 2.88 \cdot 10^{-3}$ N·m s/deg ($R^2 = 0.99$).

Giorgio Carpino

Tesi di dottorato in Ingegneria Biomedica, di Giorgio Carpino,
discussa presso l'Università Campus Bio-Medico di Roma in data 20/03/2012.
La disseminazione e la riproduzione di questo documento sono consentite per scopi di didattica e ricerca,
a condizione che ne venga citata la fonte

A handwritten signature in black ink, appearing to read "Giorgio Carpino". The signature is written in a cursive, flowing style with some loops and flourishes.

Chapter 4

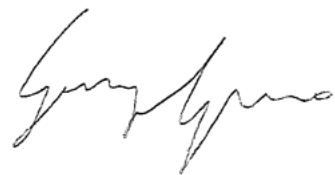
Non-anthropomorphic lower limbs wearable robot for gait assistance

4.1 Introduction

The investigation of non-anthropomorphic architectures may provide solutions to some of the problems associated with closely matching the structure of the exoskeleton to the wearer, such as the need for close alignment between the joints of the robot and the wearer [3].

Ideally, a person wearing a robot must feel no restriction to his/her natural motion patterns; if robots and humans are not kinematically compliant, a source of non-ergonomic interaction forces appears. Kinematic compatibility is of paramount importance in robotic exoskeletons working on the principle of internal forces. The typical misalignment between exoskeleton and anatomical joints results in uncomfortable interaction forces where both systems are attached to each other.

A good wearable exoskeleton design starts with the choice of a suitable kinematic structure for the device. That is to say, even before implementing actuation and control of a device, the purely mechanical structure must enable wearability, ease of use and operator comfort. Comfort depends partly on the ability of the exoskeleton to interact smoothly with the human; in other words, the exoskeleton must not limit the range of motion of the operator and must otherwise be as trans-



parent as possible. The reasons for kinematic incompatibility between HB and WR joints are the variability of biomechanical parameters between subjects, and also the variability of joint axis locations and body segment sizes within individual subjects during movement. These anatomical variations make it difficult to produce an exoskeleton design that fits a wide range of users without problems.

Causes of kinematic incompatibilities between human joint axes and exoskeleton joint axes can then be classified into two groups:

- *macromisalignments* can occur if an exoskeleton joint or joint group has less DOFs than the corresponding human joint or joint group. Macromisalignments are thus induced by a mismatch between the DOFs of human limb motion and exoskeleton link motion;
- *micromisalignments* are less obvious but occur in all wearable exoskeleton designs. Micromisalignments are caused by non coincident instantaneous centre of rotation (ICR) between the exoskeleton and the human limb. This is almost always the case because it is not possible to align an exoskeleton perfectly to the human joints, due to intersubject variability and coverage of the joints. Micromisalignment can, furthermore, be caused by slippage of the exoskeleton attachments on the human skin during motion. A significant negative effect of micromisalignments is the creation of interaction forces, such as shear forces between the exoskeleton attachment point and the human limb.

Macro and micromisalignments contribute to operator discomfort and can limit and alter the natural movement of a human limb inside an exoskeleton. This raises the question of how a kinematic structure for an exoskeleton should be designed to provide a maximum of comfort and ease of use despite the variability of anatomic properties within and between users.

A possible solution to overcome these limitations imposed by an anthropomorphic design both from a kinematic and dynamic point of view is to develop a non-anthropomorphic structure for WRs. The first design criteria for kinematically compatible wearable robots for rehabilitation was proposed by Schiele and



van der Helm [5]. For a truly ergonomic exoskeleton design to be feasible, the authors postulate that an exoskeleton must be able to:

- interact with the complete functional workspace of the human limb of interest;
- induce exact torque, position and velocities to the human joints (and hence be able to resolve the redundancy);
- must not cause discomfort or safety hazards for the user.

These kinds of WRs may possess multiple degrees of redundancy to cope with the interaction with human limbs and joints, without presenting the need of aligning the axes of rotation of artificial joints to those of human joints. These concepts have been implemented in an exoskeleton for the upper limbs developed to enable in-space force-feedback tele-manipulation with redundant robot arms [5]. The kinematic structure of the exoskeleton, which does not mimic upper limbs, offers an alternative kinematic chain bridging over the human joints. Even though the kinematics of the exoskeleton and the human arm are different, any posture of the human joints can be univocally determined by the corresponding posture of the exoskeleton, which allows the complete range of motions of human articulations.

The problem of optimal kinematic synthesis of non-anthropomorphic wearable robots may be very difficult to be solved by human intuition and engineering insight alone, due to the large number of open parameters involved in the design. This task can be simplified by automatic tools in support of the designer. In the last decade, evolutionary programming has been applied to solve the problem of co-designing from scratch both the mechanics and the control of mobile artificial machines, by just defining the basic building blocks of the structure and the rules to connect them [122]. This open-ended kind of design methodology has the advantage that it may lead to interesting and unexpected design solutions. However, such kind of design methods imply that the whole design process is completely demanded to the tool, which can autonomously decide to switch to a more complex structure during the optimization phase so to increase the fitness of the best individuals.



4.1.1 Objectives

The objective has been to develop a systematic approach for the kinematic synthesis of wearable robots. The following dissertation on the adopted novel design methodology for WR is based on the results reported in [123, 124]. The candidate contribution is focused on the hardware implementation of the optimal morphological solution related to the chosen WR topology.

In this novel approach, the design process is divided into three stages. In the first stage a systematic search of all the plausible independent generalized kinematic solutions (i.e. topologies) is performed. In the second stage, an optimization algorithm acting on a fixed number of parameters (encoding both properties pertaining to the mechanical structure and to the control) is used to define the morphology providing the best performances in terms of some design objective. In the final stage, the best morphologies produced by the optimization on each topology are compared with each other, so to define the best solution [123]. A schematization of the pursued approach is shown in Fig. 4.1.

This approach appears more reliable since optimization algorithms acting on a fixed parameter space are simpler and with faster convergence properties. Furthermore, each optimization process is independent from the others and can run in parallel on different computers. Additionally, this approach assures that all interesting generalized solutions (i.e. topologies) are evaluated before producing the final design. However, this approach requires the a-priori knowledge of the list of independent topologies having the desired kinematic properties (i.e. maximum number of links and of degrees of freedom (DOFs)) and respecting some basic criteria of kinematic compatibility with the human body.

The designed lower limbs WR comprises two modules: hip/knee flexion/extension module and hip abduction/adduction and intra/extrarotation module. As described in the following sections, only the first module acting in the sagittal plane has been optimized in this simulation environment while the other module is hand-designed.



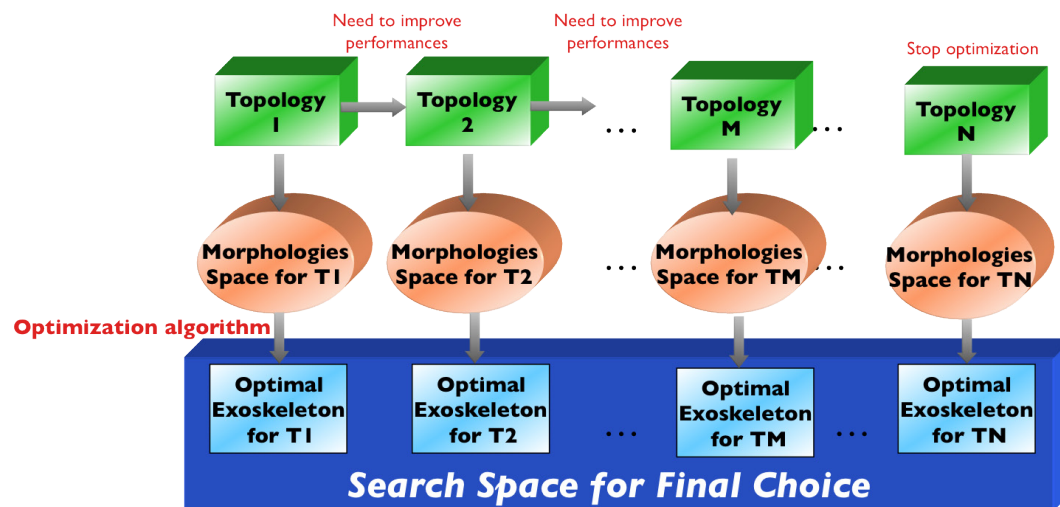


Figure 4.1: Overview of the methodology based on the multi-objective optimization of a fixed number of parameters, describing robot morphology (kinematic and dynamical properties) and actuation laws (torque applied to the robot joints). This optimization strategy requires the a-priori knowledge of the list of suitable independent solutions (i.e. topologies), which are considered valid if a certain number of kinematic properties of the set constituted by human and robot kinematic chains is respected. The generated topologies can be ordered for increasing complexity (such as number of links and number of DOFs) and the optimization process can be stopped when satisfactory performances are reached.

4.2 Hip/knee flexion/extension module

4.2.1 Wearable robot topology and morphology

A graph-based method for the exhaustive enumeration of the topologies of planar non-anthropomorphic wearable robotic orthoses has been adopted, which represents the first stage of the design methodology described in the following. The method includes two tests (i.e. the *HR-isomorphism test* and the *HR-degeneracy test*), which have purposively been devised to solve the problem of the enumeration of wearable robots kinematic structures. With the developed methodology, it was possible to derive the atlas of all the possible independent kinematic structures of a planar wearable robotic orthosis with up to 7 robot links, to assist a human limb modeled as a 4-link/3-joint serial kinematic chain, satisfying a certain set of basic kinematic requirements.


A complete dissertation about the methodology adopted to reduce the parameters space is presented in [123, 124].

Initially, an encoding needed to be defined, in order to represent the kinematic structure of robotic orthoses. Since the aim is obviously to consider in the design also the mobility of the human limbs connected to the robotic orthosis, the whole parallel kinematic chain consisting of both robot links and human limbs was considered. The description of this kinematic chain can be performed at two levels of abstraction: (i) *topology*, which defines the number of links and the connections among them and (ii) *morphology*, which instantiates a given topology, adding the geometrical properties of links and of joints.

Under some reasonable hypotheses [125], many properties of mechanisms kinematics, such as the number of DOFs, are entirely determined only by the topology of the kinematic chain and unaltered by the geometric properties of its links. At this level of abstraction, the classical analogy between undirected graphs and kinematic chains, as introduced by [126], can be employed, where graph vertexes correspond to the links of the chain and edges correspond to the joints. The focus was on planar kinematic chains containing only revolute joints. Then, the only necessary information to define robot morphology is the position of joints in a particular configuration. In such a way a binary link is represented by a bar jointed at its extremities, a ternary link by a triangle jointed at its vertices and so on.

Some constraints on the type of robot joints and links need to be defined:

- only revolute joints has been considered. By focusing on one single type of joint, the dimension of the search space to be explored by the evolutionary algorithm is reduced (in terms of both links geometry and dynamical parameters to be taken into account). This has allowed a quicker convergence of the evolutionary design process. Anyhow, this choice is not a strong limitation, since motions produced by a kinematic structure that uses linear joints can be approximated by other kinematic structures with only revolute joints.
- no flexible link will be included in the robot in order to not explode the search space and to avoid complex computational issues. A rectangular cross-section



is chosen for the links so to maximize their stiffness in the sagittal plane, while preserving a small thickness in case two or more links need to be stacked. Such overlapping could be due to the convergence of more than two links on the same joint and to the sweeping of a link over another due to the movements of the links in the kinematic chain.

The mentioned assumptions limits the relevance of the methodology for the design of assistive wearable robots for the lower limbs, since the hip and the ankle joints have spatial movements. However, it can be noticed that most of the power of the lower limbs is provided by actuation of movements in the sagittal plane, which is the dominant plane of motion during human locomotion.

The described representation is then complete in the description of kinematic chains topology and allows converting the problem of kinematic synthesis into a problem of graphs enumeration. However, as it will be more extensively discussed further, the relation between a kinematic structure and a graph is a one-to-many relation. The same kinematic structure can indeed be achieved by a different graph, by just re-labeling links numbers. This implies that any enumeration process based on a graph-based representation implies the need for an explicit isomorphism test to assess the real independence of any couple of solutions.

Once defined the specifications for robot joints and links, it is possible to derive possible constraints on the number of links and joints, which constitute the mechanical structure of the robot. Two opposing criteria will be employed for giving the boundaries, which are necessary as an input for the evolutionary design phase:

- mobility of human limbs;
- weight and complexity of the structure.

The first criterion relates to the necessity of providing an adequate mobility to the human limbs. The basic hypothesis is that the model of human limbs employed for the design of the wearable robot is a planar model acting in the sagittal plane with rigid links and revolute joints for hip, knee and ankle. This is a serial, 3 DOFs kinematic chain. Since the aim is to design robotic structures connected in parallel



to human limbs in a possibly non-anthropomorphic way, the ensemble of the robot and human links is to be regarded as a whole as a parallel planar robotic structure. A wearable robot does not apply torques to human limbs. Rather, it applies forces, which are statically equivalent to torques at human joints. As a consequence, no double limb connections are needed. A structural representation of the problem is shown in Fig. 4.2.

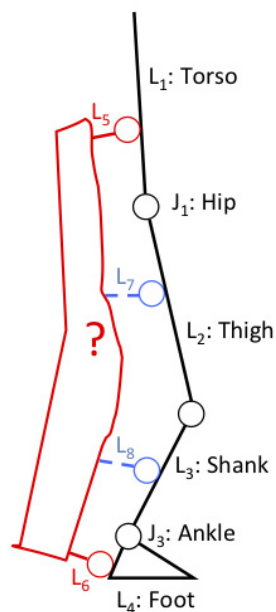


Figure 4.2: Schematic of a wearable robot (in red), attached to the planar model of a lower limb (in black). Connections with thigh and shank are reported in blue.

The kinematic structure has to preserve the range of motion of each human articulation, which is supported/assisted by the robot. For this reason the minimum number of DOFs of the whole kinematic structure is three. More DOFs can enable a better adaptation to the human body, and the achievement of better dynamical properties of the robotic structure. A systematic investigation of the set of possible kinematic structures is required to get possible constraints on the robot design.

A further selection over the list of enumerated topologies is performed, in order to filter out the kinematic chains which:

- contain rigid or over-constrained subchains;

- correspond to disconnected graphs (i.e. not all graphs vertices are connected by a path);
- impair the simultaneous motion of human joints.

A standard degenerate testing algorithm has been implemented to recognize and discard rigid subchains (such as 3 links-3 joints and 5 links-6 joints subchains) [123].

Additionally, disconnected mechanisms (i.e. such that there is not a path connecting each couple of vertices of the corresponding graph) are eliminated with a purposively developed algorithm, which verifies the existence of a path between each couple of vertices.

Furthermore, an additional test was introduced so to exclude those solutions where a subset of n human joints is part of subchain with less than n DOFs. In this case the robot would impair human movements by imposing unnatural kinematic constraints, violating the second kinematic requirement reported above. This test is called *HR-degeneracy test (Human-Robot degeneracy test)* since it applies to kinematic chains including both human and robot structures. Another test has been developed in order to eliminate the isomorphic solutions. Two kinematic chains K_1 and K_2 are said to be isomorphic if there exists a one-to-one correspondence between links of K_1 and K_2 such that any pair of links of K_1 are jointed if and only if the corresponding pair of links of K_2 are jointed. This means that from the graph corresponding to K_1 one can obtain the graph corresponding to K_2 by only relabeling link numbers. A purposively developed test, *HR-isomorphism test*, has been implemented in order to discard these solutions [123].

After making considerations on the number of additional links and joints provided by the structure, the problem is to derive a methodology which allows to explore all possible assortments of the given number of links and joints which provide a certain desired degree of mobility to the "human + robot" system.

The described algorithm has been implemented in MATLAB (The MathWorks, Inc.) and allowed to obtain the complete list of topologies describing the kinematic chains which consist of both human segments (a serial 4-link, 3-joint kine-



TABLE 4.1: NUMBER OF TOPOLOGIES GENERATED AND FILTERED FOR HR-ISOMORPHISM AND FOR HR-DEGENERACY FOR THE CASE OF HIP AND KNEE ORTHOSIS.

	4 robot links 2 DOFs	5 robot links 3 DOFs
Total combinations $\binom{l}{e}$	84	1820
Filtered including only closed chains	13	54
Filtered including only not HR-isomorphic	10	22
Filtered including only not HR-degeneracy	10	22

matic chain) and robot links. The limit to the search space of robot kinematic chains was 7 links, since a robot with more links would result in a too complex and heavy system.

4.2.1.1 Particularization to a hip/knee orthosis

In the context of a collaborative research project funded by the EC commission, the Evryon project [127], the described approach has been particularized to the case of the design of a hip/knee orthosis. This was due to the fact that the problem described in the previous section, the design of a full exoskeleton for the lower limbs, had a large possible number of solutions, which was not possible to exhaustively explore in a simulation-based optimization environment due to the strict timeline of that specific project.

The same steps used for the enumeration of the planar lower limbs WR could be followed for this new enumeration problem.

The application of the previously described set of functions for the: (i) generation of the set of admissible topologies, (ii) elimination of serial, bio-isomorphic and bio-degenerate solutions lead to the results summarized in Tab. 4.1, which comprises the cases of four and five robot links.

The atlas containing the set of admissible topologies is sufficient to implement



a kinematic-based optimization to derive the fittest morphology in terms of some kinematic or kinetostatic set of parameters. However, all enumerated topologies are parallel chains, which imply that the number of joints is higher than the number of DOFs of the structure. It is then necessary to specify which joints are actuated and which are instead not. Referring to the topologies enumerated for the case of 4 robot links and 2 DOFs (see Fig. 4.3), since the structure has a total of 2 DOFs, 2 actuators are required to determine the pose of the structure.

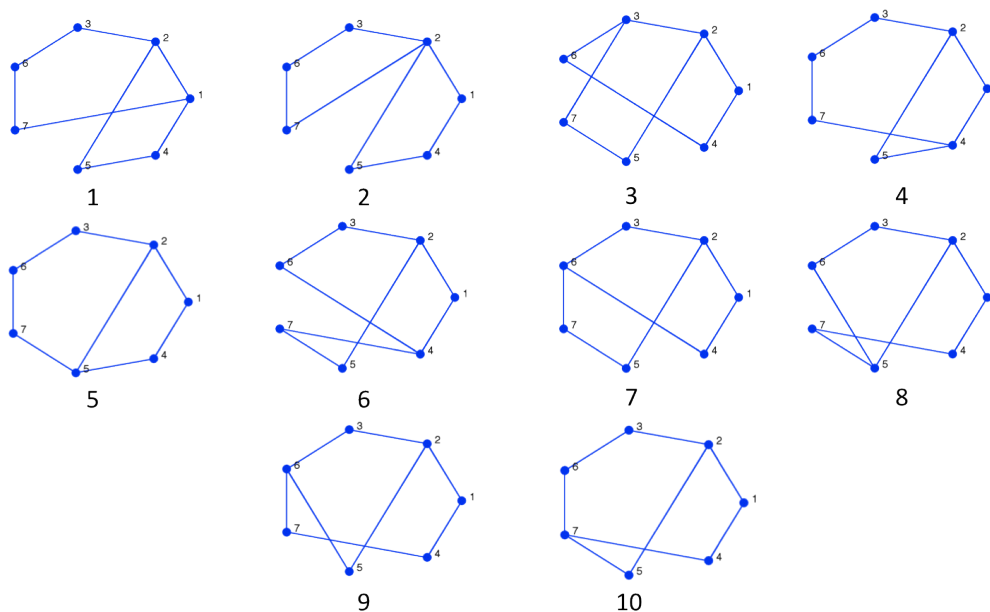


Figure 4.3: Atlas of topologies with 4 robot links, 2 DOFs, for the design of a planar orthosis assisting the hip/knee flexion/extension [124]. Graph vertexes correspond to the links of the chain and edges correspond to the joints. The same labeling scheme used in Fig. 4.2 is followed: (torso=link 1, thigh= link 2, shank= link 3); link 4 to 7 are robot links.

4.2.1.2 Simulation environment

In Fig. 4.4 shows arbitrarily defined morphologies, each of them corresponding to the topologies depicted in Fig. 4.3.

The transformation from a topology to a morphology can be encoded in several ways. The type of encoding chosen encodes for each joint its position in Cartesian

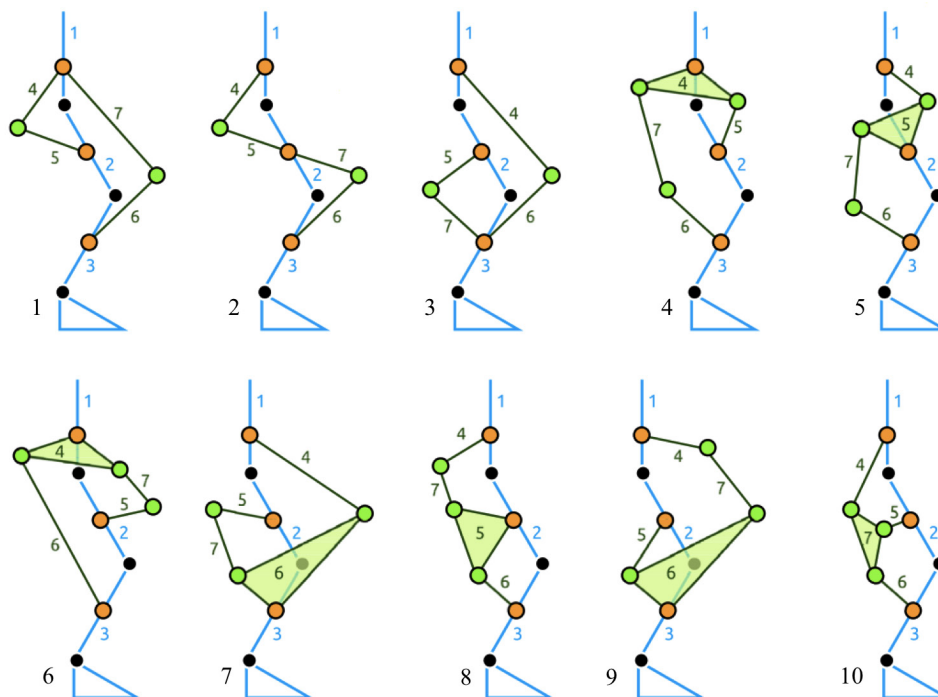


Figure 4.4: Structural representations of morphologies with 4 robot links, 2 DOFs, for the design of a planar orthosis assisting the hip and the knee flexion/extension, arbitrarily derived from the atlas shown in Fig. 4.3. In these pictures the same labeling scheme used in Fig. 4.2 is followed: (torso=link 1, thigh= link 2, shank= link 3); link 4 to 7 are robot links. Attachments with human joints are shown in orange, joints between two robot joints are in green.

space. Thus each joint needs two parameters (since the simulation is constrained in 2D, planar motion) to be realized. A change in a parameter simply moves a joint to a different initial position in space. Each change in the parameters is an independent change in the morphology. The joints can thus be placed at their Cartesian coordinates, and the joint angles resulting from connecting the different joints according to the topology provide the initial rest position of all the joints.

In order to find the best morphology for a given WR topology, the dynamics of the combined system comprising “human body + wearable robot” has been opportunely co-evolved. The evolution of the WR has been done on a passive human body which is modeled in the physics simulation environment (Webots, Cyberbotics), based on anthropometric measurements provided by [128]. This includes

accurate limb lengths, masses, inertia, passive position dependent impedance properties and ligaments modeling. The motivation for a passive human body is twofold: on one hand, the objective is to evolve the combined system of "human body + wearable robot" as a passive walker by minimizing the torque requirements of the actuators; on the other hand, the aim is to avoid the added complexity of modeling a human Central Nervous System deriving from the choice of an active human model. Furthermore, to simplify the stability issues in bipedal locomotion, the torso is constrained such that it cannot rotate (it can still move forward, backward, up and down). Although this is a very strong constraint, this type of restriction is justified by the assumption that the target population of the wearable device does not have severe balance impairments. In addition the forces and torques that are being delivered by these constraints are constantly monitored. The only biomechanical properties of the human body that are implemented are the ligaments. The ligaments essentially constrain the range of motion of each of the joints.

An additional structure representing the exoskeleton has been attached onto this human model at specific attachment points. The mass distribution (and corresponding inertial properties) of the WR can influence the dynamics and the performance of the system. In the system, there are two types of masses, (i) fixed masses (e.g. the human body and WR links) and (ii) partially free masses (e.g. actuators and added masses). The fixed masses in the system are the human body and the mass resulting from the material used for the WR links. The link mass is an open parameter which can be used to simulate added mass at links, to allow the optimization of efficient mass distribution. This mass are situated at the center of the link. In addition, the radius of gyration from which the inertia of a link can be calculated is an open parameter. This encodes for non-uniform mass distributions in the link that can potentially lead to more efficient solutions. The free masses are: (i) actuator masses and (ii) extra masses added by the optimization. The mass of each actuator is set equal to 4 kg. The additional hip module (not co-evolved in the simulation environment) has been also modeled as added masses. A total mass of 7 kg for the hip module has been attached on the lower torso of the human model.

Any design for the WR exactly features two actuators (since the need is to con-




trol two DOFs) per leg. These actuators are controlled by an impedance law which has been optimized. Equation 4.1 shows the basic control equation:

$$\tau(t) = k(t)(q_{ref}(t) - q(t)) + b(t)(\dot{q}_{ref}(t) - \dot{q}(t)) \quad (4.1)$$

where $\tau(t)$ is the torque applied at the joint, $q_{ref}(t)$, $k(t)$ and $b(t)$ are three control signals representing respectively the joint angle reference trajectory, the stiffness and the damping, $q(t)$ and $\dot{q}(t)$ are respectively the measured joint angle and joint angle velocity. Note that this equation resembles a PD control law, with the exception that the stiffness and the damping are functions of time. This allows for more complex control schemes where in some parts of the gait the control can be stiffer, or more damped, than in other parts.

The co-evolution of the WR morphology and control is governed by multiple objective functions, combined into a single objective value by means of use a weighted product [129]. To measure the performance of the WR we consider two main objectives were considered: (i) the restoration of the physiological gait and (ii) the minimization of required torque to restore the gait. In addition, several objectives were added to guide the evolutionary process to viable solutions which improve the convergence properties of the optimization. Thus, six objective functions were followed:

- Minimization of physiological gait restoration error: the error on the joint angles for both hip and knee during the gait respect to the angles of a physiological gait were measured and integrated and then minimized;
- Minimization of required torque to actuate the system;
- Minimization of excessive segment size: the maximum allowed segment size is 700 mm;
- Maximization of physiological gait speed;
- Minimization of knee overstretching;



- Maximization of simulated time: if the model falls, or if there are numerical instabilities in the simulation, the simulation is stopped prematurely, thus this objective will guide the optimization towards solutions that are stable.

From this optimization analysis, the best topology in terms of the above mentioned objective functions was topology no. 10 in Fig. 4.5, as detailed described in the next paragraph.

4.2.2 Design of hip/knee flexion/extension module

The hip/knee flexion/extension module has been designed in order to assist the flexion/extension movements of hip and knee during gait. The module is composed by: (i) the kinematics described and chosen from the set of possible topologies listed in the previous paragraphs, (ii) two actuators actuating the relative sub-chains acting in parallel to the human hip and knee and (iii) two cuffs connecting the WR to the thigh and the calf so to transmit the motion between WR and HB.

The selected topology was topology no. 10; the choice was driven by a trade-off between the optimization of the objective functions described above and the minimization of design complexity for the WR design (also related to the users acceptability of the WR).

The selected morphology, instantiating topology 10, has shown in Fig. 4.5. The kinematic chain, in red, is shown in five configurations of the right leg, in blue as the entire human lower limbs model. The 3D CAD model of the human lower limbs has been retrieved from Jack (Tecnomatix, Siemens) and is characterized by real human anthropometric dimensions. In the rest configuration, all the joints have been labeled, in particular: H , T and C are the attachments sites of the WR to the hip, thigh and calf segments respectively. Joints a and d are the vertex of the link ad and the joints d , e and f are the vertex of the ternary link (link 7 of topology no. 10 shown in Fig. 4.4–10).

In order to obtain a compact design and to reduce the inertia perceived by the leg during gait, the two actuators have been arranged along the same link (link ad in Fig. 4.5) in correspondence to the thigh actuating the joints a and d of the robot



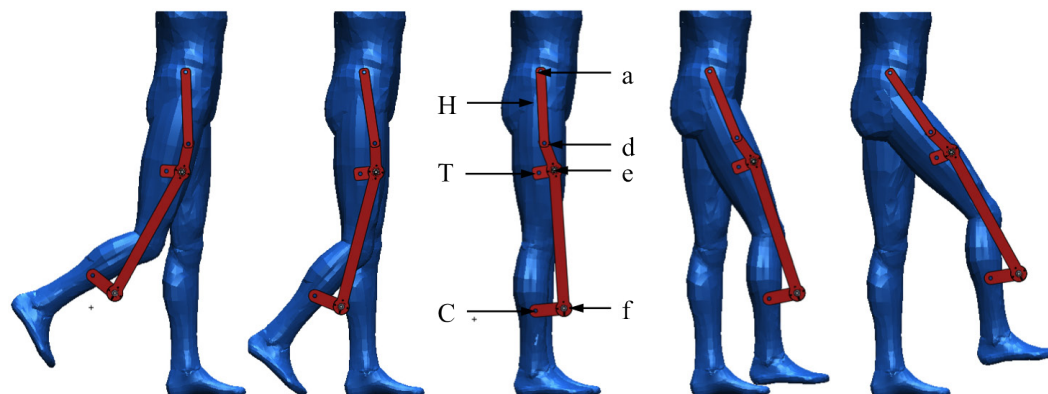


Figure 4.5: Selected morphology for the hip/knee flexion/extension module (in red) attached to anthropometric human lower limbs model (in blue). Five configurations of the right leg are reported. Joints H , T and C represent the attachment sites of the WR to the hip, thigh and calf respectively; link AD is the WR link incorporating the two SEA 300W actuating the hip and knee parallel independent subchains. The ternary link def is the link 7 of topology no. 10 shown in Fig. 4.4-10.

and respectively allowing the independent motions of the two parallel hip and knee subchains.

The peak torque exerted by the actuator of the knee subchain occurs during the 14% of the gait cycle and has a value of 58.4 N·m, while the peak torque exerted by the actuator of the hip subchain occurs during the 0% of the gait cycle with a value of 42.7 N·m. Under these requirements of peak torque the most suitable choice for the WR actuation is the second version of SEA 300W described in the previous chapter. As already discussed, this is the most appropriate solution in terms of required power, torque, and non co-located distribution of actuator mass. The link ad has, thus, a total weight of 6.5 kg and an inertia of 10^8 g/mm² and embeds the most part of the total weight of the hip/knee flexion/extension module. The torques required to the actuators in topology 10 are not smaller than those required by anthropomorphic kinematics. Compared to other non-anthropomorphic solutions, the one depicted in fig. 4.6 minimizes the forces exchanged with the human body, statically equivalent to the joints torques reported in the Winter dataset [96].

The WR links will have a rectangular cross section so to maximize their stiffness in the sagittal plane while preserving a small thickness and will be manufactured in

Ergal (Aluminum alloy, 7000) due to its low density and high yield stress. The WR passive joints (e and f) have been provided with ball bearings in order to adequately transfer the loads.

The attachments of the WR to the lower limbs have been realized through ap-
posite cuffs able to transfer the torque from the WR to the limbs, as better explained
in the next paragraph.

A 3D CAD view of the module connected to the human lower limbs model is
shown in Fig. 4.6. The weight of the module is about 9 kg.

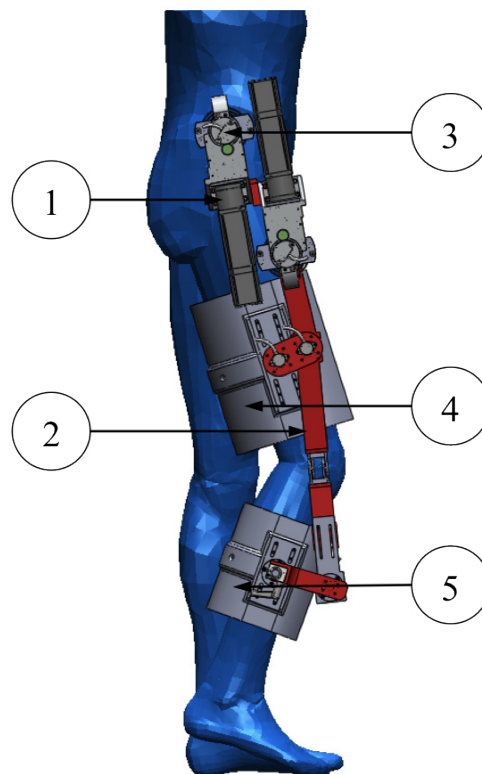


Figure 4.6: 3D CAD of hip/knee flexion/extension module. 1: link ad incorporating the two SEA 300W actuating the WR hip and knee subchains; 2: WR kinematic chain deriving from topology no.10; 3: connection site to the hip module; 4: thigh cuff; 5: calf cuff.

Giorgio Carpino

4.2.2.1 Thigh and calf cuffs

A powered wearable robot works in intimate mechanical contact with its human user. The design of an effective WR requires extraordinary attention to the details of this coupling. A well-engineered WR can still fail if it does not mesh seamlessly with the user's mobility, if it applies unusual or excessive forces to the body, or if it loads the body in a manner that causes discomfort or even pain to the users.

The physical attachment of machine to human must be designed carefully in order to tackle the problem of applying significant forces to the skeleton while keeping skin loading to acceptable levels. Shear loads are important because they are disruptive for skin, but a small shear load is acceptable even over many cycles. The friction of the material against the skin has a role in the damage process [130]. It appears that skin tolerates high cycles of low shear loads better than few cycles of high loads which bodes well for a WR designed with low shear loads which cycle with each step. Moisture and temperature influence the ability of skin to maintain integrity under load. The wearable robot attachment points must be kept away from heat generating sources.

As with any orthosis, the challenge in designing attachments is the trade-off between rigid coupling to the skeleton and comfort for the user. Because rigid coupling is not feasible at all, any connection will move relative to the skeleton. A well-designed attachment point meets these requirements: *(i)* distributes the load, *(ii)* minimizes shear, *(iii)* avoids bony points, and *(iv)* keeps the skin cool. Another critical design criteria for the attachments are that the exoskeleton be easily donned and doffed.

Off-the-shelf, commercial orthosis (GYSGY Reha Kft., Budapest, Hungary) have been chosen to couple the WR to the thigh. An opportunely shaped orthosis has been designed and produced, always by the same company, to couple the WR to the calf. The orthoses are provided with a hard polyethylene outer shell provided with an aluminum bar with tapped holes for mounting components and are lined with soft padding. The orthoses are disposable in different sizes and the shape of the shell conforms closely to the thigh and the calf which results in a close, comfortable fit when the component is closed. In Fig. 4.7 pictures of the thigh and calf cuffs are



shown.



Figure 4.7: Three pictures of the worn thigh and calf cuffs produced by GYSGY Reha Kft. (Budapest, Hungary).

The objective is to render the cuffs as stiff as possible in order to transmit only pulling and pushing forces (avoiding shear forces) from the WR to the human limbs and still guaranteeing wearability and comfort to the users. To achieve this tradeoff an aluminum C-shaped insert has been designed to be integrated in the polyethylene shell. The brace presents a plate connecting the WR to the cuffs and an arched part with an aperture of 120 deg in contact with the back of the thigh and calf segments.

The braces have been opportunely dimensioned taking into account the anthropometric data used by GYSGY Reha Kft. FEM analyses have been conducted on the thigh and calf braces so to verify their robustness and rigidity. As it is shown in Fig. 4.8-(a-b), the braces have been fixed in correspondence of the tapped holes connecting the WR to the cuffs and have been loaded with a normal distributed forces on the C-shaped parts of the inserts. The applied forces were calculated as the ratio between the peak torques at the hip and knee joints (retrieved by the Winter dataset [96]) and the distance between the center of the cuffs and the human

A handwritten signature in black ink, appearing to read 'Giorgio Carpino'.

hip and knee center of rotation respectively. In Fig. 4.8-(c-d) the 1:1 deformation and the maximum von Mises stress for the thigh and calf C-brace are respectively shown; considering an aluminum alloy for the brace like Anticorodal (aluminum alloy 6082, yield stress 240 MPa), a total thickness of 5 mm and a height of the C-shaped part of 30 mm for both braces, the inserts are verified with a SF of 2.8 and 2.6 with a maximum deflection of 2.7 deg and 2.2 deg for the thigh and calf cuffs respectively.

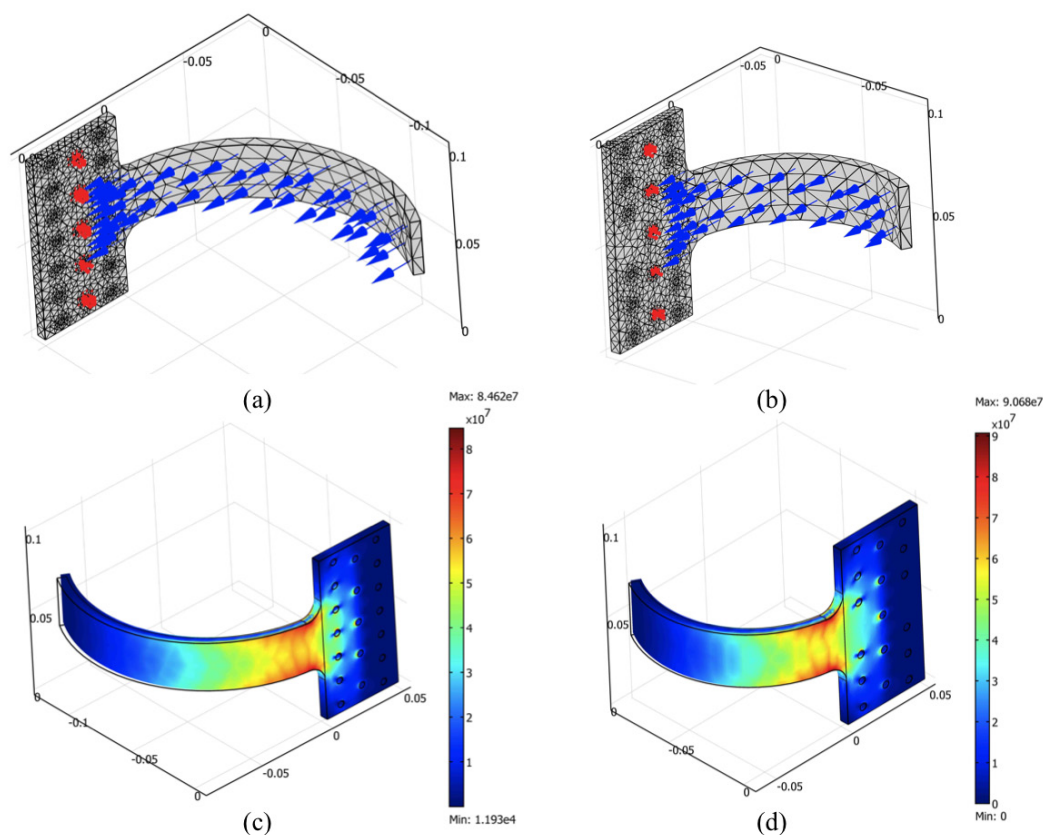


Figure 4.8: FEM analysis of the C-shaped inserts of thigh and calf cuffs. (a-b): boundary conditions and mesh for thigh and calf braces respectively; (c-d): 1:1 deformation and von Mises stress for thigh and calf braces respectively.

The presence of other tapped holes on the inserts plates is due to the possibility of regulate the height of the attachments to the WR depending on the different users limbs length. Other types of regulation will be implemented in order to properly tune the angle and the distance between the planes defined by the inserts plates of

the thigh and calf cuffs in order to avoid possible misalignments that could cause wrong torque transmission from the WR to the human limbs and consequent pain for the users.

4.3 Hip module

The *actively controlled hip module* (ACHM) extends the original idea of WR that powers the lower limbs only in the sagittal plane by assisting hip/knee flexion/extension. ACHM controls two anatomic motions of the hip by implementing actively assisted hip adduction/abduction and intra/extrarotation. One of the added value of the introduction of the hip module are that the role of the hip in the emerging dynamics of a robotic walking can be investigated.

Initially, a major simplification concerning the topology of WR was introduced in order to reduce the size of the parameters search space: only WRs with revolute joints in the sagittal plane were planned to be investigated. This choice is not critical for the validation of the proposed design approach, though the actual transfer to application of the WR as a real assistive device will require the inclusion of additional DOFs in the system. For example, movements outside the sagittal plane have been shown to be important in a physiological gait, mostly for maintaining stability in the frontal plane. This was also evidenced by clinicians, who established that six determinants can be used to assess the ability of a person to walk with a physiological pattern, and three of them describe movements outside the sagittal plane [131]. In [5], a list of requirements for a successful human-robot interaction is provided. Among them it is reported that a human-interfacing rehabilitation or assisting robot should be able to selectively apply torques to each human DOF which is relevant for a given motor task. Under these considerations, it is possible to conclude that hip adduction/abduction is a relevant DOF for assisting and restoring natural human walking; similar considerations can be also inferred for the possible inclusion also of the intra/extrarotation hip DOF. No other exoskeletons or wearable robots including a wearable hip module actively controlling all the three DOFs has been retrieved in the literature survey. The analysis of the state of the art of wearable robotics for the lower limbs has shown that the natural anatomical motions of the



hip are not supported at all, or supported with passive joints, or supported at most with active hip abduction/adduction. From a biomechanical point of view the use of passive compliant joints in the hip module are acceptable but compromised solutions. The hip abduction/adduction and intra/extrarotation require active control by the orthosis during the restoration of the normal gait.

Other practical benefits of adding ACHM to the WR, originally acting only in the sagittal plane, are the expected significant improvements in terms of ergonomics, thanks to the better compliance to human anatomy.

The design of the module has been developed by the Department of Manufacturing Science and Technology of Budapest University of Technology and Economics in collaboration with the Laboratory of Biomedical Robotics and Biomechanics of University Campus Bio-Medico of Rome. The candidate has spent three months in this department working on the the integration of the WR sub-modules.

4.3.1 Hip abduction/adduction and intra/extrarotation module

4.3.1.1 ACHM requirements

Table 4.2 lists the ROM during walking, the peak torque and the peak power for hip joint for the abduction/adduction and intra/extrarotation movements [132] and the expected minimum and maximum ranges of motion, peak torque and peak power for the ACHM module. The ACHM minimum ranges of motion coincide with the ranges of motion during walking for the four considered hip movements while the maximum ranges of motion coincide with the maximum physiologic ranges of motion for the hip joint in the frontal and transverse anatomical planes. The ACHM expected torque and power are calculated as the 30% of the hip joint peak torque and power; this percentage has been considered enough to provide assistance to lower limbs movements the frontal and transverse planes during gait.

The maximum weight of the ACHM has been set to 7 kg. This constraint, as already described in the previous paragraphs, has been also implemented as added mass at torso level in the simulation environment. In order to allow the wearability of the module, ACHM centers of rotation and hip centers of rotation should be



TABLE 4.2: PHYSIOLOGICAL RANGE OF MOTION (ROM), PEAK TORQUE AND PEAK POWER OF HIP DURING NORMAL GAIT FOR A 75 KG PERSON [132]. ALSO THE EXPECTED VALUES FOR ACHM ROM, MINIMUM TORQUE AND MINIMUM POWER ARE LISTED.


Hip DOFs	ROM during walking [deg]	Peak torque [Nm]	Peak power [W]	ACHM min. ROM [deg]	ACHM max. ROM [deg]	ACHM min. torque [Nm]	ACHM min. power [W]
Abduction	6	90	45	6	40	30	15
Adduction	4	15	60	4	15	5	20
Intrarotation	5	15	4	5	33	5	1.5
Extrarotation	5	15	15	5	34	5	5

aligned as much as possible in order to avoid misalignments, which could cause discomfort or pain to the users; the maximum allowed misalignment error is tolerated within a circle of 10 mm in diameter. The ACHM should guarantee users adaptability because it will be worn by different users with different anthropometric data (the adjustability has to fulfill with the full anthropometric size ranges of dataset reported in [128]). The maximum allowed temperature for the ACHM components is 40 °C. The module has to provide a flange to connect the hip/knee flexion/extension module.

4.3.1.2 ACHM design

A number of design iterations has been carried on considering both parallel or serial mechanisms; a serial configuration has been chosen in order to fulfill the requirements listed above. 3D CAD views of the ACHM resultant module are depicted in Fig. 4.9. As it is clear from the figure, the ACHM dimensions are 170 mm in the sagittal plane and 70 mm in the frontal plane considering in both cases as dimensions the distance between the human body and the end of the hip module.

In Fig. 4.10 the ACHM serial mechanism is shown; for the sake of clarity only the right leg mechanism is reported. The module presents four equal actuation systems (Fig. 4.10-2,4), two per each leg, to actuate the hip abduction/adduction and intra/extrarotation DOFs and to fulfill the requirements in terms of required torque and power listed in Tab. 4.2. The actuators are composed by a Maxon brushed



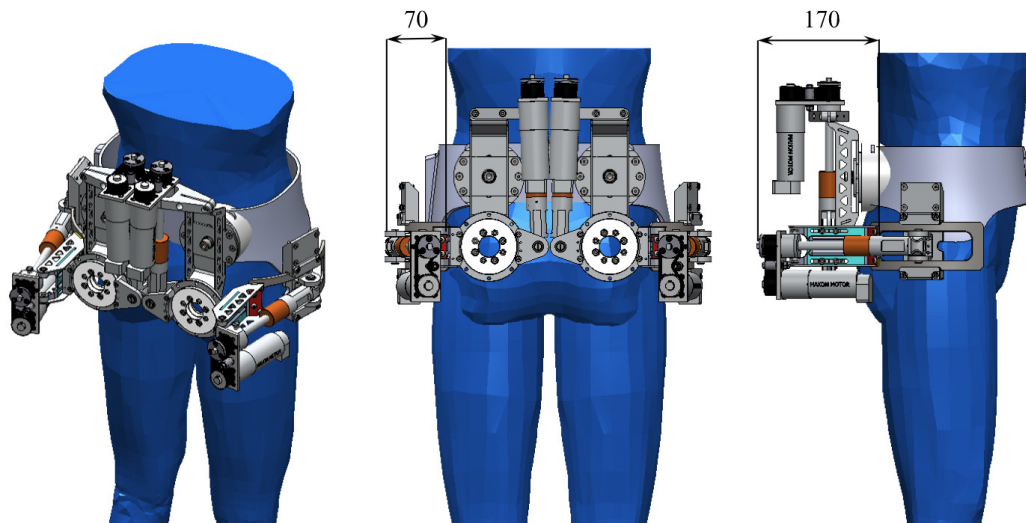


Figure 4.9: Three views of ACHM module 3D CAD. Dimensions in the sagittal and frontal anatomical planes are shown in [mm].

motor RE 40 150W equipped with a Maxon planetary gearhead GP 42C with a reduction ratio of 4.3:1 and an optimal incremental encoder Maxon HEDS 5540 with 500 cpt. The gearmotor is connected to a SKF spindle drive equipped with a miniature ball screw with ball recirculation. The coupling between the gearmotor and the spindle is realized thanks to a timing belt-pulley mechanism with a reduction ratio of 1:1.

For the abduction/adduction actuation the force exerted by the actuator (Fig. 4.10-2) is transmitted to the slewing ring bearing (Fig. 4.10-3) that in turn transmits the force to the interface with hip/knee flexion/extension module (Fig. 4.10-7) through the sliding flange (Fig. 4.10-6). The chosen slewing ring bearing is a IGUS iglidur PRT with extremely low weight and an external diameter of 100 mm; the outer ring is made of anodized aluminum while the inner rings is made of iglidur J4 run without lubricants directly against the outer ring.

For the intra/extrarotation, instead, the force exerted by the actuator (Fig. 4.10-4) is transmitted to the interface with hip/knee flexion/extension module (Fig. 4.10-7) causing the sliding of the module on the flange (Fig. 4.10-6). Silicon dampers are placed at the end of the ball screw in order to act as shock absorbers.

A force sensor based on the use of strain gauges (Fig. 4.10-5) is placed in the

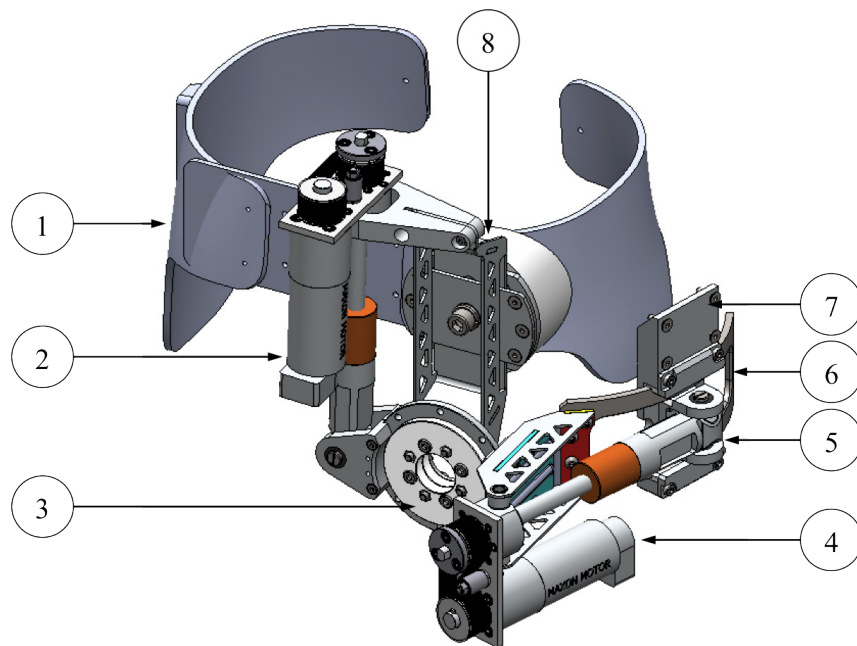


Figure 4.10: Serial mechanism of ACHM module. 1: hip belt; 2 and 4: equal actuation systems for the abduction/adduction and intra/extrarotation DOFs composed by a Maxon gearmotor of 150W and a spindle drive coupled through a timing belt mechanism; 3: IGUS slewing ring bearing; 5: shaft integrating strain gauges for force measurement; 6: sliding flange for intra/extra rotation; 7: interface with hip/knee flexion/extension module; 8: connection to the hip belt with to the possibility to adapt the module to different anthropometric sizes.

shaft at the end of the spindle drive of the actuator for the intra/extrarotation. The arrangement of the force sensor has been decided after FEM analyses showing that this zone is the most stressed of the entire ACHM and thus the more eligible to place the sensor.

The entire hip module is connected to the human waist through a custom-made hip orthosis developed by GYSGY Reha Kft. The mechanisms for the two legs are connected through apposite pads enabling also the regulation of the module to different anthropometric sizes of the users.

The ACHM mechanism is able to provide a maximum ROM of 25 deg for all the four actuated hip DOFs thus fulfilling the ROM requirements listed in Tab. 4.2. Only the abduction ROM is limited to 10 deg because to avoid the penetration in the user torso of the actuator of the hip/knee flexion/extension module actuating

A handwritten signature in black ink, appearing to read 'Giorgio Carpino'.

the hip subchain.

4.4 Modules integration and future works

In Fig. 4.11 four views of the rendering of the full WR concept, integrating the two submodules described above, are shown. The weight of the WR is about 25 kg.

An ankle module is also under development. The *actively controlled ankle module* (ACAM) actuates the dorsi/plantar flexion of the ankle and passively allows the other movements in the frontal and transverse plane. The actuation of the ankle joint is expected to improve gait stability and to achieve a better physiological gait. The presence of the ankle module allows the transfer of the WR load to the ground.

The ankle module will be composed by an ankle/foot orthosis (developed by GYSGY Kft. as for the other cuffs) and by a mechanism allowing the active control of the dorsi/plantarflexion through a brushed motor and allowing the spring-based passive motion of the feet in the other two anatomical planes. The ACAM will be connected to the WR through the calf cuff of the hip/knee flexion/extension module.

Some improvements will be also implemented in the evolutionary design of WR. Although the exclusive use of revolute joints will be considered as a first choice in planning the design phase, in order not to limit the open-endedness of robotic solutions provided by the evolutionary algorithm, it would be useful also to consider prismatic joints in the evolutionary co-design process. Prismatic joints could be considered in the simulations in order to evaluate advantages and disadvantages of the two solutions (with and without prismatic joints). The optimization in the simulation environment also of the kinematic chains actuating the DOFs outside the sagittal plane will lead to the optimization of the mechanism actuating the movements in the other two anatomical planes (in this case at the hip and ankle level).

The WR will be initially tested on healthy subjects walking on a treadmill in order to validate the outputs of the novel design methodology described in the first paragraphs. The final prototype of the robot will need a structured environment to be tested. The use of a treadmill is thus mandatory to keep fixed all external



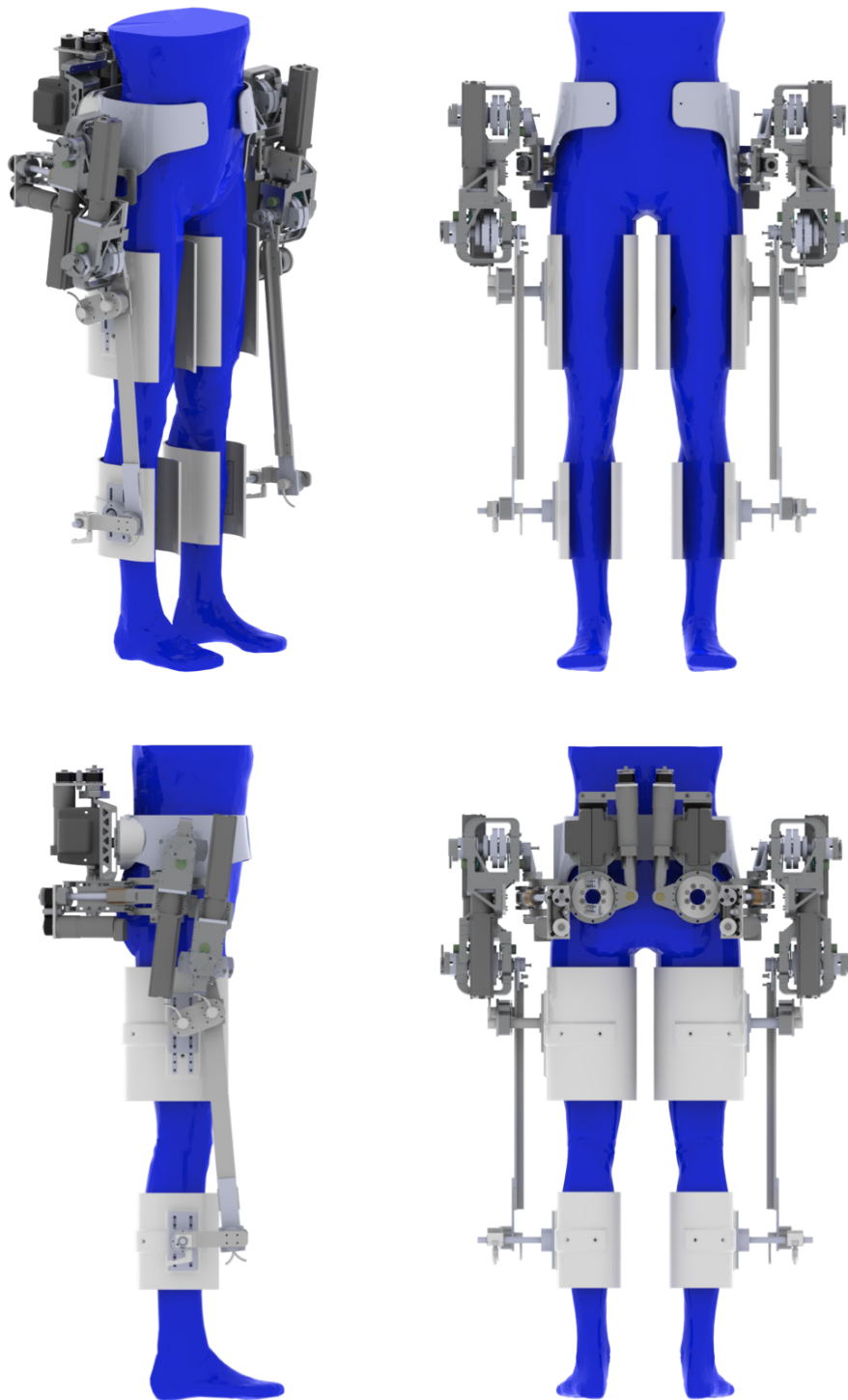


Figure 4.11: Four views of the rendering of the lower limbs WR concept.

Giorgio Carpino

components (electronics and power supply); in this first phase, the focus will be on the evaluation of the enhancements introduced by the adoption of the novel design methodology not focusing on the optimization of such aspects related to wearability such as integration of electronic components (motor drivers, acquisition boards, computation units, etc.) or power supply. A harness will be adopted to guarantee safety for the testers. The objective of the prototype is to demonstrate the advantages of structural intelligence in assisting steady straight walking. As such, other tasks, involving the assistance of a wearable robot (e.g. sitting), are not central to the feasibility proof. Anyhow, the actuators described in this thesis can be conveniently used also with other kinematic structures, including anthropomorphic ones.

The emerging dynamic behaviours arisen from the coupling of the dynamics of human body and wearable robot will be evaluated through the analysis of the metabolic consumption of the testers and the monitoring of the ECG activity of the lower limbs muscles.

The target users will then be switched to elderly people with chronic gait impairments. Since in this case the subjects will not have balance problems and with significant motor residual capabilities, the harness will be useful only for safety reasons and not for support function. The hypothesis to test the robot on users with lower limbs disabilities will be also taken into account.



Chapter 5

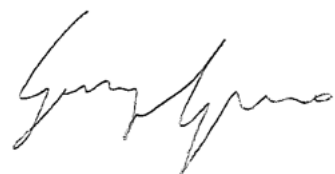
Conclusions

In 2000 elderly people in Europe aged 65 or over were more than 60 million (16.4% of the EU population). The rise in life expectancy is set to continue; combined with falling birth rates, this will accelerate the aging of the population. The EU population aged 60 and over is expected to rise by 37% by 2050. This will certainly have a great impact on the development of the wearable robotic devices.

The development of efficient robotic systems for rehabilitation and assistive purposes requires the synergistic deployment of advanced solutions from multiple aspects, including the choice of the kinematic structure, actuation systems and from a comprehensive knowledge of relevant biomechanical and neural properties of the human component.

This thesis investigates the application of biomechatronic design methods in the design of two concepts of wearable robotic orthoses for gait assistance. In both contexts, the described contributions represented advancements with respect to the current state of the art.

An analysis of the state-of-the-art of currently existing devices allowed to formulate a research hypothesis. The introduction in the field of wearable robotics of the concept of embodied intelligence, in particular structural intelligence, and of the concepts derived from the findings in the field of passive walkers, can lead to the design of optimal solutions in terms of kinematics and thus ergonomics and in terms of dynamics and thus the emergence of dynamic behaviours arisen from the



coupling between the human and robot components. The embodiment of robotic artefacts has so far been intended as a principle useful to achieve a strict interrelation between cognitive and physical processes, exploiting the interaction with the environment. Many embodied intelligence robots designed so far are animal-like artificial artefacts whose physical and cognitive functions are conceived to exploit the embodied interaction with a more or less complex and variable ecological niche. If the ecological niche is the human body, an enormous, extremely variable amount of physical, dynamical and neuromuscular properties has to be taken into account, which a robot should symbiotically exploit for a positive interaction. In order to obtain this symbiotic interaction robot topology and morphology need not to be predefined but must emerge from an evolutionary design phase in which the interaction with the physical interaction with the human body is taken into account and optimized. The effect of the process of designing robots in order to optimize dynamically the interaction between the machine and the environment has already been investigated for bipedal walking robots, and the advantages in terms of energy consumption and biomimicry have been analyzed.

The development of novel compliant active and passive joints allows to design new robot for human gait assistance exploiting the above-mentioned concept of structural intelligence. In the attempt to overcome the mentioned challenges, the design methodology followed in this work involves developing custom elements with minimal dimensions and mass, such as the monolithic torsional spring, and carefully selecting commercial components where possible able to satisfy given different design requirements. The developed torsional springs have been integrated in two Series Elastic Actuators with different architectures due to the differences in power and torque specifications. A passive viscoelastic joint, integrating a stiffness and a damping modules able to regulate joint stiffness and damping respectively, has been also developed and characterized.

The SEA 90W has been integrated in a frame of a knee orthosis for the assistance of human knee movements. The SEA 300W, instead, has been adopted for the actuation system of a non-anthropomorphic lower limbs wearable robot for human gait assistance. The choice of non-anthropomorphic kinematic solution can provide



improvements over the currently available anthropomorphic solutions both from an ergonomics standpoint and from the chance of exploiting the intrinsic dynamics of the system comprising both human and robot.


Once defined the robot kinematic chain, the solutions adopted for the design of the different submodules of the wearable robot have been discussed. The design choices and the requirements for the assistance in the sagittal and in the frontal anatomical planes of all the hip and knee DOFs have been accurately analyzed. A concept of the resultant wearable robot and future works regarding a novel ankle module and the WR testing on different target populations are finally reported and discussed.

An estimation of the possible social impact of a well-conducted validation test in humans of a device that allows restoring of walking is given by the consideration that the average age of population is dramatically increasing as described above. Furthermore, the reduction or loosing in gait abilities is commonly accepted as one of the most indicative parameters in the evaluation of the grade of disability and it is strictly linked with the cost sustained by the national health systems.

The long-term goal is to develop and test a novel methodology for the design of wearable robots, which can serve the specific needs of selected groups of people with similar walking anomalies. This design method is expected to lead to a new generation of wearable robots, expected to be more energy-efficient through the symbiotic dynamics interaction and able to adapt to a wider population of impaired users, thanks to the tunability of the hardware and the flexibility of the adaptive control.



Tesi di dottorato in Ingegneria Biomedica, di Giorgio Carpino,
discussa presso l'Università Campus Bio-Medico di Roma in data 20/03/2012.
La disseminazione e la riproduzione di questo documento sono consentite per scopi di didattica e ricerca,
a condizione che ne venga citata la fonte

A handwritten signature in black ink, appearing to read "Giorgio Carpino". The signature is fluid and cursive, with the first name "Giorgio" and the last name "Carpino" clearly distinguishable.

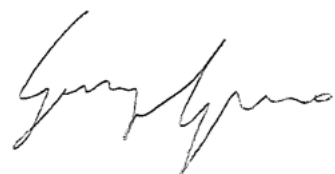
Appendix A

Selection of spring stiffness for SEA

Ideally, a SEA can be considered a pure force source within the controlled bandwidth. The deflection of the spring can be used to estimated as feedback signal for the force control (see Fig. A.1). The compliant element lowers the loop gain of the closed-loop system; for this reason the controller gain can be proportionally increased to maintain the overall loop gain of the actuator at desired stability margins. This allows to have:

- low output impedance;
- tolerance to shock loading;
- robustness to changing loads;
- reduction of the effects of internal stiction and other transmission non-linearities (friction and backlash);
- clean force output;
- simple force control.

The minimal model and the block diagram of Fig. A.1 can help understanding some important features of a SEA, to define indications for the choice of its components in the design phase.



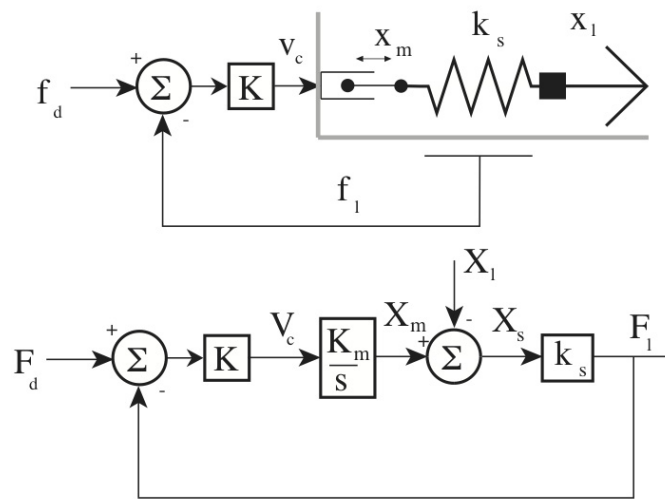


Figure A.1: Minimal model and block diagram for a Series Elastic Actuator (from [80])

For simplicity the motor is modeled as a high impedance velocity source (motor inertia is neglected and it is assumed that the actuator can perfectly generate the output velocity given the commanded one); moreover, force controller only consists in a proportional gain (K). f_d is the desired force; f_l is the measured force; V_c is the motor commanded voltage; x_m is the motor position; x_l is the load position; k_s is the stiffness of the series elastic element.

The closed loop function in these conditions is:

$$\frac{F_l}{F_d} = \frac{k_s \cdot K \cdot K_m}{s + k_s \cdot K \cdot K_m} \quad (\text{A.1})$$

in which ω_c ($\omega_c = k_s \cdot K \cdot K_m$) is the cutting frequency. It can be noticed that a decrease in spring stiffness is compensated for an increase in control gain in order to maintain a high closed-loop bandwidth. For this reason bandwidth limit is independent from spring stiffness. The large force bandwidth (LFB) is the frequency range over which the actuator can oscillate at a force amplitude equivalent to the maximum force. It can be demonstrated (see [80]) that it is independent of the control system. The mechanical output impedance is defined as the minimum force an actuator outputs for a given load motion. Ideally, the impedance of a force controlled device is zero.

Low impedance means that the actuator appears to the robot as a pure force source with negligible internal dynamics.

The output impedance (referred to the model in Fig. A.1) is expressed by:

$$\frac{F_l}{x_l} = \frac{-k_s \cdot s}{s + k_s \cdot K \cdot K_m} \quad (\text{A.2})$$

It is:

- minimal at low frequency (it is equivalent to having a zero rate spring connected to the load; any load mass will move around and react to the actuator force commands almost entirely decoupled from the dynamics of the actuator itself);
- equal to the physical spring at high frequencies.

The selection of the spring stiffness emerges as a tradeoff between the large force bandwidth and low intrinsic impedance. The guidelines for this choice are reported in [80]:

- selection of a motor and transmission based on the force, speed, and power requirements;
- definition of an operational bandwidth for which the actuator will need large forces (the large force bandwidth profile is independent of controller); this places a lower bound on the stiffness;
- definition of the minimum tolerable impedance; this places an upper bound on the stiffness;
- choice of a spring within the two set bounds. It may be necessary to iterate the process.



Tesi di dottorato in Ingegneria Biomedica, di Giorgio Carpino,
discussa presso l'Università Campus Bio-Medico di Roma in data 20/03/2012.
La disseminazione e la riproduzione di questo documento sono consentite per scopi di didattica e ricerca,
a condizione che ne venga citata la fonte

A handwritten signature in black ink, appearing to read "Giorgio Carpino". The signature is fluid and cursive, with the first name "Giorgio" and the last name "Carpino" clearly distinguishable.

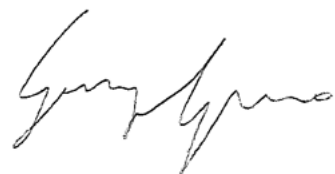
List of Publications

Journal papers

1. F. Sergi, D. Accoto, N. L. Tagliamonte, **G. Carpino**, E. Guglielmelli, "A systematic graph-based method for the kinematic synthesis of non-anthropomorphic wearable robots for the lower limbs", *Frontiers of Mechanical Engineering*, vol. 6, no. 1, pp. 61-70, 2011.
2. **G. Carpino**, D. Accoto, F. Sergi, N. L. Tagliamonte, E. Guglielmelli, "A novel compact torsional spring for Series Elastic Actuators", Under review for *ASME Journal of Mechanical Design*, September 2011.
3. N. L. Tagliamonte, F. Sergi, D. Accoto, **G. Carpino**, E. Guglielmelli, "Double actuation architectures for varying impedance in compliant robots", Under review for *Mechatronics*, January 2012.

Peer-reviewed international conferences


1. F. Sergi, D. Accoto, **G. Carpino**, N. L. Tagliamonte, E. Guglielmelli, "Design and Characterization of a Compact Rotary Series Elastic Actuator for Knee Assistance During Overground Walking", Submitted to *International Conference on Biomedical Robotics and Biomechatronics (BIOROB 2012)*, Rome, Italy, June 2012.
2. D. Accoto, N. L. Tagliamonte, **G. Carpino**, F. Sergi, M. Di Palo, E. Guglielmelli, "A novel modular passive viscoelastic joint for wearable robots", Accepted for the *International Conference on Robotics and Automation 2012 (ICRA 2012)*, St. Paul, Minnesota, USA, May 2012.



3. **G. Carpino**, D. Accoto, M. Di Palo, N. L. Tagliamonte, F. Sergi, E. Guglielmelli, "Design of a rotary passive viscoelastic joint for wearable robots", *Proceedings of the International Conference of Rehabilitation Robotics (ICORR 2011)*, Zurich, Switzerland, pp. 1-6, July 2011.
4. N. L. Tagliamonte, F. Sergi, **G. Carpino**, D. Accoto, E. Guglielmelli, "Design of a variable impedance differential actuator for wearable robotics applications", *Proceedings of the 2010 IEEE/RSJ International Conference on Intelligent Robots and Systems (IROS 2010)*, Taipei, Taiwan, pp. 2639-2644, 2010.
5. F. Sergi, D. Accoto, N. L. Tagliamonte, **G. Carpino**, E. Guglielmelli, "Graph-based methodology for the kinematic synthesis of wearable assistive robots for the lower limbs", *Proceedings of the 32nd International Conference of the IEEE Engineering in Medicine and Biology Society (EMBC 2010)*, Buenos Aires, Argentina, pp. 3682-5, 2010.
6. F. Sergi, D. Accoto, N. L. Tagliamonte, **G. Carpino**, L. Pathiyil, E. Guglielmelli, "A systematic graph-based method for the kinematic synthesis of non anthropomorphic wearable robots", *Proceedings of the IEEE International Conference on Robotics, Automation and Mechatronics (CIS-RAM 2010)*, Singapore, pp. 100-105, 2010.
7. L. Pecchia, **G. Carpino**, L. Mirarchi, M. Bracale, "The preservation of the CE mark for a medical device further to a maintenance process", *Proceedings of International Conference on Information Technology and Applications in Biomedicine (ITAB 2009)*, Larnaca, Cyprus, pp. 1-4, 2009.

Abstracts in international conferences

1. D. Accoto, **G. Carpino**, N. L. Tagliamonte, M. Di Palo, F. Sergi, E. Guglielmelli, "Active and passive devices for tuning impedance in wearable robotics", *Workshop on Biologically-inspired Actuation at the International Conference on Robotics and Automation 2011 (ICRA 2011)*, Shanghai, China, May 2011.



2. D. Accoto, F. Sergi, **G. Carpino**, N. L. Tagliamonte, E. Guglielmelli, "A design methodology for neurorehabilitative and assistive wearable robots incorporating embodied intelligence", *14th European Congress on Clinical Neurophysiology (ECCN 2011)*, Rome, Italy, May 2011.
3. D. Accoto, N. L. Tagliamonte, F. Sergi, **G. Carpino**, E. Guglielmelli, "VIDA: a Variable Impedance Differential Actuator", *Workshop on New variable impedance actuators for the next generation of robots (ICRA 2010)* Anchorage, AK, USA, May 2010.

Peer-reviewed national conferences

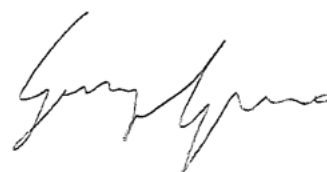
1. **G. Carpino**, F. Sergi, N. L. Tagliamonte, D. Accoto, E. Guglielmelli, "Series Elastic Actuators for lower limbs wearable robots for assistance during over-ground walking", Submitted to *GNB 2012*, Rome, Italy, June 2012.
2. D. Accoto, F. Sergi, N. L. Tagliamonte, **G. Carpino**, E. Guglielmelli, "Biomechatronic design of a non-anthropomorphic 2DOFs wearable orthosis for gait assistance", Submitted to *GNB 2012*, Rome, Italy, June 2012.
3. **G. Carpino**, F. Sergi, D. Accoto, E. Fischetti, N. Tagliamonte, E. Guglielmelli, "Design di giunti rotoidali per robot indossabili non antropomorfi", *Neuroriabilitazione Robotica dell'Arto Superiore*, Genova, Italy, December 2009.
4. N. Tagliamonte, F. Sergi, D. Accoto, **G. Carpino**, E. Guglielmelli, "Modelazione e controllo di un attuatore differenziale ad impedenza variabile per robot esoscheletrici", *Neuroriabilitazione robotica dell'arto superiore*, Genova, Italy, December 2009.

Technical reports

1. N. L. Tagliamonte, **G. Carpino**, F. Sergi, M. Di Palo, D. Accoto, E. Guglielmelli, "Development of VIJs", *Deliverable 5.2 of the Evryon Project, FP7-ICT-2007.8.5-231451*, March 2011.

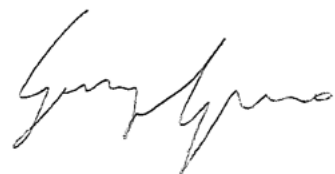


2. **G. Carpino**, A. Toth, N. L. Tagliamonte, S. De Rossi, T. Lenzi, N. Vitiello, "Report on the basic requirements of the design of the actively controlled hip module", *Deliverable 9.1 of the Evryon-Project, FP7-ICT-2007.8.5-231451*, October 2010.
3. F. Sergi, **G. Carpino**, N. L. Tagliamonte, D. Accoto, E. Guglielmelli, "Basic constraints on robot design", *Deliverable 5.1 of the Evryon-EEU-Project, FP7-ICT-2007.8.5-231451*, July 2009.



Bibliography

- [1] A. De Santis, B. Siciliano, A. De Luca, and A. Bicchi. An atlas of physical human-robot interaction. *Mechanism and Machine Theory*, 43:253–270, Feb. 2008.
- [2] J. L. Pons. *Wearable Robots: Biomechatronic Exoskeletons*. John Wiley & Sons, Ltd, 2008.
- [3] A. Dollar and H. Herr. Lower extremity exoskeletons and active orthoses: Challenges and state-of-the-art. *Robotics, IEEE Transactions on*, 24(1):144 – 158, 2008.
- [4] E. Guglielmelli, M. Johnson, and T. Shibata. Guest editorial special issue on rehabilitation robotics. *Robotics, IEEE Transactions on*, 25(3):477 – 480, 2009.
- [5] A. Schiele and F. C. van der Helm. Kinematic design to improve ergonomics in human machine interaction. *IEEE Trans Neural Syst Rehabil Eng*, 14(4):456–69, Dec. 2006.
- [6] H. Herr. Exoskeletons and orthoses: classification, design challenges and future directions. *Journal of NeuroEngineering and Rehabilitation*, 6(1):21, 2009.
- [7] E. Guizzo and H. Goldstein. The rise of the body bots [robotic exoskeletons]. *Spectrum, IEEE*, 42(10):50 – 56, Oct. 2005.
- [8] K. H. Low. Robot-assisted gait rehabilitation: From exoskeletons to gait systems. In *Defense Science Research Conference and Expo (DSR), 2011*, pages 1 –10, Aug. 2011.
- [9] S. Mohammed and Y. Amirat. Towards intelligent lower limb wearable robots: Challenges and perspectives - state of the art. In *Robotics and Biomimetics, 2008. ROBIO 2008. IEEE International Conference on*, pages 312 –317, Feb. 2009.
- [10] J. L. Pons. Rehabilitation exoskeletal robotics. *Engineering in Medicine and Biology Magazine, IEEE*, 29(3):57 –63, 2010.
- [11] R. Bogue. Exoskeletons and robotic prosthetics: a review of recent developments. *Industrial Robot An International Journal*, 36(5):421–427, 2009.



- [12] W. S. Harwin, J. L. Patton, and V. R. Edgerton. Challenges and opportunities for robot-mediated neurorehabilitation. *Proceedings of the IEEE*, 94(9):1717–1726, Sept. 2006.
- [13] N. Yagn. Apparatus for facilitating walking, running and jumping. *US Patent 420179*, Jan. 1890.
- [14] H. Kazerooni and R. Steger. The Berkeley lower extremity exoskeleton. *Journal of Dynamic Systems, Measurement, and Control*, 128:14–25, 2006.
- [15] A. Zoss, H. Kazerooni, and A. Chu. Biomechanical design of the berkeley lower extremity exoskeleton (BLEEX). *Mechatronics, IEEE/ASME Transactions on*, 11(2):128–138, 2006.
- [16] A. Chu, H. Kazerooni, and A. Zoss. On the biomimetic design of the berkeley lower extremity exoskeleton (BLEEX). In *Robotics and Automation, 2005. ICRA 2005. Proceedings of the 2005 IEEE International Conference on*, pages 4345–4352, April 2005.
- [17] A. Zoss and H. Kazerooni. Design of an electrically actuated lower extremity exoskeleton. *Advanced Robotics*, 20(9):967–988, 2006.
- [18] S. C. Jacobsen. On the development of XOS, a powerful exoskeletal robot. *IEEE/RSJ IROS, Plenary Talk*, 2007.
- [19] S. Collins and A. Ruina. A bipedal walking robot with efficient and human-like gait. pages 1963–1968, 2005.
- [20] M. Vukobratovic and D. Juricic. Contribution to the synthesis of biped gait. *Biomedical Engineering, IEEE Transactions on*, 16(1):1–6, 1969.
- [21] M. Vukobratovic and B. Borovac. Zero-moment point - thirty five years of its life. *International Journal of Humanoid Robots*, 1(1):157–173, 2004.
- [22] C. H. Walsh, K. Endo, and H. Herr. A quasi-passive leg exoskeleton for load-carrying augmentation. *International Journal of Humanoid Robotics*, 4(3):487–506, Jan. 2007.
- [23] H. Kawamoto and Y. Sankai. Power assist system HAL-3 for gait disorder person. *Lecture Notes in Computer Science, Springer-Verlag*, (2398):196–203, Jan. 2002.
- [24] K. Suzuki, Y. Kawamura, T. Hayashi, T. Sakurai, Y. Hasegawa, and Y. Sankai. Intention-based walking support for paraplegia patient. *Systems, Man and Cybernetics, 2005 IEEE International Conference on*, 3:2707–2713, 2006.



- [25] H. Kawamoto, Suwoong Lee, S. Kanbe, and Y. Sankai. Power assist method for hal-3 using emg-based feedback controller. In *Systems, Man and Cybernetics, 2003. IEEE International Conference on*, volume 2, pages 1648 – 1653 vol.2, Oct. 2003.
- [26] K. Kasaoka and Y. Sankai. Predictive control estimating operator's intention for stepping-up motion by exo-skeleton type power assist system hal. In *Intelligent Robots and Systems, 2001. Proceedings. 2001 IEEE/RSJ International Conference on*, volume 3, pages 1578 –1583 vol.3, 2001.
- [27] H. Kawamoto, S. Kanbe, and Y. Sankai. Power assist method for hal-3 estimating operator's intention based on motion information. In *Robot and Human Interactive Communication, 2003. Proceedings. ROMAN 2003. The 12th IEEE International Workshop on*, pages 67 – 72, 2003.
- [28] X. Liu, K. H. Low, and H. Y. Yu. Development of a lower extremity exoskeleton for human performance enhancement. In *Intelligent Robots and Systems, 2004. (IROS 2004). Proceedings. 2004 IEEE/RSJ International Conference on*, volume 4, pages 3889 – 3894, 2004.
- [29] K.H. Low, X. Liu, and H. Y. Yu. Development of ntu wearable exoskeleton system for assistive technologies. In *Mechatronics and Automation, 2005 IEEE International Conference*, volume 2, pages 1099 – 1106, 2005.
- [30] Ekso bionics website, <http://berkeleybionics.com>.
- [31] K. A. Strausser and H. Kazerooni. The development and testing of a human machine interface for a mobile medical exoskeleton. In *Intelligent Robots and Systems (IROS), 2011 IEEE/RSJ International Conference on*, pages 4911 –4916, Sept. 2011.
- [32] K. A. Strausser, T. A. Swift, A. Zoss, and H. Kazerooni. Prototype medical exoskeleton for paraplegic mobility: First experimental results. *3rd Annual Dynamic Systems and Control Conference, September 13-15, 2010, Cambridge, MA, USA*, Jul. 2010.
- [33] T. A. Swift, K. A. Strausser, A. Zoss, and H. Kazerooni. Control and experimental results for post stroke gait rehabilitation with a prototype mobile medical exoskeleton. *3rd Annual Dynamic Systems and Control Conference*, Jul. 2010.
- [34] P. D. Neuhaus, J. H. Noorden, T. J. Craig, T. Torres, J. Kirschbaum, and J. E. Pratt. Design and evaluation of mina: A robotic orthosis for paraplegics. In *Rehabilitation Robotics (ICORR), 2011 IEEE International Conference on*, pages 1 –8, 2011.



- [35] H. K. Kwa, J. H. Noorden, M. Missel, T. Craig, J. E. Pratt, and P.D. Neuhaus. Development of the ihmc mobility assist exoskeleton. In *Robotics and Automation, 2009. ICRA '09. IEEE International Conference on*, pages 2556–2562, May 2009.
- [36] R. Farris, H. Quintero, and M. Goldfarb. Preliminary evaluation of a powered lower limb orthosis to aid walking in paraplegic individuals. *Neural Systems and Rehabilitation Engineering, IEEE Transactions on*, PP(99):1, 2011.
- [37] T. Nakamura, K. Saito, ZhiDong Wang, and K. Kosuge. Realizing a posture-based wearable antigravity muscles support system for lower extremities. In *Rehabilitation Robotics, 2005. ICORR 2005. 9th International Conference on*, pages 273–276, 2005.
- [38] T. Nakamura, K. Saito, and K. Kosuge. Control of wearable walking support system based on human-model and grf. In *Robotics and Automation, 2005. ICRA 2005. Proceedings of the 2005 IEEE International Conference on*, pages 4394–4399, April 2005.
- [39] T. Nakamura, K. Saito, ZhiDong Wang, and K. Kosuge. Realizing model-based wearable antigravity muscles support with dynamics terms. In *Intelligent Robots and Systems, 2005. (IROS 2005). 2005 IEEE/RSJ International Conference on*, pages 2694–2699, Aug. 2005.
- [40] Y. Mori, J. Okada, and K. Takayama. Development of a standing style transfer system "ABLE" for disabled lower limbs. *Mechatronics, IEEE/ASME Transactions on*, 11(4):372–380, Aug. 2006.
- [41] N. Costa and D.G. Caldwell. Control of a biomimetic "soft-actuated" 10dof lower body exoskeleton. In *Biomedical Robotics and Biomechatronics, 2006. BioRob 2006. The First IEEE/RAS-EMBS International Conference on*, pages 495–501, Feb. 2006.
- [42] Y. Fang, Y. Yu, F. Chen, and Y. Ge. Dynamic analysis and control strategy of the wearable power assist leg. In *Automation and Logistics, 2008. ICAL 2008. IEEE International Conference on*, pages 1060–1065, Sept. 2008.
- [43] M. Visintin, H. Barbeau, N. Korner-Bitensky, and N. E. Mayo. A new approach to retrain gait in stroke patients through body weight support and treadmill stimulation. *Stroke*, 29(6):1122–1128, 1998.
- [44] M. Frey, G. Colombo, M. Vaglio, R. Bucher, M. Jorg, and R. Riener. A novel mechatronic body weight support system. *Neural Systems and Rehabilitation Engineering, IEEE Transactions on*, 14(3):311–321, sept. 2006.



- [45] G. Colombo, M. Joerg, R. Schreier, and V. Dietz. Treadmill training of paraplegic patients using a robotic orthosis. *Journal of Rehabilitation Research and Development*, 37(6):693–700, May 2000.
- [46] L. L Cai, A. J Fong, C. K Otoshi, Y Liang, J. W Burdick, R. R Roy, and V. R Edgerton. Implications of assist-as-needed robotic step training after a complete spinal cord injury on intrinsic strategies of motor learning. *Journal of Neuroscience*, 26(41):10564–10568, Oct. 2006.
- [47] S. Jezernik, G. Colombo, and M. Morari. Automatic gait-pattern adaptation algorithms for rehabilitation with a 4-DOF robotic orthosis. *Robotics and Automation, IEEE Transactions on*, 20(3):574 – 582, 2004.
- [48] J. Veneman, R. Kruidhof, E. Hekman, R. Ekkelenkamp, E. Van Asseldonk, and H. van der Kooij. Design and evaluation of the Lopes exoskeleton robot for interactive gait rehabilitation. *Neural Systems and Rehabilitation Engineering, IEEE Transactions on*, 15(3):379 – 386, 2007.
- [49] E. Van Asseldonk, M. Wessels, A. H. Stienen, F. C. van der Helm, and H. van der Kooij. Influence of haptic guidance in learning a novel visuomotor task. *Journal of physiology, Paris*, 103:276–285, 2009.
- [50] R. G. West. Powered gait orthosis and method of utilizing same. *US Patent 7041069*, Jan 2006.
- [51] S. Banala, S. Agrawal, A. Fattah, V. Krishnamoorthy, W. L. Hsu, J. Scholz, and K. Rudolph. Gravity-balancing leg orthosis and its performance evaluation. *IEEE Transactions on Robotics*, 22(6):1228–1239, Nov. 2006.
- [52] S. Banala, S. H. Kim, S. Agrawal, and J. Scholz. Robot Assisted Gait Training With Active Leg Exoskeleton (ALEX). *Neural Systems and Rehabilitation Engineering, IEEE Transactions on*, 17(1):2 – 8, 2009.
- [53] D. Aoyagi, W.E. Ichinose, S.J. Harkema, D.J. Reinkensmeyer, and J.E. Bobrow. A robot and control algorithm that can synchronously assist in naturalistic motion during body-weight-supported gait training following neurologic injury. *Neural Systems and Rehabilitation Engineering, IEEE Transactions on*, 15(3):387 –400, Sept. 2007.
- [54] K. Kong and J. Doyoung. Design and control of an exoskeleton for the elderly and patients. *Mechatronics, IEEE/ASME Transactions on*, 11(4):428 – 432, 2006.



- [55] K. Kong, M. Tomizuka, H. Moon, B. Hwang, and D. Jeon. Mechanical design and impedance compensation of subar (sogang university's biomedical assist robot). In *Advanced Intelligent Mechatronics, 2008. AIM 2008. IEEE/ASME International Conference on*, pages 377–382, July 2008.
- [56] Y. Stauffer, Y. Allemand, M. Bouri, J. Fournier, R. Clavel, P. Metrailler, R. Brodard, and F. Reynard. The walktrainer - a new generation of walking reeducation device combining orthoses and muscle stimulation. *Neural Systems and Rehabilitation Engineering, IEEE Transactions on*, 17(1):38–45, Feb. 2009.
- [57] P. Wang, K.H. Low, A. Tow, and P.H. Lim. Initial system evaluation of an overground rehabilitation gait training robot (nature-gaits). *Advanced Robotics*, 25(15):1927–1948, 2011.
- [58] J. Burgess, G. Weibel, and D. Brown. Overground walking speed changes when subjected to body weight support conditions for nonimpaired and post stroke individuals. *Journal of NeuroEngineering and Rehabilitation*, 7(1):6, 2010.
- [59] T. Kubow and R. J. Full. The role of the mechanical system in control: a hypothesis of self-stabilization in hexapedal runners. *Philosophical Transactions of the Royal Society, Part B*, 354(1385):849–861, Jan. 1999.
- [60] R. Pfeifer and F. Iida. Morphological computation: connecting body, brain, and environment. *Japanese Scientific Monthly*, 2005.
- [61] R. Pfeifer, M. Lungarella, and F. Iida. Self-organization, embodiment, and biologically inspired robotics. *Science*, 318:1088–1093, 2007.
- [62] I. E. Brown and G. E. Loeb. *Biomechanics and Neuro-Control of Posture and Movement*, chapter A reductionist approach to creating and using neuromusculoskeletal movement. 2000.
- [63] R. J. Full and M. S. Tu. Mechanics of six-legged runners. *Journal of Experimental Biology*, 148:129–46, Jan. 1990.
- [64] J. G. Cham, S. A. Bailey, and M. R. Cutkosky. Robust dynamic locomotion through feedforward-preflex interaction. In *ASME IMECE Proceedings*, pages 5–10, 2000.
- [65] T. Mc Geer. Passive dynamic walking. *The International Journal of Robotics Research*, 9(2):62–82, 1990.



- [66] S. Collins, M. Wisse, and A. Ruina. A three-dimensional passive-dynamic walking robots with two legs and knees. *The International Journal of Robotics Research*, 20(7):607–615, Jul. 2001.
- [67] K. Matsushita, H. Yokoi, and T. Arai. Pseudo-passive dynamic walkers designed by coupled evolution of the controller and morphology. *Robotics and Autonomous Systems*, 54(8):674–685, 2006.
- [68] S. Krut, M. Benoit, E. Dombre, and F. Pierrot. Moonwalker, a lower limb exoskeleton able to sustain bodyweight using a passive force balancer. In *Robotics and Automation (ICRA), 2010 IEEE International Conference on*, pages 2215 –2220, May 2010.
- [69] A. Mokhtarian, A. Fattah, and S.K. Agrawal. A novel passive pelvic device for assistance during locomotion. In *Robotics and Automation (ICRA), 2010 IEEE International Conference on*, pages 2241 –2246, May 2010.
- [70] H. Vallery, A. Duschau-Wicke, and R. Riener. Hiding robot inertia using resonance. In *Engineering in Medicine and Biology Society (EMBC), 2010 Annual International Conference of the IEEE*, pages 1271 –1274, 2010.
- [71] C. J. Bosecker and H. I. Krebs. Mit-skywalker. In *Rehabilitation Robotics, 2009. ICORR 2009. IEEE International Conference on*, pages 542 –549, June 2009.
- [72] M. S. Cherry, S. Kota, and D. P. Ferris. An elastic exoskeleton for assisting human running. In *Proceedings of the ASME 2009 International Design Engineering Technical Conferences & Computers and Information in Engineering Conference, IDETC/CIE 2009*, pages 1–12, 2009.
- [73] P. Beyl, K. Knaepen, S. Duerinck, M. Van Damme, B. Vanderborght, R. Meeusen, and D. Lefeber. Safe and compliant guidance by a powered knee exoskeleton for robot-assisted rehabilitation of gait. *Advanced Robotics*, 25(5):513–535, 2011.
- [74] H.I. Krebs, N. Hogan, M.L. Aisen, and B.T. Volpe. Robot-aided neurorehabilitation. *IEEE Transactions on Rehabilitation Engineering*, 6(1):75–87, 1998.
- [75] M. H. Raibert and E. R. Tello. Legged robots that balance. *IEEE Expert*, 1(4):89, Nov. 1986.
- [76] J. W. Hurst, J. E. Chestnutt, and A. A. Rizzi. An actuator with physically variable stiffness for highly dynamic legged locomotion. *Proceedings of the IEEE International Conference on Robotics and Automation*, 5:4662–4667, 2004.



- [77] A. van den Bogert. Exotendons for assistance of human locomotion. *BioMedical Engineering OnLine*, 2(1):17, 2003.
- [78] R. Van Ham, T. Sugar, B. Vanderborght, K. Hollander, and D. Lefeber. Compliant actuator designs. *Robotics & Automation Magazine, IEEE*, 16(3):81 – 94, 2009.
- [79] G. Pratt and M. Williamson. Series elastic actuators. *Proceedings of the IEEE/RSJ International Conference on Intelligent Robots and Systems*, 1:399 – 406, 1995.
- [80] D. Robinson. Design and analysis of series elasticity in closed-loop actuator force control. *Ph.D. dissertation, Massachusetts Inst. Technol. (MIT), Cambridge*, 2000.
- [81] D. Paluska and H. Herr. The effect of series elasticity on actuator power and work output: Implications for robotic and prosthetic joint design. *Robotics and Autonomous Systems*, 54(8):667–673, 2006.
- [82] H. Vallery, J. Veneman, E. van Asseldonk, R. Ekkelenkamp, M. Buss, and H. van der Kooij. Compliant actuation of rehabilitation robots: benefits and limitations of series elastic actuators. *IEEE Robotics & Automation Magazine*, 15(3):60–69, 2008.
- [83] G. Pratt. Legged robots at MIT: what's new since Raibert? *IEEE Robotics & Automation Magazine*, 7(3):15 – 19, 2000.
- [84] J F Veneman, R Ekkelenkamp, R Kruidhof, F van der Helm, and H van der Kooij. A series elastic- and bowden-cable-based actuation system for use as torque actuator in exoskeleton-type robots. *The International Journal of Robotics Research*, 25(3):261–281, 2006.
- [85] K. Kong, J. Bae, and M. Tomizuka. A compact rotary series elastic actuator for knee joint assistive system. *Proceedings of the 2010 IEEE International Conference on Robotics and Automation*, pages 2940–2945, 2010.
- [86] N. Tsagarakis, M. Laffranchi, B. Vanderborght, and D. Caldwell. A compact soft actuator unit for small scale human friendly robots. *IEEE International Conference on Robotics and Automation*, pages 4356 – 4362, 2009.
- [87] S. Yoon, S. Kang, S. Kim, Y. Kim, M. Kim, and C. Lee. Safe arm with MR-based passive compliant joints and visco-elastic covering for service robot applications. *Intelligent Robots and Systems, 2003. (IROS 2003). Proceedings. 2003 IEEE/RSJ International Conference on*, 3:2191 – 2196 vol.3, 2003.



- [88] G. Wyeth. Demonstrating the safety and performance of a velocity sourced series elastic actuator. *Proc. IEEE International Conference on Robotics and Automation*, pages 3642 – 3647, 2008.
- [89] C. Lagoda, A. Schouten, A. Stienen, E. Hekman, and H. van der Kooij. Design of an electric series elastic actuated joint for robotic gait rehabilitation training. *3rd IEEE RAS and EMBS International Conference on Biomedical Robotics and Biomechanics*, pages 21 – 26, 2010.
- [90] A. Stienen, E. Hekman, H. ter Braak, A. Aalsma, F. van der Helm, and H. van der Kooij. Design of a rotational hydroelastic actuator for a powered exoskeleton for upper limb rehabilitation. *IEEE Transactions on Biomedical Engineering*, 57(3):728 – 735, 2010.
- [91] B. T. Knox and J. P. Schmiedeler. A unidirectional series-elastic actuator design using a spiral torsion spring. *ASME Journal of Mechanical Design*, 131(125001):1–5, 2009.
- [92] J. O. JudgeRoy, B. Davis, and Sylvia Ounpuu. Step length reductions in advanced age: The role of ankle and hip kinetics. *The Journals of Gerontology Series A: Biological Sciences and Medical Sciences*, 51(6):303–312, 1996.
- [93] M. P. Murray, R. C. Kory, and B. H. Clarkson. Walking patterns in healthy old men. *Journal of Gerontology*, 24(2):169–178, 1969.
- [94] J. Rose and J.G. Gamble. *Human Walking*. Eds. Lippincott USA, 2005.
- [95] H. B. Menz, S. R. Lord, and R. C. Fitzpatrick. Age-related differences in walking stability. *Age and Ageing*, 32(2):137–142, 2003.
- [96] D.A. Winter. *Biomechanics and Motor Control of Human Movement*. Wiley, 2009.
- [97] J. W. Sensinger and R. F. ff. Weir. Improvements to series elastic actuators. In *Proc. 2nd IEEE/ASME International Conference on Mechatronic and Embedded Systems and Applications*, pages 1–7, 2006.
- [98] N Tagliamonte, F Sergi, G Carpino, D Accoto, and E Guglielmelli. Design of a variable impedance differential actuator for wearable robotics applications. *Intelligent Robots and Systems (IROS), 2010 IEEE/RSJ International Conference on*, pages 2639 – 2644, 2010.



- [99] J. Veneman, R. Ekkelenkamp, R. Kruidhof, F. van der Helm, and H. van der Kooij. Design of a series elastic- and bowden cable-based actuation system for use as torque-actuator in exoskeleton-type training. *Rehabilitation Robotics, 2005. ICORR 2005. 9th International Conference on*, pages 496 – 499, 2005.
- [100] G. Wyeth. Control issues for velocity sourced series elastic actuators. *Proceedings of Australasian Conference on Robotics and Automation 2006*, 2006.
- [101] L. Zhang, G. Nuber, J. Butler, M. Bowen, and W. Z. Rymer. In vivo human knee joint dynamic properties as functions of muscle contraction and joint position. *Journal of Biomechanics*, 31(1):71 – 76, 1997.
- [102] I. D. Loram and M. Lakie. Direct measurement of human ankle stiffness during quiet standing: the intrinsic mechanical stiffness is insufficient for stability. *The Journal of Physiology*, 545(3):1041–1053, 2002.
- [103] R. C. Juvinall and K. M. Marshek. *Fundamentals of machine component design*, Chap. 8, pages 290–347. John Wiley & Sons, 2006.
- [104] A. Bicchi and G. Tonietti. Fast and “soft-arm” tactics [robot arm design]. *Robotics & Automation Magazine, IEEE*, 11(2):22 – 33, 2004.
- [105] R. Schiavi, G. Grioli, S. Sen, and A. Bicchi. VSA-II: a novel prototype of variable stiffness actuator for safe and performing robots interacting with humans. *Robotics and Automation, 2008. ICRA 2008. IEEE International Conference on*, pages 2171 – 2176, 2008.
- [106] B. S. Kim, J. B. Song, and J. J. Park. A serial-type dual actuator unit with planetary gear train: Basic design and applications. *Mechatronics, IEEE/ASME Transactions on*, 15(1):108 – 116, 2010.
- [107] J. Choi, S. Hong, W. Lee, and S. Kang. A variable stiffness joint using leaf springs for robot manipulators. *Robotics and Automation, 2009. ICRA '09. IEEE International Conference on*, pages 4363 – 4368, 2009.
- [108] S. Wolf and G. Hirzinger. A new variable stiffness design: Matching requirements of the next robot generation. *Robotics and Automation, 2008. ICRA 2008. IEEE International Conference on*, pages 1741–1746, 2008.



- [109] O. Eiberger, S. Haddadin, M. Weis, A. Albu-Schäffer, and G. Hirzinger. On joint design with intrinsic variable compliance: derivation of the DLR QA-Joint. *Robotics and Automation (ICRA), 2010 IEEE International Conference on*, pages 1687–1694, 2010.
- [110] N. Tsagarakis, A. Jafari, and D. Caldwell. A novel variable stiffness actuator: Minimizing the energy requirements for the stiffness regulation. *Engineering in Medicine and Biology Society (EMBC), 2010 Annual International Conference of the IEEE*, pages 1275 – 1278, 2010.
- [111] B. S. Kim and J. B. Song. Hybrid dual actuator unit: A design of a variable stiffness actuator based on an adjustable moment arm mechanism. *Robotics and Automation (ICRA), 2010 IEEE International Conference on*, pages 1655 – 1660, 2010.
- [112] R. Van Ham, B. Vanderborght, M. Van Damme, B. Verrelst, and D. Lefeber. MACCEPA, the mechanically adjustable compliance and controllable equilibrium position actuator: Design and implementation in a biped robot. *Robotics and Autonomous Systems*, 55(10):761 – 768, 2007.
- [113] B. Vanderborght, N. Tsagarakis, C. Semini, R. Van Ham, and D. Caldwell. MACCEPA 2.0: Adjustable compliant actuator with stiffening characteristic for energy efficient hopping. *Robotics and Automation, 2009. ICRA '09. IEEE International Conference on*, pages 544 – 549, 2009.
- [114] J. Li, D. Jin, X. Zhang, J. Zhang, and W. Gruver. An electrorheological fluid damper for robots. *Robotics and Automation, 1995. Proceedings., 1995 IEEE International Conference on*, 3:2631 – 2636 vol.3, 1995.
- [115] N. Takesue, G. Zhang, M. Sakaguchi, J. Furusho, and Y. Kiyosawa. Development and analysis of actuator with ER damper. *Robotics and Automation, 2000. Proceedings. ICRA '00. IEEE International Conference on*, 2:1328 – 1333 vol.2, 2000.
- [116] M. Unsal, C. Niezrecki, and C. Crane. Two semi-active approaches for vibration isolation: piezoelectric friction damper and magnetorheological damper. *Mechatronics, 2004. ICM '04. Proceedings of the IEEE International Conference on*, pages 60 – 65, 2004.
- [117] A. S. Shafer and M. R. Kermani. Design and validation of a magneto-rheological clutch for practical control applications in human-friendly manipulation. *Robotics and Automation (ICRA), 2011 IEEE International Conference on*, pages 4266 – 4271, 2011.



- [118] M. Laffranchi, N.G. Tsagarakis, and D.G. Caldwell. A variable physical damping actuator (VPDA) for compliant robotic joints. *Robotics and Automation (ICRA), 2010 IEEE International Conference on*, pages 1668–1674, 2010.
- [119] R. Farris and M. Goldfarb. Design of a multi-disc electromechanical modulated dissipator. *Robotics and Automation (ICRA), 2010 IEEE International Conference on*, pages 2189 – 2196, 2010.
- [120] N. Lauzier and C. Gosselin. Series clutch actuators for safe physical human-robot interaction. *Robotics and Automation (ICRA), 2011 IEEE International Conference on*, pages 5401 – 5406, 2011.
- [121] G. Carpino, D. Accoto, M. Di Palo, N. L. Tagliamonte, F. Sergi, and E. Guglielmelli. Design of a rotary passive viscoelastic joint for wearable robots. In *Rehabilitation Robotics (ICORR), 2011 IEEE International Conference on*, pages 1–6, Jul. 2011.
- [122] H. Lipson and J. B. Pollack. Automatic design and manufacture of robotic lifeforms. *Nature*, 406(6799):974–978, 2000.
- [123] F. Sergi, D. Accoto, N. Tagliamonte, G. Carpino, and E. Guglielmelli. A systematic graph-based method for the kinematic synthesis of non-anthropomorphic wearable robots for the lower limbs. *Frontiers of Mechanical Engineering*, 6:61–70, 2011. 10.1007/s11465-011-0206-2.
- [124] F. Sergi. Biomechatronic design of wearable and operational robots for rehabilitation and assistive applications. *Ph.D. dissertation, University Campus Bio-Medico of Rome, Rome, Italy*, 2011.
- [125] T. S. Mruthyunjaya. Kinematic structure of mechanisms revisited. *Mechanism and Machine Theory*, 38(4):279–320, Jan. 2003.
- [126] L. Dobrjanskyj and F. Freudenstein. Some applications of graph theory to structural analysis of mechanisms. *Journal of Engineering for Industry-Transactions of the ASME, Series B*, 89:153–158, 1967.
- [127] Evryon website, <http://www.evryon.eu>.
- [128] TUDelft (<http://dined.io.tudelft.nl>). Population “dined 2004 (20-30 years)”. *Dataset “Dutch Adults”*, 2004.



- [129] J. van den Kieboom, F. Sergi, G. Carpino, N. L. Tagliamonte, D. Accoto, E. Guglielmelli, R. Ronsse, and A. J. Ijspeert. Co-evolution of morphology and control of a wearable robot for human locomotion assistance exploiting variable impedance actuators. *Procedia Computer Science*, 7:223 – 225, 2011.
- [130] J. E. Sanders, J. M. Greve, S. B. Mitchell, and S. G. Zachariah. Material properties of commonly-used interface materials and their static coefficients of friction with skin and socks. *J Rehabil Res Dev*, 35(2):161–76, 1998.
- [131] J. B. dec. M. Saunders, V. T. Inman, and H. D. Eberhart. The major determinants in normal and pathological gait. *The Journal of Bone and Joint Surgery (American)*, 35(3):543–558, 1953.
- [132] H. P. Crowell III, A. C. Boynton, and M. Mungiole. Exoskeleton power and torque requirements based on human biomechanics. *ARL-TR-2764*, pages 1–51, Nov. 2002.

